NEURONAL MITOCHONDRIAL CALCIUM UNIPORTER DEFICIENCY EXACERBATES AXONAL INJURY AND SUPPRESSES REMYELINATION IN MICE SUBJECTED TO EXPERIMENTAL AUTOIMMUNE ENCEPHALOMYELITIS

by

Scott Phillip Holman

Submitted in partial fulfillment of the requirements
for the degree of Master of Science

at

Dalhousie University
Halifax, Nova Scotia
July 2020

Dedicated to my family.

Table of Contents

List of Tables

List of Figures

Abstract

High-capacity mitochondrial calcium (Ca^{2+}) uptake by the mitochondrial Ca^{2+} uniporter (MCU) is strategically positioned to support the survival and remyelination of axons in multiple sclerosis (MS) by undocking mitochondria, buffering Ca^{2+} and elevating adenosine triphosphate (ATP) synthesis at metabolically stressed sites. Respiratory chain deficits in MS are proposed to metabolically compromise axon survival and remyelination by suppressing MCU activity. In support of this hypothesis, clinical scores, mitochondrial dysfunction, myelin loss, axon damage and inflammation were elevated while remyelination was blocked in neuronal MCU deficient (Thy1-MCU Def) mice relative to Thy1 controls subjected to experimental autoimmune encephalomyelitis (EAE). At the first sign of walking deficits, mitochondria in EAE/Thy1 axons showed signs of activation. By contrast, cytoskeletal damage, fragmented mitochondria and large autophagosomes were seen in EAE/Thy1-MCU Def axons. As EAE severity increased, EAE/Thy1 axons were filled with massively swollen mitochondria with damaged cristae while EAE/Thy1-MCU Def axons were riddled with late autophagosomes. ATP concentrations and mitochondrial gene expression were suppressed while calpain activity, autophagy-related gene mRNA levels and autophagosome marker (LC3) co-localization in Thy1-expressing neurons were elevated in the spinal cords of EAE/Thy1-MCU Def compared to EAE/Thy1 mice. Suppression of remyelination and exacerbation of axonal damage in EAE/Thy1-MCU Def mice replicates key features of progressive MS and suggests that MCU inhibition contributes to axonal damage that drives MS disease progression.

List of Abbreviations and Symbols Used

ACK	Ammonium-chloride-potassium
AMPK	Adenosine monophosphate kinase
APC	Antigen presenting cell
ASIC1	Acid-sensing ion channel 1
Atg	Autophagy-related
ATP	Adenosine triphosphate
ATPase	Adenosine triphosphatase
Ca^{2+}	Calcium
CCR2	C-C chemokine receptor 2
CFA	Complete Freund's Adjuvant
CIS	Clinically isolated syndrome
CNS	Central nervous system
CS	Clinical score
CX3CR1	CX3C chemokine receptor 1
DMT	Disease modifying therapy
DPI	Day(s) post immunization
EAE	Experimental Autoimmune Encephalomyelitis
EBNA	Epstein-Barr nuclear antigen
EBV	Epstein-Barr virus
ECR	Eriochrome cyanine
EM	Electron microscopy
EDTA	Ethylenediaminetetraacetic acid

eYFP	Enhanced yellow florescent protein
FACS	Fluorescence-activated cell sorter
FBS	Fetal bovine serum
HBSS	Hank's balanced salt solution
HHV-6	Human herpesvirus 6
IFA	Incomplete Freund's adjuvant
ip	Intraperitoneal
K^+	Potassium
L2-5	Lumbar vertebrae 2-5
LC3	Microtubule-associated protein 1A/1B light chain 3
MA-5	Mitochonic acid 5
MCU	Mitochondrial Calcium Uniporter
$MCU^{fl/fl}$	MCU-floxed
MOG_{35-55}	Myelin oligodendrocyte glycoprotein peptide 35-55
MS	Multiple sclerosis
mt-CO4	Mitochondrial cytochrome oxidase subunit 4
Na^+	Sodium
NCX	Na^+/Ca^{2+} exchanger
NG2	Neuron-glia antigen 2
NOD	Non-obese diabetic
NR	Neutral red
OCT	Tissue-Tek® optimal cutting temperature
OSP	Oligodendrocyte specific protein

PBS	Phosphate buffered saline
PFA	Paraformaldehyde
PGC-1α	Peroxisome proliferator-activated receptor gamma coactivator 1 alpha
$PLP_{139-151}$	Proteolipid protein 139-151
po	Orally gavaged
PPMS	Primary progressive multiple sclerosis
PRMS	Progressive relapsing multiple sclerosis
PTX	*Bordetella pertussis* toxin
PVDF	Polyvinylidene fluoride
qRT-PCR	Quantitative reverse transcription polymerase chain reaction
RIN	RNA integrity number
RFU	Relative florescent units
ROS	Reactive oxygen species
rpm	Revolutions per minute
RRMS	Relapse-remitting multiple sclerosis
RT	Room temperature
RXR	Retinoic acid receptor
sc	Subcutaneous
SD	Standard deviation
SDHA	Succinate dehydrogenase subunit A
SEM	Standard Error of the Mean
SFV	Semliki Forest virus

SIP	Stock isotonic percoll
SLICK-H	Single-neuron Labelling with Inducible Cre-mediated Knockout-H
SPMS	Secondary progressive multiple sclerosis
SNPH	Syntaphilin
TAE	Tris-acetate-EDTA
TMX	Tamoxifen
WMA	White matter area
WML	White matter loss
WMLA	White matter lesion area
α	Alpha
~	Approximately
β	Beta
°C	Degrees Celsius
γ	Gamma
Ψ_m	Mitochondrial membrane potential
%	Percent
±	Plus-minus

Acknowledgements

I would first like to thank Dr. George S. Robertson for your supervision of nearly 5 years. Your inquisitiveness and dedication have taught me to be a better scientist, a harder working person and to seek passion in the work that I do. I am floored by your commitment to your students, to quality work and to an accurate golf swing. Many of the lessons I have learned in your lab will influence the decisions I make for the rest of my life. You once told me, “It’s good to be sensitive to the things that are important but not to let it bother you when you mess up along the way.” This wisdom always reminds me to be kinder to myself and others. Thank you for your bearing on my life, I will never forget my time in the GSR lab. Aurelio, thank you so much for your emotional support, your technical support and your friendship. I would not have gotten very far through this degree without you. Arul, thank you for your kindness and our life chats, I could always rely on you (and your generous supply of food) to make me feel better. Elizabeth, thank you so much for your dedication to the lab and your wealth of knowledge. You saved countless of my faulty experiments, even if I’d rather not admit it. Dan Kim, I am so unbelievably grateful to have had you along with me through this degree and in every degree since grade 10. Having you to grab lunch with, complain to, play cribbage with and just have around has kept me going through the hard parts. I will miss you dearly as we move on to different things for the first time in 9 years. You are my definition of a good friend. Robyn, thank you for being my companion through this degree. I’m glad to have had you along for the ride and I wish you all the best in your PhD. Gracious, thank you for being a bright light to the lab. I am glad we got to know each other, and I will miss our philosophical chats in the kinematics room. I wish you all the best as you replace me as George’s favourite. Thank you to Anjali, Sam, Janet, Maddy and Sydney for making a memorable summer and for humbling me at lunch games of President. Thank you to my friend and mentor Matthew for the countless hikes, movies, cideys, late-night chats and many words of guidance. In so many ways I could not have gotten through this without you. You have taught me so much about life and friendship and I look forward to making many more memories together. Max, thank you for all your help and training, you are a stunning example of a good friend and climbing buddy. AC, thank you so much for your friendship and your down to earth demeanor, camping trips with you are a real treat. Jordan, thank you for your strong example and for almost helping me weigh endothelin. Thank you to my advisory committee members Eileen Denovan-Wright and Kishore Pasumarthi for your guidance and compelling conversations. Thank you to my examining committee Deniz Top and Kerry Goralski for taking the time to read my thesis and attend my defense. Luisa Vaughan, thank you for being a huge support and reliable place to turn whenever I needed help.

And the biggest thank you I reserve for my family and friends who have been my strength. Mom, Dad, Jessie and Jodie, thank you so much for all that you have done for me and for all the encouragement that has gotten me this far. Your confidence in me has always saved me when I have lacked confidence in myself. You have made everything possible.

Chapter 1 – Introduction

Portions of this dissertation appear in the following manuscript:

Holman SP, Lobo AS, Novorolsky RJ, Nichols M, Fiander MD, Konda P, Kennedy BE, Gujar S, and Robertson GS. 2020. Neuronal mitochondrial calcium uniporter deficiency exacerbates axonal injury and suppresses remyelination in mice subjected to experimental autoimmune encephalomyelitis. *Experimental Neurology* 333: 113430.

Student contributions to the manuscript: SPH performed the EAE studies, histology, statistical analysis, and preparation of the manuscript with assistance from AL, MDJF, MN and RJN. BEK, PK and SG performed the flow cytometry and statistical analysis of the resultant data and assisted with the preparation of the manuscript. GSR assisted with the statistical analysis and preparation of the manuscript.

1.1 Multiple Sclerosis

1.1.1 Epidemiology of Multiple Sclerosis

Multiple sclerosis (MS) is a chronic, autoimmune-mediated disease characterized by demyelination and neurodegeneration of the central nervous system (CNS) (Faissner et al., 2019; GBD, 2019). MS is the most common neurological disease in adults under the age of 30 with approximately 2.3 million cases worldwide as of 2016 (GBD, 2019). However, the exact disease etiology remains unknown (Faissner et al., 2019). Canadians are one of the highest risk populations for MS in the world with a prevalence of 290 per 100,000 individuals (GBD, 2019; Mao and Reddy, 2010). Incidence of disease has traditionally been thought to increase with distance from the equator, but re-assessment of these correlations has shown that geographical associations are decreasing while female-male ratios are increasing (Alonso and Hernan, 2008). Women currently have a higher rate of MS than men with a sex ratio of 2.6:1 (female-male) (Gilmour et al., 2018). However, this ratio has been increasing in Canada and globally over time

(Gilmour et al., 2018; Koch-Henriksen and Sorensen, 2010). Global incidence rates have also been increasing over the last decade (Gilmour et al., 2018; Koch-Henriksen and Sorensen, 2010).

Some of the factors that may contribute to MS disease onset are genetic, environmental, or viral in nature (Milo and Kahana, 2010). Geographical and ancestral associations of onset have shown that individuals of Scandinavian descent may be at higher risk for MS (Page et al., 1993). Twin studies have revealed a 25-30% disease concordance rate in monozygotic twins indicating some degree of familial inheritance (Hawkes and Macgregor, 2009; Milo and Kahana, 2010). Genome wide studies have implicated major histocompatibility complex (MHC), human leukocyte antigen (HLA) and mitochondrial genes as potential contributors to MS disease onset (Dutta et al., 2006; Hafler et al., 2007; Mao and Reddy, 2010). However, the genetic makeup of MS is complex and can only account for a fraction of disease occurrences. Indeed, migration of at-risk individuals from a high- to a low-risk area reduces the risk of developing MS by two-fold (Kurtzke et al., 1985). Latitudinal associations with MS incidence may be due to seasonal decreases in sun exposure leading to vitamin D deficiency (Holick, 2004). There is also a correlation between low serum levels of vitamin D and likelihood of developing MS (Ascherio and Munger, 2007b; Sintzel et al., 2018). Smoking is another environmental risk factor for MS showing a relative risk of 1.5 for smokers compared to non-smokers (Riise et al., 2003; Wingerchuk, 2012). In addition to environmental and genetic risk factors, particular viral infections of the CNS show strong correlation with MS disease onset. For

example, individuals seropositive for Epstein-Barr virus nuclear antigen (EBNA) have been shown to be 15 times more likely to develop MS than EBNA-seronegative individuals (Ahmed et al., 2019; Ascherio and Munger, 2007a). Similarly, human herpesvirus 6 (HHV-6) is found more often in MS plaques than in normal appearing white matter of MS patients or non-diseased controls (Virtanen and Jacobson, 2012). There are other studies linking saturated fats and estrogen levels to the risk of developing MS, but these studies do not offer strong correlations or very compelling cases to explain MS lineage (Ascherio and Munger, 2007b).

1.1.2 Types of MS and Their Clinical Presentations

The clinical onset of MS is unique to the individual, but it can be generally classified into 4 different subtypes. The most common type is relapse-remitting MS (RRMS) which occurs in approximately 85% of patients (Loma and Heyman, 2011; Weiner, 2008). RRMS is characterized by recurrent autoimmune demyelination in the CNS (termed relapses) causing variable degrees of neurological impairment followed by a recession of inflammation and varying degrees of functional recovery (termed remission) (Loma and Heyman, 2011). Relapses cause a variety of symptoms including impaired vision, reasoning, emotion, memory, and motor function (Grzegorski and Losy, 2017; Loma and Heyman, 2011). These relapses occur sporadically but rarely exceed 1.5 per year and each remission is often accompanied by permanent neurological deficits (Compston and Coles, 2008). As sclerotic plaques build up after repeated immune attacks, most RRMS patients will transition to secondary progressive MS

(SPMS) (Compston and Coles, 2008; Weiner, 2008). SPMS is thought to be initiated by the accumulation of axonal damage and neural degeneration produced by persistent relapses resulting in a continuous worsening of disease severity (Faissner et al., 2019; Lublin et al., 2014). Primary progressive MS (PPMS) occurs in 10% of MS patients and presents in very similar ways to SPMS. Based on similarities with SPMS, researchers are unsure whether SPMS and PPMS are unique forms of the disease or whether PPMS is a form of SPMS in which relapses did not present at a clinical level (Baecher-Allan et al., 2018; Compston and Coles, 2008). PPMS and SPMS present challenges in the development of effective disease modifying therapies (DMTs) because of their complex underlying pathophysiology thereby making this a research field ripe with opportunity (Faissner et al., 2019). The fourth and least common form of MS is progressive relapsing MS (PRMS). This subtype presents initially with the persistent progressive characteristics of PPMS which are later combined with the intermittent and recurring relapses characteristic of RRMS (Loma and Heyman, 2011).

1.1.3 Pathophysiology of MS

MS disease onset is characterized by the infiltration of autoreactive $CD4^+$ T cells into the CNS which initiate a pro-inflammatory environment leading to recruitment of monocytes and B cells to the site of inflammation (Chitnis, 2007; Dendrou et al., 2015; Olsson et al., 1990). Cytotoxic $CD8^+$ T cells are then recruited to the CNS where they predominate in the perivascular spaces of chronic lesions (Chitnis, 2007; Gay et al., 1997). Autoimmune attack of the CNS promotes active

demyelination of axons and suppresses remyelination by inducing the apoptosis of myelin-producing oligodendrocytes (Barnett and Prineas, 2004; Dendrou et al., 2015). These events lead to neuronal degeneration and subsequent motor deficits observed in people living with MS (Compston and Coles, 2008). Autoreactive neuroinflammation has historically been considered the primary event in MS whereby there is an “outside-in” demyelinating immune attack leading to CNS damage (Geurts et al., 2010; Tsunoda and Fujinami, 2002). More recently, convergent evidence from genetic association, transcriptional profiling, proteomic, biochemical, and imaging studies have implicated a host of mitochondrial deficits in the unrelenting loss of CNS axons responsible for MS disease progression. The mitochondrial deficits observed in the CNS of patients with MS include impaired respiratory chain activities, Ca^{2+} buffering, motility, undocking and integrity (Campbell and Mahad, 2018; Campbell and Mahad, 2012; Dutta et al., 2006; Franklin et al., 2012; Trapp et al., 1998; Witte et al., 2014). The precise mechanisms at work are unclear (Peruzzotti-Jametti and Pluchino, 2018) but these events seem to cause axonal damage that stimulates inflammation resulting in disease progression according to the “inside-out” theory of MS (Geurts et al., 2010).

Impaired mitochondrial respiration could affect a host of cellular processes including suppressed ion pumping by sodium/potassium adenosine triphosphatase (Na^+/K^+ ATPase), excessive autophagy, overactivation of calpain, and failed mitochondrial undocking (Alizadeh et al., 2015; Trapp and Stys, 2009). In fully myelinated spinal cord axons, voltage gated Na^+, K^+ and calcium (Ca^{2+})

channels are strategically positioned at the nodes of Ranvier to enable the saltatory conduction of action potentials (Hamada and Kole, 2015; Trapp and Stys, 2009). Na^+/K^+ ATPase consumes ~40% of the energy supply in the brain to maintain the electrochemical gradient essential for the active propagation of action potential along the axon (Purves et al., 2001). Demyelination causes axons to transition from saltatory to continuous conduction mediated by an increase in the number of voltage gated Na^+ channels that distribute evenly along the length of the axon (Alizadeh et al., 2015; Trapp and Stys, 2009). The resultant influx of Na^+ places a further metabolic demand on denuded axons to support increased Na^+/K^+ ATPase activity (Trapp and Stys, 2009). Increased Na^+ and K^+ pumping therefore places a huge metabolic burden on denuded axons which leads to the failure of action potential conduction, axonal transection and neurodegeneration in MS (Coggan et al., 2015; Trapp et al., 1998; Trapp and Stys, 2009; Young et al., 2008a). Compromised Ca^{2+} uptake by mitochondria resulting from depolarization of the mitochondrial membrane potential (Ψ_m) leads to elevated axoplasmic Ca^{2+} levels that induce injurious calpain activity. Additionally, energy failure may create a starvation state that activates excessive autophagy in denuded axons (Giorgi et al., 2012; Jeon, 2016; Sun et al., 2016). Finally, the positioning of functional mitochondria at denuded sites essential for increased Ca^{2+} buffering and ATP production may also be impaired in MS (Cai and Sheng, 2009; Sheng and Cai, 2012). It has therefore been hypothesized that in tandem with genetic, infectious and environmental factors, impaired mitochondrial function is a key factor in the initiation of CNS damage which

drives MS progression (Geurts et al., 2010; Geurts and Barkhof, 2008; Stys et al., 2012; Trapp and Stys, 2009). Understanding the metabolic mechanisms underlying MS disease progression would thus enable the development of more effective treatments for this chronic neurodegenerative disorder.

1.1.4 Drug Therapies for Progressive MS

MS therapeutics have been steadily advancing; there are currently 20 DMTs available for reduction of MS disease severity, mitigating symptoms and delaying the conversion of RRMS to SPMS (Brown et al., 2019; Thompson et al., 2010; Torkildsen et al., 2016). However, all of these FDA approved therapies are primarily immune targeting in nature and therefore reduce disease relapse but have limited value in halting the neurodegenerative processes responsible for MS disease progression (1998; Dendrou et al., 2015; Kapoor et al., 2018; Lublin et al., 2016; Montalban et al., 2017). The FDA has recently approved two new DMTs which, in addition to being effective in RRMS, also show promise in improving progressive forms of MS. One such DMT, Siponimod, is a sphingosine-1-phosphate receptor modulator the same chemical class as the analog compound - fingolimod (Faissner et al., 2019). Although extremely effective at preventing relapses by suppressing immune cell egress from lymph nodes, fingolimod fails to show any efficacy in reducing MS disease progression (Chun and Hartung, 2010; Lublin et al., 2016). However, siponimod has shown success in reducing the progression of neurological disabilities by 21% in SPMS and is the first approved drug for this form of MS (Kappos et al., 2018). The second DMT, ocrelizumab, is an anti-B cell therapy that opposes

neuroinflammation and is the first drug approved for PPMS, however, the therapeutic benefits against disease progression are modest (Montalban et al., 2017). The mechanisms by which these drugs reduce MS disease progression are not yet well understood but it appears that they may improve the clearance of inflammatory debris from brain lesions essential for remyelination (Frischer et al., 2009; Kappos et al., 2018; Montalban et al., 2017). Current immune-based therapies therefore fail to target metabolic features of progressive MS thereby highlighting the need for a new therapeutic approach (Faissner et al., 2019).

1.2 Preclinical Models of MS

There are multiple common methods by which different pathological aspects of MS can be recapitulated in rodents that include experimental autoimmune encephalomyelitis (EAE), CNS injections of lysolecithin, the cuprizone diet, non-obese diabetic (NOD) mice, Semliki Forest virus (SFV) and others. In an attempt to replicate key features of MS these models employ different mechanisms to induce CNS demyelination (Faissner et al., 2019). However, none of them fully recapitulate all aspects of MS.

1.2.1 EAE Pathophysiology and Drug Discovery

EAE was first described in non-human primates in 1933 and remains the most used model of MS (Handel et al., 2011; Rivers et al., 1933). EAE is induced in rodents and non-human primates by peripheral immunization with a myelin antigen combined with an immune adjuvant which activates autoreactive populations of $CD4^+$ T cells (Chitnis, 2007; Constantinescu et al., 2011). Activated $CD4^+$ T cells then migrate to the CNS where they release pro-

inflammatory cytokines IFN-γ and TNF-α that mobilize the innate immune system resulting in inflammatory spinal cord damage (Corsini et al., 1996; Dendrou et al., 2015; Olsson et al., 1990; Olsson, 1995). This promotes the recruitment and infiltration of monocytes to the CNS (Dendrou et al., 2015; Monaghan et al., 2019). Cross-presentation by dendritic cells induces the activation and recruitment of $CD8^+$ cytotoxic T cells whose numbers are correlated with higher rates of axonal damage in MS (Bitsch et al., 2000; Dendrou et al., 2015). The disease course taken by EAE mice depends on the genetic background and the myelin antigen used for immunization (Constantinescu et al., 2011). For example, immunization of SJL mice with proteolipid protein amino acids 139-151 ($PLP_{139-151}$) induces a relapse-remitting form of EAE that recapitulates RRMS (Constantinescu et al., 2011; McRae et al., 1995). In the current study, we immunized sexually mature female C57BL/6 mice with myelin oligodendrocyte glycoprotein peptide 35-55 (MOG_{35-55}) suspended in complete Freund's adjuvant (CFA) followed by pertussis toxin (PTX) that boosts immune activation. The MOG_{35-55} model leads to a monophasic immune infiltration that produces permanent motor deficit (Constantinescu et al., 2011). Autoimmune demyelination in this EAE model recapitulates oligodendrocyte cell death, axonal transection, incomplete remyelination, motor deficit and permanent neurological impairments seen in MS (Constantinescu et al., 2011; Jones et al., 2013; Mei et al., 2016; Prinz et al., 2015; Recks et al., 2013; Smith, 1999). EAE models have been used to identify several FDA approved DMTs such as glatiramer acetate, natalizumab, mitoxantrone, fingolimod and most recently ocrelizumab (Faissner

et al., 2019; Robinson et al., 2014; Steinman and Zamvil, 2006). However, EAE fails to reproduce unrelenting neurodegeneration in inactive lesions typical of progressive MS (Faissner et al., 2019).

1.2.2 Limitations and Shortcomings for Preclinical Models of MS

Despite having proven useful in the development of multiple FDA approved drugs, the EAE model has also failed to deliver on multiple occasions. EAE models that simply use peripheral immunization with an exogenous antigen to initiate an immune response are limited by our incomplete understanding of the neurodegenerative disease mechanisms in MS (Constantinescu et al., 2011; Faissner et al., 2019; Friese et al., 2006; Handel et al., 2011). Furthermore, the overall genetic makeup of mice and humans are different in multiple ways. For instance, the T cell responses in murine EAE models and MS differ – autoreactive $CD4^+$ T cells predominate in EAE while $CD8^+$ T cells play a greater pathogenic role than $CD4^+$ T cells in MS (Handel et al., 2011; Seok et al., 2013). Such differences may thus account for the failure of the EAE model to predict clinical efficacy in some cases (Friese et al., 2006). This has been particularly evident for treatments designed to improve myelin repair. Opicinumab (anti-LINGO-1 monoclonal antibody) improves remyelination in models of chemical and autoimmune-mediated demyelination but has been ineffective in MS patients. In the case of Lenercept (anti-TNF monoclonal antibody), disease relapses were actually exacerbated (1999; Cadavid et al., 2019; Friese et al., 2006). These translational failures indicate a lack of fidelity for EAE as a model of MS.

There are a number of other animal models that recapitulate, to varying degrees, immune mediated damage in MS. Cuprizone and lysolecithin use chemicals to induce lysis of oligodendrocytes and disrupt the myelin sheath leading to demyelination (Denic et al., 2011; Friese et al., 2006; Skripuletz et al., 2010). Although these models are useful for investigating demyelination and remyelination in animals, they do not recapitulate the immune mechanisms impacted in MS (Denic et al., 2011). More recently, immune based models more relevant to progressive MS have been developed. NOD mice subjected to EAE present with an initial $CD4^+$ and $CD8^+$ T cell recruitment to the CNS resulting in a relapse-remitting form of EAE followed by a secondary progressive phase similar to SPMS (Ignatius Arokia Doss et al., 2015). The SFV model of CNS demyelination supports the theory that viral infection may be a contributor to T cell-mediated disease onset in MS (Amor et al., 2005; Mokhtarian et al., 2003). The NOD and SFV models effectively recapitulate aspects of MS but still rely on the assumption that MS is primarily immune mediated and that progression is driven by a continuous immune-mediated destruction of the CNS rather than mechanisms which promote chronic neuronal degeneration (Faissner et al., 2019; Ignatius Arokia Doss et al., 2015). Recently, it was shown that the intravenous administration of T cells reactive to β-synuclein causes gray matter demyelination and neurodegeneration in Lewis rats reminiscent of neurodegeneration in progressive MS (Calabrese et al., 2015; Faissner et al., 2019; Lodygin et al., 2019). However, it is not yet clear whether grey matter loss in MS simply results from the retrograde degeneration of demyelinated white

matter tracts or if white and grey matter damage are mediated by different mechanisms. Nevertheless, this model offers a new avenue to study grey matter degeneration in progressive MS (Calabrese et al., 2015).

Overall, the current preclinical models do not mimic critical aspects of progressive MS (Faissner et al., 2019). In particular, the potential contribution of mitochondrial collapse as a driver of CNS damage that induces chronic neuroinflammation according to the inside-out theory of MS are lacking (Faissner et al., 2019; Mao and Reddy, 2010). To be relevant for progressive MS, we propose that disease models should reproduce features of mitochondrial dysfunction in a manner that closely precedes CNS axon injury. In addition to improving our understanding of how mitochondrial dysfunction promotes MS progression by damaging axons and disrupting remyelination, such models would also assist the development of more effective treatments.

1.3 The Mitochondrial Calcium Uniporter

Mitochondrial Ca^{2+} uptake, driven by the Ψ_m, was clearly demonstrated in 1961 (Deluca and Engstrom, 1961). Genetic identification of the mitochondrial Ca^{2+} uniporter (MCU) in 2011 revealed that high-capacity mitochondrial Ca^{2+} uptake is mediated by the MCU (Baughman et al., 2011; De et al., 2011). MCU-mediated Ca^{2+} uptake buffers Ca^{2+} and induces adenosine triphosphate (ATP) synthesis. This mechanism for mitochondrial Ca^{2+} uptake therefore has important implications for impaired Ca^{2+} buffering and energy production leading to axonal loss that promotes MS disease progression.

1.3.1 Conditional Ablation of the MCU and Mitochondrial Function

Identification of the MCU has allowed for the generation of conditional MCU deficient murine lines for which MCU activity in cardiac myocytes or CNS neurons is suppressed by tamoxifen- (TMX) induced *cre* recombination at floxed sites critical for MCU function (Heimer-McGinn and Young, 2011; Luongo et al., 2015). These inducible knockout lines have shown that the MCU regulates both cell death and survival. With respect to the former, excessive MCU activity triggers mitochondrial Ca^{2+} overloading resulting in ischemic/reperfusion heart and brain injury (Kwong et al., 2015; Luongo et al., 2015; Nichols et al., 2018). In the case of the latter, enhanced entry of Ca^{2+} into the mitochondrial matrix via the MCU increases ATP synthesis by allosterically activating dehydrogenases that produce reducing equivalents which fuel complex I activity (Denton et al., 1972; Nichols et al., 2017; Rizzuto et al., 2012). MCU-mediated mitochondrial Ca^{2+} uptake may also promote neuronal survival by buffering intracellular Ca^{2+} concentrations that oppose injurious Ca^{2+}-dependent phospholipase and protease activities (Stirling and Stys, 2010; Trapp and Stys, 2009). In response to the dynamic energy demands imposed by neurotransmission, mitochondria are rapidly transported along the axon by cytoskeletal motors to metabolically active sites (Saxton and Hollenbeck, 2012; Schwarz, 2013). Increased MCU-mediated Ca^{2+} uptake, triggered by elevated Ca^{2+} concentrations at these active sites, undocks mitochondria from their cytoskeletal motors (Chang et al., 2011; Niescier et al., 2013; Niescier et al., 2018). This positions mitochondria at metabolically active neuronal sites in need of increased Ca^{2+} buffering and ATP synthesis.

1.3.2 The MCU and Progressive MS

Demyelination places a considerable metabolic burden on axons that must produce massive amounts of ATP to support increased ion pumping by Na^+/K^+ ATPases (Stys and Lopachin, 1998; Trapp and Stys, 2009; Tsutsui and Stys, 2013). Increased MCU activity may thus be required to meet the prodigious metabolic demands imposed by demyelination on axons. Oxidative phosphorylation generates the Ψ_m by the pumping of hydrogen ions into the intermembrane space (Lehninger, 1979). ATP synthase harvests this proton gradient to produce ATP (Hahn et al., 2018). Respiratory deficits seen in progressive MS axons (Campbell and Mahad, 2012; Dutta and Trapp, 2012; Fischer et al., 2012; Mahad et al., 2009; Witte et al., 2014) would thus suppress ATP synthesis by depolarizing the Ψ_m. Since the Ψ_m drives mitochondrial Ca^{2+} uptake (Rottenberg and Scarpa, 1974) we propose that respiratory deficits in progressive MS reduce axonal MCU activity. Confocal imaging has shown that depolarization of the Ψ_m in spinal cord axons is also associated with increased disease severity while recovery is accompanied by repolarization of the Ψ_m (Sadeghian et al., 2016). These findings indicate that autoimmune-mediated demyelination places a massive metabolic stress on spinal cord axons leading to the impairment of movement in patients with MS and EAE mice.

1.4 Rationale

The MS community continues to be in the utmost need of DMTs that safely and effectively halt long-term disease progression. At the centre of this issue is the “paucity of relevant preclinical animal models” that replicate the metabolic and neurodegenerative features of progressive MS (Faissner et al., 2019). EAE has

been used as a model of autoimmune mediated demyelination that has led to the FDA approval of DMTs for relapses in MS but lacks the fidelity and complexity to reliably identify drugs that reduce MS progression (Friese et al., 2006). In view of the potential for impaired axonal MCU activity to promote MS disease progression, the present study examines the effects of MCU deletion in the neurons of mice subjected to EAE in the hopes of replicating the degenerative mechanisms implicated in MS progression.

1.5 Research Aims

The current study has three main research aims: 1) to determine whether there are any differences in EAE disease severity between Thy1-MCU Def mice and their Thy1 controls, 2) to measure pathophysiological features of progressive MS in the spinal cords of EAE/Thy1 and EAE/Thy1-MCU Def mice and 3) to quantify the inflammatory environment of EAE/Thy1 and EAE/Thy1-MCU Def mice.

1.5.1 Aim 1

The first aim of this study is to determine whether MCU deletion in the CNS of mice subjected to EAE increases EAE disease severity. Quantification of clinical scores, spinal cord white matter loss (WML) and axonal injury were used to measure disease outcomes. The MCU is critical for proper Ca^{2+} regulation, energy production and mitochondrial positioning (Chang et al., 2011; Denton, 2009; Nichols et al., 2017; Niescier et al., 2018; Schwarz, 2013; Stirling and Stys, 2010; Trapp and Stys, 2009). It was therefore hypothesized that conditional Thy1-MCU deletion would lead to an exacerbation of disease severity in mice subjected to EAE as observed through an elevation of clinical score, WML and axonal damage of the spinal cord.

1.5.2 Aim 2

Given that mitochondrial deficits are hypothesized to contribute to MS disease progression (Campbell and Mahad, 2012; Mahad et al., 2009; Witte et al., 2014), aim 2 sought to determine whether Thy1-MCU Def in mice subjected to EAE replicated key neurophysiological features seen in the lesions of patients with progressive MS. Spinal cord ATP concentrations and mitochondrial gene expression were measured to assess metabolic function. Calpain activation was measured to determine the degree of Ca^{2+} overloading. Mitochondrial morphologies indicative of activation, swelling and fragmentation and cytoskeletal loss, autophagosome formation, axonal damage and remyelination were quantified in electron microscopic images of axons located within L5 of the spinal cord at different stages of disease development in EAE/Thy1 and EAE/Thy1-MCU Def mice. Autophagy markers were also compared in the spinal cords of these mice. It was hypothesized that EAE/Thy1-MCU Def would compromise Ca^{2+} buffering and ATP production resulting in calpain overactivation, excessive autophagy, mitochondrial damage and increased cytoskeletal loss thus replicating key features of progressive MS not present in wild-type mice subjected to EAE (Faissner et al., 2019).

1.5.3 Aim 3

The final aim sought to determine whether EAE/Thy1-MCU Def mice showed changes in immune activation compared to EAE/Thy1 mice. Given that there appears to be an interplay between immune dysregulation and neuronal degeneration in MS (Faissner et al., 2019; Mallucci et al., 2015), it seemed possible that increased spinal cord pathology would lead to enhanced immune

activation. Therefore, immune cell activation and infiltration were examined by the flow cytometric analysis of T cell and myeloid cell populations in the spleens and CNS of EAE/Thy1 and EAE/Thy1-MCU Def mice. Quantitative RT-PCR measurements of mRNA levels for pro-inflammatory and pro-repair cytokines within the spinal cords of these mice were also performed to determine whether there were changes of inflammatory activation and the polarization of immune cells from a damaging to a repair phenotype. It was hypothesized that EAE/Thy1-MCU Def mice would show an upregulation of immune activation compared to EAE/Thy1 controls.

Chapter 2- Materials and Methods

2.1 Animal Care

All experimentation for this project was approved by the Dalhousie University Committee on Laboratory Animals (DUCLA) in accordance with the Canadian Council on Animal Care and ARRIVE Guidelines. Mice were housed in the Life Sciences Research Institution on a 12-hour light/dark cycle (7:00am/7:00pm) with water and food provided *ad libitum*.

2.2 Generation of Neuronal Specific MCU Deficient Mice

Single-neuron Labelling with Inducible Cre-mediated Knockout-H (SLICK-H; The Jackson Laboratory; Stock No: 012708) mice expressing a Thy1-creER^{T2}-enhanced yellow florescent protein (eYFP) construct were crossed with C57BL/6 MCU-floxed (MCU$^{fl/fl}$) mice (Dr. Jeffrey Molkentin, Philadelphia, OH, USA) to generate Thy1-creER^{T2}-eYFP$^{+/-}$/MCU$^{fl/fl}$ mice. Mice received daily TMX dosing (80 mg/kg) by oral (po) gavage for 5 days followed by a 3-week washout period to ablate the MCU in Thy1-expressing neurons. These mice were subsequently titled Thy1-MCU Def mice while SLICK-H mice expressing Thy1-creER^{T2}-eYFP that were treated in the same manner served as controls and were titled Thy1 mice. All experimentation was performed on female Thy1 and Thy1-MCU Def mice at 8-12 weeks of age.

2.3 Experimental Autoimmune Encephalomyelitis

2.3.1 Preparation of Reagents

Heat-killed *Mycobacterium tuberculosis* H37RA (Difco Laboratories, Detroit, MI, USA) was thoroughly suspended in incomplete Freund's adjuvant (IFA) to make complete Freund's adjuvant (CFA) with a 10 mg/ml concentration. A peptide corresponding to amino acids 35-55 (MEVGWYRSPFSRWHLYRNGK; Gen Script, Piscataway, NJ, USA) of myelin oligodendrocyte glycoprotein (MOG_{35-55}) was dissolved in sterile phosphate buffered saline (PBS) to produce a solution at concentration of 3 mg/ml. MOG_{35-55} was combined with CFA in a 1:1 ratio to produce CFA/MOG_{35-55} and was used to induce experimental autoimmune encephalomyelitis (EAE). *Bordetella pertussis* toxin (PTX; Sigma-Aldrich, St. Louis, MO, USA) was reconstituted in sterile saline to create a concentration of 100 µg/ml. PTX was further diluted in PBS to create a final injection concentration of 1.5 ng/µl.

2.3.2 Induction of EAE

Thy1 and Thy1-MCU Def mice were anesthetized using isoflurane (2%; 1 litre/min O_2) before receiving bilateral (2 injections/mouse) subcutaneous (sc) injections (100 µl/injection) of CFA/MOG_{35-55} near the base of the tail on day(s) post immunization (DPI) 0. At DPI 0 and 2 an intraperitoneal (ip) injection containing 300 ng of PTX was administered to each mouse in a volume of 200 µl at each timepoint. Mice receiving this treatment developed EAE and are hereafter referred to as EAE/Thy1 and EAE/Thy1-MCU Def mice. Thy1 and Thy1-MCU Def mice that received bilateral sc injections of CFA emulsified with

PBS instead of MOG_{35-55} (100 µl/injection) followed by PTX on DPI 0 and 2 did not develop EAE and served as MOG_{35-55} immunization controls (CFA/Thy1 and CFA/Thy1-MCU Def mice). The 4 resulting experimental groups were CFA/Thy1, EAE/Thy1, CFA/Thy1-MCU Def and EAE/Thy1-MCU Def mice.

2.3.3 Clinical Scoring

EAE severity was assessed by tracking daily changes in weight and motor function. The following ordinal scale was used to clinically score (CS) the animals for degree of motor deficit: 0, no clinical signs; 0.5, hooked tail (inability to lift the tip of the tail from the ground); 1, fully flaccid tail or mostly flaccid tail with splay; 1.5, flaccid tail with splay; 2, minor walking deficits, mild ataxia and general weakness of the lower body (may include uneven gait or waddling); 2.5, severe walking deficits, which may include paraparesis, severe swaying and weakness of the hindlimbs; 3, dropped pelvis (characterized by a total inability of the hindlimbs to lift the pelvis from the ground) in addition to severe walking deficits and chronic ataxia; 3.5, unilateral hindlimb paralysis; 4, bilateral hindlimb paralysis; 4.5, forelimb paralysis; 5, moribund (Table 1). A trained observer blinded to the treatment conditions recorded all CS and weights starting at DPI 7.

Table 1. Ordinal scale of clinical scores used to assess disease severity in EAE

CLINICAL SCORE	DESCRIPTION
0	No clinical signs
0.5	Hooked tail (inability to lift the tip of the tail from the ground)
1	Fully flaccid tail or mostly flaccid tail with splay
1.5	Flaccid tail with splay
2	Minor walking deficits, mild ataxia and general weakness of the lower body (may include uneven gait or waddling)
2.5	Severe walking deficits, which may include paraparesis, severe swaying and weakness of the hindlimbs
3	Dropped pelvis (a total inability of the hindlimbs to lift the pelvis from the ground) in addition to severe walking deficits and chronic ataxia
3.5	Unilateral hindlimb paralysis
4	Bilateral hindlimb paralysis
4.5	Forelimb paralysis
5	Moribund

2.3.4 Animal Husbandry

Mice were provided mashed kibble, Dietgel® Recovery and Dietgel® Boost (ClearH_2O, Westbrook, ME, USA) *ad libitum* beginning at DPI 9 until experiments' end. If body weight loss exceeded 10% of pre-immunization values, mice were handfed Nutri-Cal® gel (Vetoquinol, DE, USA) and given sc injections of 0.9% Na^+ chloride solution (25 ml/kg/day) to maintain hydration and nutrition. Humane end-points as agreed upon by DUCLA, were defined as follows: 1) weight loss exceeded 20% of the pre-immunization values; 2) CS of 4.5 or higher (unilateral forelimb paralysis and/or moribund); 3) loss of righting reflex or 4) inability to access food or water for 24 hours. Any mice breaching any of the humane endpoints were humanely euthanized and excluded from experimental results.

2.4 Histology and Immunohistochemistry

2.4.1 Preparation of Spinal Cord Tissue for Histology and Immunohistochemistry

Mice were humanely euthanized at DPI 16 or 30 with an overdose of Na^+ pentobarbital (150 mg/kg, ip; Euthansol; Schering, Canada, Pointe-Claire, QC) and underwent cardiac perfusion with PBS (10 ml) followed by 4% paraformaldehyde (PFA, 10 ml; Fisher Scientific, Fair Lawn, NJ, USA). Spinal cords were isolated from the spinal column by microdissection, post-fixed in 4% PFA for 24 hr and placed in 15% sucrose (24 hr) followed by 30% sucrose (24 hr) for cryoprotection. The spinal cords were then cut to a segment spanning lumbar vertebrae 2-5 (L2-5) and embedded horizontally in Tissue-Tek® optimal cutting temperature (OCT; Sakura® Finetek, CA, USA). Serial sagittal sections

(30 µm thick) were then cut at -18˚C with a CM1950 cryostat (Leica Biosystems, Concord, ON, Canada).

2.4.2 Eriochrome Cyanine and Neutral Red Staining

Spinal cord sections at DPI 16 and 30 were rehydrated with descending concentrations of ethanol (100% to 70%) before being immersed in tap water. Sections were then stained with eriochrome cyanine (ECR; myelin stained blue; Sigma-Aldrich, St. Louis, MO, USA) for 15 min, differentiated in 0.5% ammonium hydroxide solution and rinsed in tap water. Sections were counterstained with neutral red (NR; neurons and exposed axons stained red; Acros Organics, Geel, Belgium) for 2 min and rinsed once more with tap water. Sections were then dehydrated in ascending concentrations of ethanol (70%-100%), washed in xylene and cover-slipped with Cytoseal™ 60 (Thermo Scientific, Waltham, MA, USA).

2.4.3 Quantification of WML

Slides were imaged using the Axioplan II with an Axiocam HRC Colour Camera (Zeiss, Pleasanton, CA, USA) and analyzed using ImageJ. One serial slide from each mouse was taken for imaging. The spinal cord sections with the largest white matter lesion area (WMLA; defined by the occurrence of NR staining within ECR stained white matter) from each mouse were imaged for quantification. All white matter area (WMA) was traced by a trained experimenter that was blinded to experimental conditions. WMLAs within WMA were traced, summed and calculated as a percentage of WMA to produce spinal cord WML ($\frac{WMLA}{WMA} * 100\% =$

WML). WML for each mouse was an average of the three most damaged sections of that mouse.

2.4.4 Immunohistochemistry for LC3 and eYFP

Immunohistochemistry was performed on longitudinal spinal cord sections of DPI 16 mice. Sections were blocked for 1 hr at room temperature (RT) with 20% normal goat serum in PBS/0.5% Triton™ X-100 (Sigma-Aldrich, St. Louis, MO, USA). Slides were then incubated overnight in rabbit anti-LC3b (1:400; L7543, Sigma-Aldrich, St. Louis, MO, USA) at 4°C. Slides were washed 3 times with PBS and incubated in goat anti-rabbit Alexa Fluor 647 (1:250; ab150079, Abcam, Cambridge, UK) at RT for 1 hr. Fluoromount™ (Sigma-Aldrich, St. Louis, MO, USA) was used to coverslip slides before eYFP/LC3b was visualized using a Zeiss Axio Imager Z2 with monochrome camera (Zeiss, Pleasanton, CA, USA). A trained experimenter blinded to the experimental groups counted the number of neurons positive for LC3b staining, eYFP expression and LC3b/eYFP co-staining. 3 representative images were counted and averaged for each animal.

2.4.5 Quantification of Punctate eYFP Labelling of the Corticospinal Tract

Endogenous eYFP fluorescence within axonal tracts of the corticospinal tract was also visualized using the Zeiss Axio Imager Z2 with monochrome camera (Zeiss, Pleasanton, CA, USA). Punctate labelling of eYFP aggregation was used as a marker of axonal transection and spinal cord damage. The Yen auto thresholding tool in ImageJ was then used to establish a threshold that would exclude all normal eYFP fluorescence and include only areas of punctate

labelling. Damaged areas were summed for each section and the final value for each animal was an average of three sections.

2.5 Western Blotting

Spinal cords from CFA/Thy1, EAE/Thy1, CFA/Thy1-MCU Def and EAE/Thy1-MCU Def mice euthanized at DPI 16 were homogenized in 500 μl RIPA buffer including a protease inhibitor cocktail (Sigma-Aldrich, Oakville, ON, Canada) and then spun at 14,000 g for 15 min at 4˚C. The supernatant was collected into fresh microtubes and the protein concentration determined by Bradford assay (Bio-Rad Laboratories Inc., Mississauga, ON, Canada). After thawing, 10 μg protein samples were electrophoretically separated on 10% Na^+ dodecyl sulfate polyacrylamide gels and transferred onto Amersham Hybond 0.2 μm PVDF membranes (GE Healthcare Life sciences, Germany) at 220 mA for 2 hr. The protein containing PVDF membranes were then blocked in 5% non-fat milk (Santa Cruz Biotechnology, Dallas, TX, USA) for 1 hour and washed 3x in Tris-base Saline with 0.05% Tween®-20 (Sigma-Aldrich, St. Louis, MO, USA). The membranes were incubated overnight at 4˚C in primary antibodies prepared in 1% non-fat milk and at dilutions according to manufacturer's instructions. The antibodies utilized included: rabbit anti-MCU D2Z3B (149975, Cell Signaling Technology, Danvers, MA, USA), mouse anti-β-actin antibody (055K4854, Sigma-Aldrich, St. Louis, MO, USA), rabbit anti-β-tubulin (ab6046, Abcam, Cambridge, UK) and mouse anti-α-Fodrin (AA6; BML-FG6090-0100, Enzo Life Sciences Inc., Cedarlane, Burlington, ON, Canada). Blots were incubated with peroxidase-labelled goat anti-rabbit IgG PI-1000 or goat anti-mouse IgG PI-2000

(Vector Laboratories, Burlingame, CA, USA) for 1 hr and washed. Amersham ECL prime western blotting detection reagent (GE Healthcare Life Sciences, Germany) was applied uniformly to the membrane immediately before imaging. Images were captured with a ChemiDoc Touch and analysed with Image Lab 6.0 software (Bio-Rad Laboratories, Inc., Mississauga, ON, Canada). MCU levels are shown as a ratio relative to the β-tubulin signal in spinal cord tissue and β-actin signal in splenocytes. Calpain activation reflected the optical density ratio of the calpain-cleaved fragment of αII-spectrin (150 kDa) divided by the intact αII-spectrin strand (285 kDa).

2.6 Transmission Electron Microscopy (EM)

2.6.1 Preparation and Staining of Spinal Cord Tissue for EM

Mice were humanely euthanized at DPI 16 and underwent cardiac perfusion with PBS (10 ml) followed by 2.5% glutaraldehyde in PBS (10 ml; pH 7.4; Sigma-Aldrich, St. Louis, MO, USA). Spinal cords were isolated from the spinal column by microdissection, rinsed 3 times in 0.1 M Na^+ cacodylate buffer (Sigma-Aldrich, St. Louis, MO, USA) and post-fixed in 1% osmium tetroxide (Sigma-Aldrich, St. Louis, MO, USA) for 2 hr. The samples were then dehydrated, trimmed to the L5 region and embedded in epon araldite resin (Agar Scientific, Stansted, Essex, UK). Sections were cut to 100 nm thickness with an ultramicrotome (Leica Biosystems, Concord, ON, Canada) and placed on mesh copper grids for staining. Sections were stained with 2% aqueous uranyl acetate, rinsed, and treated with lead citrate, then rinsed again and air dried. Images were captured with a Jeol Jem 1230 transmission EM (Jeol, Peabody, MA, USA) at 80 kV

equipped with a Hamamatsu ORCA-HR digital camera (Hamamatsu, Naka-ku, Hamamatsu, Japan).

2.6.2 Quantification of Mitochondrial Activation, Damage and Autophagosomal Formation

Mitochondria (activated, condensed/fragmented or swollen) per axon, autophagosomes per axon, damaged axons, remyelinating axons and mitochondria per remyelinating axon were manually counted within an area (10 X 10 μm) in the L5 spinal cord. Four regions within ten serially sectioned images, selected at random, were quantified for each of the EAE/Thy1 (n=20) and EAE/Thy1-MCU Def (n=20) mice with CS=0, 2.0, 2.5, 3.0 or 3.5 (n=4/CS). Optical densities were also measured within an area (2 X 2 μm) located within L5 spinal cord axons of EAE/Thy1 and EAE/Thy1-MCU Def mice at CS=2.0 using ImageJ software for the purpose of quantifying cytoskeletal densities. The average values for measurements made by two individuals blinded to the experimental conditions were used for the statistical comparisons.

2.7 Flow Cytometry

2.7.1 Cell Preparation of Spleens for Flow cytometry

Mice were humanely euthanized at DPI 16, their spleens were harvested aseptically and were kept in chilled, sterile Ca^{2+} and Mg^{2+} free PBS (Gibco; Life technologies, Grand Island, NY, USA) on ice. Individual spleens were filtered through a 40 μm Nylon cell strainer (BD Falcon, Bedford, MA, USA) into a 50 ml conical tube. The crushed cells were filtered, washed with 5 ml PBS, and centrifuged at 500 rpm for 10 min at 4˚C. The supernatant was aspirated and

discarded while the pellet was resuspended in 4 ml/spleen of 1X sterile Ammonium-Chloride-Potassium lysis buffer (ACK; ThermoFisher Scientific, Waltham, MA, USA) and allowed to stand at RT for 15 min. The lysis buffer was then neutralized with 6 ml of sterile complete RPMI medium (Gibco; Life technologies, Grand Island, NY, USA) which contained 1% heat inactivated fetal bovine serum (FBS, Mediatech, Inc., Corning subsidiary, Manassas, VA, USA). The neutralized cell suspension was then passed through a 40 µm Nylon cell strainer to exclude any cell clumps and was centrifuged at 500 rpm for 10 min at 4˚C. The supernatant was discarded, and cells resuspended in complete RPMI medium at 10 x 106 cells/ml before fluorescence-activated cell sorter (FACS) analysis.

2.7.2 Cell Preparation of CNS Tissues for Flow Cytometry

The same mice were then perfused with ice-cold 1X Hank's Balanced Salt Solution (HBSS, Gibco by Life Technologies, Grand Island, NY, USA) without Ca^{2+} and Mg^{2+}. Brain and spinal cord tissues were harvested and maintained in RPMI without phenol red (Gibco by Life Technologies, Grand Island, NY, USA) until all mice were sacrificed. CNS tissues from individual mice were homogenized together in a Dounce homogenizer in RPMI and the cell suspension was then made up to 7 ml with RPMI. Stock isotonic percoll (SIP) was prepared by mixing 9 parts percoll (MP Biomedicals, LLC, Santa Ana, CA, USA) with one-part 10X HBSS without Ca^{2+} and Mg^{2+}. The cell suspension was mixed with 3 ml SIP to get 30% SIP which was slowly overlayered on top of 2 ml of 70% SIP in 1X HBSS. The overlayered cells were centrifuged at 500 rpm for

30 min at 18˚C with minimal or no breaks so that the interface was not disturbed. Approximately 2-3 ml of the 70-30% interphase was collected into a fresh tube and washed twice by resuspending the cells in 1X HBSS and centrifugated at 500 rpm for 7 min at 18˚C. The pellet was resuspended in complete RPMI medium.

2.7.3 FACS Analysis

For all experiments, approximately 1 x 106 cells were resuspended in FACS buffer (1% FBS in PBS with 5 mM Ethylenediaminetetraacetic acid (EDTA)). Centrifugation was carried out at 500 rpm for 5 min at 4˚C. Cells were incubated in purified anti-mouse CD16/CD32 (BD Biosciences, San Jose, CA, USA) in FACS buffer for 30 min at 4˚C to block the F_C binding sites. Surface staining was performed in the dark for 30 min at 4˚C in FACS buffer. Cells were then washed twice with FACS buffer and fixed in 4% PFA (VWR, West Chester, PA, USA) for 20 min at RT. Cells were then washed twice, resuspended in FACS buffer, and stored at 4˚C until FACS analysis. Surface markers for these experiments include: anti-mouse CD4 antibody clone RM4-5 FITC (1:200; BioLegend, San Diego, CA, USA); anti-mouse CD3ε antibody clone 145-2C11 PE (1:200; BioLegend); anti-mouse CD8a antibody clone 53-6.7 PerCP (1:200; BD Biosciences); anti-mouse Ly-6G antibody clone 1A8 FITC (1:400; BD Biosciences); anti-mouse Ly-6C antibody clone HK1.4 PE (1:150; BioLegend); anti-mouse/human CD11b antibody clone M1/70 PerCP (1:400; BioLegend); anti-mouse CD45 antibody clone 30-F11 APC/Cy7 (1:200; BioLegend). The FACS experiments were performed using the FACS Canto II instrument (BD

Immunocytometry systems, San Jose, CA, USA) equipped with 405 nm, 488 nm, 561 nm and 640 nm excitation lasers located in the Dalhousie University Faculty of Medicine Core Facility, Halifax, NS, Canada. All data collections were performed using the BD FACS Diva software (BD Biosciences, San Jose, CA, USA) and the data analyses were performed using Flowing software (Turku Centre for Biotechnology, University of Turku, Finland). Compensation was performed using single colour controls prepared for each fluorochrome on positive cell populations for the cell surface staining. Doublet discrimination was performed manually to exclude any composite events due to clumped cells.

2.8 Quantitative Reverse Transcription Polymerase Chain Reaction (qRT-PCR)

Mice were humanely euthanized at DPI 16 and spinal cords were homogenized in 1 ml PureZOL (Bio-Rad Laboratories Inc., Mississauga, ON, Canada) in the Benchmark Scientific D1030 homogenizer (Cole-Parmer Canada Company, Montreal, QC, Canada). Total RNA was extracted using the Aurum Total RNA Fatty and Fibrous Tissue kit (Cat. #732-6870, Bio-Rad Laboratories Inc., Mississauga, ON, Canada) following the spin protocol as per the manufacturer's instructions. On elution, the concentration and purity of RNA was estimated spectrophotometrically on the SPECTROstar Nano spectrophotometer (BMG Labtech, Mandel Scientific Company Inc., Guelph, ON, Canada). To measure the quality and overall integrity of the isolated total RNA, the Experion bioanalyzer along with the RNA StdSens Analysis Kit (Bio-Rad Laboratories Inc., Mississauga, ON, Canada) was used. Only samples with RNA integrity number

(RIN) values of 7.5 or more were considered acceptable and used for further analysis. Reverse transcription was carried out with the iScript cDNA synthesis kit (Bio-Rad Laboratories Inc., Mississauga, ON, Canada) using 1 µg of RNA as template for each sample. Real-Time qRT-PCR was performed with the SsoFast EvaGreen Supermix kit (Bio-Rad Laboratories Inc., Mississauga, ON, Canada) with β-actin, GAPDH, β2M and HPRT1 evaluated as reference genes (see Table 2). The individual genes were optimized for both annealing temperature and conditions. PCR cycling conditions were: (95˚C for 30 sec) + (95˚C x 5 sec + 60˚C x 5 sec + fluorescence read) x 40 cycles + melt curve analysis. The melting curve program was a 2 sec hold time with plate readings for every 0.5˚C increase from 65˚C to 95˚C. All qRT-PCR protocols were done in accordance with the MIQE guidelines (Bustin et al*.,* 2009) and were performed with the Bio-Rad CFX96 real-time system C1000 touch thermal cycler (Bio-Rad Laboratories Inc., Mississauga, ON, Canada). Data analysis was performed using the CFX Maestro software (Bio-Rad Laboratories, Inc., Mississauga, ON, Canada) using the $^{\Delta\Delta}$Cq method. Statistical comparisons were performed using the average value of triplicate technical replicates for all experiments. Target genes quantified in qRT-PCR include IFN-γ, TNF-α, IL-1β, IL-6, IL-12A (p35), CCL5, TGF-β, IL-10, atg5, atg7, SDHA, mt-CO4, and PGC-1α. The primer sequences are shown in Table 2.

Table 2. Primer sequences of target genes in qRT-PCR

Target Genes	Forward	Reverse
β-actin	GTGACGTTGACATCCGTAAA	GCCGGACTCATCGTACTCC
GAPDH	AGGTCGGTGTGAACGGATT	GGGGTCGTTGATGGCAACA
β2M	TTCTGGTGCTTGTGTCACTG	CAGTATGTTCGGCTTCCCATT
HPRT1	TCAGTCAACGGGGGACATA	GGGGCTGTACTGTTAACCAG
IFN-γ	ATGAACGCTACACACTGCAT	CCATCCTTTTGCCAGTTCCTC
TNF-α	CAGGCGGTGCCTATGTCTC	CGATCACCCCGAAGTTCAGT
IL-1β	GAAATGCCACCTTTTGACAG	CTGGATGCTCTCATCAGGAC
IL-6	CTGCAAGAGACTTCCATCCA	AGTGGTATAGACAGGTCTGT
IL-12A (p35)	CATCGATGAGCTGATGCAG	CAGATAGCCCATCACCCTGT
CCL5	GCTGCTTTGCCTACCTCTC	TCGAGTGACAAACACGACTG
TGF-β	AGCTGGTGAAACGGAAGCG	GCGAGCCTTAGTTTGGACAG
IL-10	GCTCTTACTGACTGACTGG	CGCAGCTCTAGGAGCATGTG
atg5	TGTGCTTCGAGATGTGTGG	GTCAAATAGCTGACTCTTGG
atg7	GTTCGCCCCCTTTAATAGTG	TGAACTCCAACGTCAAGCGG
SDHA	TGTTCAGTTCCACCCCACA	TCTCCACGACACCCTTCTGT
mt-CO4	ATTGGCAAGAGAGCCATTTC	CACGCCGATCAGCGTAAGT
PGC-1α	CAATGAATGCAGCGGTCTTA	GTGTGAGGAGGGTCATCGTT

2.9 Fluorometric Calpain Activity Assay

Calpain activity was measured in the spinal cord at DPI 16 using a fluorometric calpain cleavage assay (K240-100; BioVision Inc., CA, USA) according to the manufacturer's protocol. Each well of a 96-well black plate was loaded with protein (50 µg) extracted from the spinal cord and reaction buffer. Active Calpain I (provided in the kit) was used as a positive control and treatment with the calpain inhibitor Z-LLY-FMK (provided in the kit) was used to confirm assay specificity. After incubation at 37˚C for 1 hr in the dark, fluorescence was measured using a Synergy H1 hybrid multi-mode plate reader (BioTek Instruments, Inc., Vermont, USA).

2.10 Adenosine Triphosphate (ATP) Measurements in the Spinal Cord

2.10.1 Sample Preparation for ATP Assay

Spinal cords harvested at DPI 16 were placed in ice-cold 2% trichloroacetic acid (Sigma-Aldrich, St. Louis, MO, USA), homogenized for 1 min and neutralized with 10 mM Tris-acetate in 2 mM EDTA (TAE; pH 7.75). The homogenate was centrifuged at 13,000 rpm for 20 min at 4˚C and then flash frozen in liquid nitrogen to be stored at -80˚C until analysis. The pellet obtained after centrifugation was washed twice in ice cold acetone and dried overnight at 37˚C in an oven. The dried pellet was reconstituted with 3 M Urea (Sigma-Aldrich, St. Louis, MO, USA) and protein estimation was carried out by Bradford assay using 3 M urea as the blank. The ATP concentration was measured using the Invitrogen™ Molecular Probes™ ATP Determination Kit (Molecular Probes Inc., Eugene, OR, USA). A 100 µL aliquot of supernatant was adjusted to 7.75 using

Tris base (pH=10; Sigma-Aldrich, St. Louis, MO, USA) immediately before ATP determination.

2.10.2 ATP Determinations

10 µL of either the neutralized acid soluble supernatant or the diluted ATP standards were added to 96-well white microplates. The reaction was started by adding 90 µL of standard reaction solution to each well and immediately reading the luminescence using the FLUOstar Omega plate reader (BMG Labtech, Ortenberg, Germany). Standard curves produced by measuring luminescence vs. ATP concentrations had an $R^2 > 0.9890$. The amount of ATP in the experimental samples was calculated from the standard curve. The ATP content of the spinal cord samples was expressed as pmol ATP per mg protein.

2.11 Power Calculations

Power calculations were performed to determine the group sizes required to detect statistical differences at an alpha level of 0.05. A group size of 10 mice with a standard deviation (SD) of 45% was needed to detect a 50% difference between the means for measurements of CS, number of days a CS was ≥1.5, myelin loss and axonal injury with 100% accuracy. Four mice per group with a SD of 25% detects a 65% difference between means for each of the EM measurements. A group size of six mice with a SD of 30% was required to detect a 50% difference between the means for measurements of calpain activity, ATP concentrations, and mitochondrial mRNA levels. Five animals per group with a SD of 25% was required to detect a 40% difference between the means for the cytometry measurements and counts for eYFP, LC3b and eYFP/LC3b positive

cells in the spinal cord. A group size of eight mice with an SD of 35% was needed to detect a 50% difference between the means for measurements of cytokines and atg mRNA levels.

2.12 Statistical Analyses

EAE CS curves were analysed using area under the curve followed by a student's t-test for EAE/Thy1 and EAE/Thy1-MCU Def mice (Fleming et al., 2005). A Kruskal-Wallace Test followed by Dunn post-hoc testing was performed to assess potential differences between myelin loss, calpain activation, ATP concentrations, atg mRNA levels, LC3b co-localization in Thy1-expression neurons, T lymphocyte and myeloid cell populations and cytokine mRNA levels. The Mann-Whitney U test was used to compare differences in the number of days a CS was ≥1.5 and optical densities for eYFP labelling in the corticospinal axons of EAE/Thy1 and EAE/Thy1-MCU Def mice at DPI 30. The Mann-Whitney U test was also used to compare EM measurements of mitochondrial morphologies, autophagy, axonal damage, demyelination and remyelination in these mice at DPI 16. All statistical tests were performed using GraphPad Prism (Version 8.00; GraphPad Software, San Diego, CA, USA) with an alpha level set to 0.05. All bar graphs represent the mean ± standard error of the mean (SEM).

Chapter 3- Results

3.1 Assessment of the Effects of Conditional Ablation of the MCU in Thy1-Expressing Neurons on EAE Disease Severity and Spinal Cord Pathology

To assess the effects of MCU deletion in Thy1-expressing neurons on EAE disease severity, Thy1 and Thy1-MCU Def mice between 8-12 weeks of age were subjected to MOG_{35-55}-induced EAE. For the first experiment, starting at DPI 7, mice were weighed and assigned a clinical score (CS) daily based on their disease severity. Mice were humanely euthanized at DPI 30 and their spinal cords were dissected to assess the percentage of WML and degree of axonal damage. Subsequent experiments mirrored the first but included CFA/Thy1 and CFA/Thy1-MCU Def controls and were terminated at DPI 16 so that spinal cords could be assessed for WML, axonal damage, calpain activation and ATP content at peak EAE disease severity. After confirming successful MCU deletion in the spinal cord, results showed that EAE/Thy1-MCU Def mice undergo a more severe disease course than EAE/Thy1 controls, characterized by enhanced remyelination failure, axonal damage, calpain activation and suppression of ATP production.

3.1.1 MCU Protein Levels are Reduced in the Spinal Cords but not the Splenocytes of Thy1-MCU Def Relative to Thy1 Mice

After treatment with TMX, western blots were performed to validate that MCU knockdown was successful in the spinal cords of Thy1-MCU Def but not Thy1

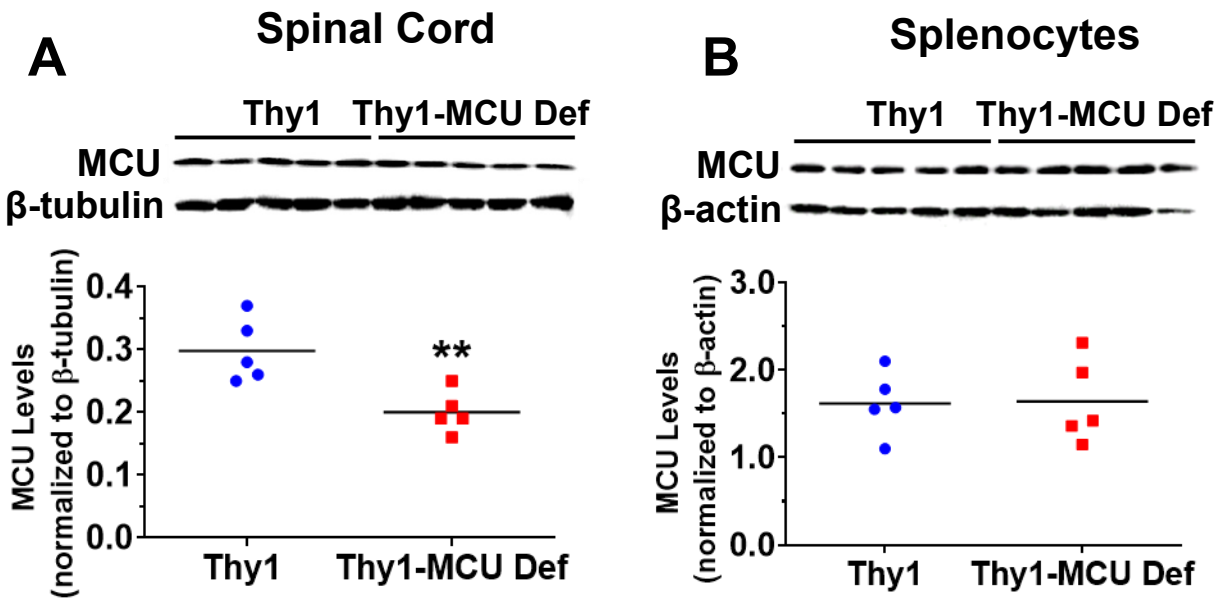

Figure 1. Western blotting and quantification of protein extracts isolated from the spinal cords and splenocytes of adult female Thy1 and Thy1-MCU Def mice. (A) MCU levels in relation to β-tubulin were significantly reduced in the spinal cords of EAE/Thy1-MCU Def when compared to EAE/Thy1 mice (**p<0.01). (B) MCU levels in relation to β-actin showed no significant difference in splenocytes between EAE/Thy1 and EAE/Thy1-MCU Def mice. Bars represent the mean. Potential group differences were analyzed by Mann-Whitney U test (n=5/group). Adapted from (Holman et al., 2020).

mice. Thy1-MCU Def mice showed a 30% reduction in MCU protein levels in relation to β-Tubulin levels when compared to Thy1 mice (Fig. 1A). Next, due to Thy1 promoter expression being diffuse within T cells (Haeryfar and Hoskin, 2004; Vidal et al., 1990), MCU levels were also measured within immune cells to ensure that MCU deletion would not alter the autoimmune response characteristic of the EAE model. Western blotting revealed that MCU protein levels relative to β-actin were not altered in the splenocytes of Thy1-MCU Def compared to Thy1 mice indicating that there should be no MCU related changes in immune cell function (Fig. 1B).

3.1.2 Clinical Scores are Markedly Elevated in EAE/Thy1-MCU Def Mice Relative to EAE/Thy1 Controls

Using a semi-quantitative system of clinical scoring to assess for degree of motor deficit, it was found that, relative to the CS for EAE/Thy1 controls, disease severity was significantly higher in EAE/Thy1-MCU Def mice from DPI 12-30 (Fig. 2A). Disease course was accelerated as onset occurred 2 days earlier (DPI 12 rather than 14; red arrow and blue arrow) and peaked 3 days earlier (DPI 17 rather than 20) in EAE/Thy1 -MCU Def compared to EAE/Thy1 mice (Fig. 2A). EAE/Thy1-MCU Def mice spent on average 17 days at a CS of 1.5 or higher whereas EAE/Thy1 controls spent on average 7 days at 1.5 or higher indicating that EAE/Thy1 MCU Def mice underwent a more severe disease course than EAE/Thy1 controls (Fig. 2B).

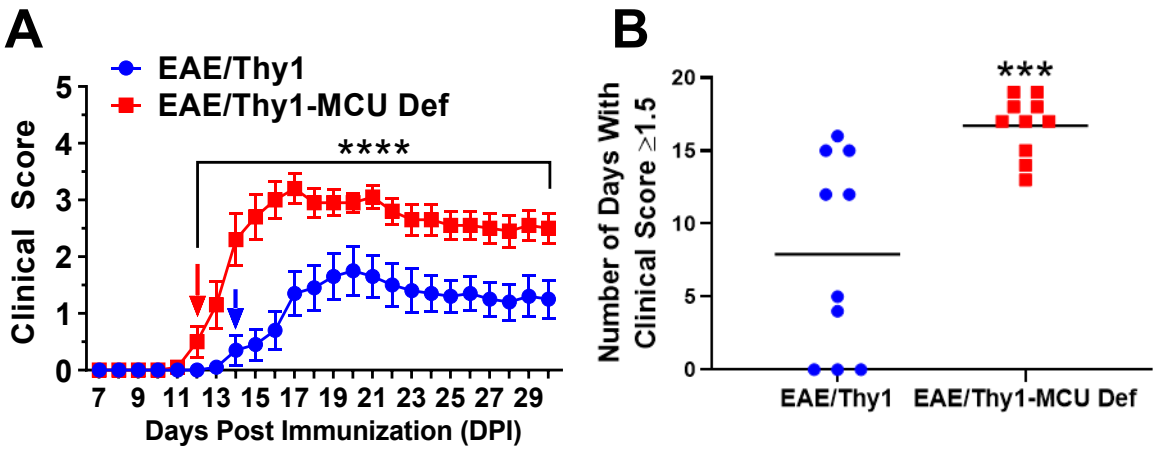

Figure 2. CS in adult female C57Bl/6 Thy1 and Thy1-MCU Def mice subjected to EAE. (A) Disease onset and peak disease occurred earlier in EAE/Thy1-MCU Def mice (DPI 12 and 17, respectively) than EAE/Thy1 controls (DPI 14 and 20, respectively). CS were consistently higher in EAE/Thy1-MCU Def mice than EAE/Thy1 controls beginning at DPI 12 and persisting until DPI 30 (****p<0.0001). (B) EAE/Thy1-MCU Def mice spent a greater number of days at a CS greater than or equal to 1.5 than EAE/Thy1 counterparts (***p<0.001). Bars represent the mean ± SEM. Data were analyzed by area under the curve followed by a student's t-test (A) and a Mann-Whitney U test (B; n=10/group). Adapted from (Holman et al., 2020).

3.1.3 Remyelination is Blocked in EAE/Thy1-MCU Def Mice When Compared to EAE/Thy1 Controls

ECR was used to stain myelin blue and was counterstained with NR to reveal lesion area within white matter (yellow arrows; Fig. 3A). This was then used to analyze differences in WML between EAE/Thy1 and EAE/Thy1-MCU Def mice. Staining revealed that there was not a significant difference in degree of demyelination between Thy1 and Thy1-MCU Def mice at DPI 16 (Fig. 3B) indicating that differences in motor deficit observed at peak disease in Fig 2A were caused by something other than spinal cord demyelination. However, there were significant differences in degree of WML between EAE/Thy1 and EAE/Thy1-MCU Def mice at DPI 30 (Fig. 3B). EAE/Thy1 mice showed a degree of remyelination by DPI 30 from DPI 16 that was not shared by EAE/Thy1-MCU Def mice indicating that the differences between the two groups at DPI 30 were likely due to a suppression of remyelination in EAE/Thy1-MCU Def mice.

3.1.4 Axonal Injury is Enhanced in EAE/Thy1-MCU Def Mice Compared to EAE/Thy1 Controls

Both Thy1 and Thy1-MCU Def mice express a transgene encoding eYFP within Thy1-expressing neurons of the corticospinal tract. In CFA/Thy1 mice that did not develop EAE, faint eYFP labelling is visible in individual axons of Thy1 neurons (arrows; Fig. 4A). Axonal transection in EAE/Thy1 mice results in aggregation of eYFP at transected ends leading to visible punctate labelling (arrowheads; Fig. 4B). This feature of axonal injury was substantially increased in EAE/Thy1-MCU Def mice (arrowheads; Fig. 4C). Punctate eYFP labelling was markedly elevated in the spinal cords of EAE/Thy1-MCU Def mice at both DPI 16 and 30 (Fig. 4D).

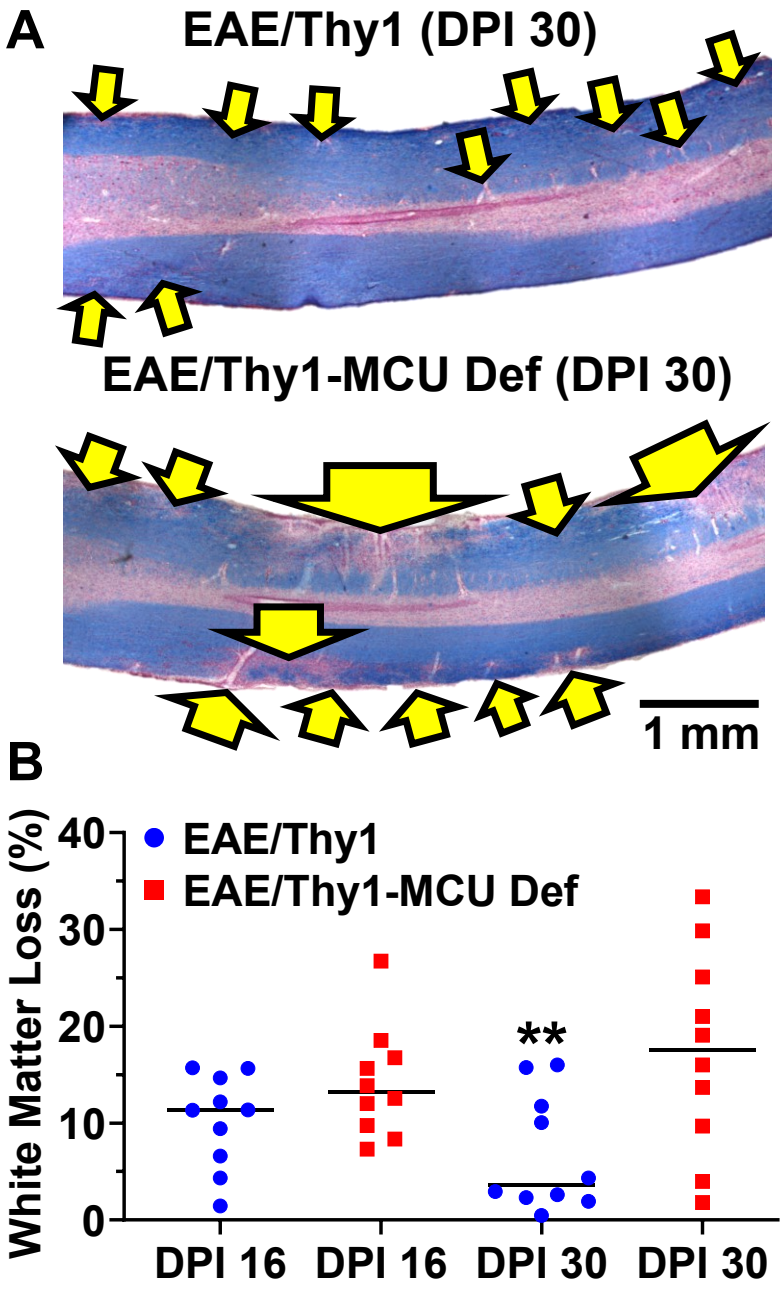

Figure 3. ECR (white matter stained blue) and NR (exposed cell bodies and axons stained red) staining showing myelin loss in EAE/Thy1 and EAE/Thy1-MCU Def mice. (A) Representative longitudinal spinal cord sections of EAE/Thy1 and EAE/Thy1-MCU Def mice at DPI 30. Demyelination is indicated by the occurrence of NR staining in a region of ECR staining (yellow arrows). (B) No differences in WML were seen between EAE/Thy1 and EAE/Thy1-MCU Def mice at peak disease (DPI 16) but EAE/Thy1 mice underwent significant remyelination by DPI 30 while EAE/Thy1-MCU Def mice failed to remyelinate (**$p<0.01$). Bars represent the mean. Data were analyzed by a Kruskal-Wallace ANOVA followed by Dunn post-hoc testing. Adapted from (Holman et al., 2020).

Additionally, axonal damage in EAE/Thy1-MCU Def mice increased from DPI 16 to DPI 30 whereas damage within EAE/Thy1 mice did not significantly change between these time points (Fig. 4D).

3.1.5 Spinal Cord Injury is Accompanied by Increased Calpain Activity and Suppressed ATP Concentrations in EAE/Thy1-MCU Def Compared to EAE/Thy1 Mice

Calpain is a Ca^{2+}-dependent protease that when activated, cleaves αII-spectrin (green arrow; 285 kDa) leaving a 150 kDa fragment (yellow arrow; Fig. 5A). Increased protein levels of αII-spectrin relative to the amount of intact protein is therefore an indicator of increased calpain activation. Western blots of spinal cords taken from CFA/Thy1, EAE/Thy1, CFA/Thy1-MCU Def and EAE/Thy1-MCU Def mice at DPI 16 revealed that both EAE groups had a significant increase in cleavage of αII-spectrin when compared to CFA controls. Simultaneously, there was a 4.0-fold elevation of calpain-cleaved αII spectrin levels in EAE/Thy1-MCU Def over EAE/Thy1 mice (Fig. 5B). EAE/Thy1-MCU Def mice also showed higher levels of calpain activation by relative florescent unit readings than EAE/Thy1 controls (Fig. 5C). ATP levels were also measured at peak disease to assess degree of mitochondrial activity. In keeping with the metabolic collapse that is present at peak EAE disease severity (Kurnellas et al., 2005; Sadeghian et al., 2016). ATP concentrations were 90% lower in EAE/Thy1 than CFA/Thy1 mice (Fig. 5D). Additionally, spinal cord ATP levels declined in EAE/Thy1-MCU Def mice to 15% of those detected in EAE/Thy1 mice (Fig. 5D).

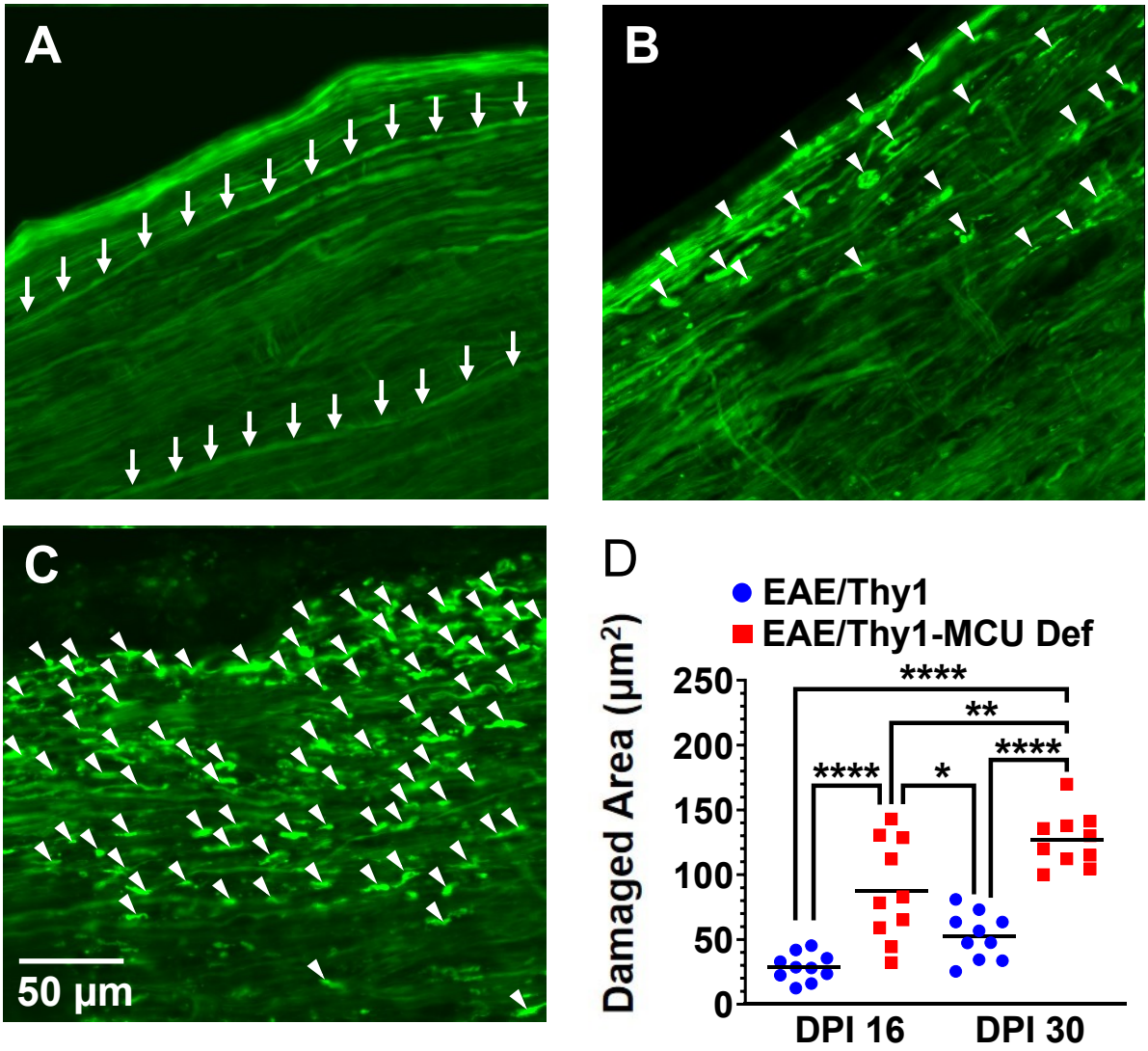

Figure 4. Quantification of axonal damage within the corticospinal tract of EAE/Thy1 and EAE/Thy1-MCU Def mice at DPI 16 and 30. (A) eYFP labelling within Thy1 neurons allows for precise imaging of intact axons (white arrows) within the corticospinal tract of spinal cords in SLICK-H mice. CFA mice do not exhibit punctate labelling indicative of damaged axons. (B) EAE/Thy1 and (C) EAE/Thy1-MCU Def mice show punctate eYFP labelling (white arrowheads) which is indicative of damage, unlike CFA controls. (D) Axon damage was assessed by quantifying the area occupied by punctate eYFP labelling and it was found that EAE/Thy1-MCU Def mice have significantly higher axonal damage when compared to EAE/Thy1 mice at both DPI 16 and 30 (****$p<0.0001$). Additionally, spinal axon damage increased from DPI 16 to 30 in EAE/Thy1-MCU def mice (**$p<0.01$) but not EAE/Thy1 mice. Bars represent the mean. Data were analyzed by a Kruskal-Wallace ANOVA followed by Dunn post-hoc testing. Adapted from (Holman et al., 2020).

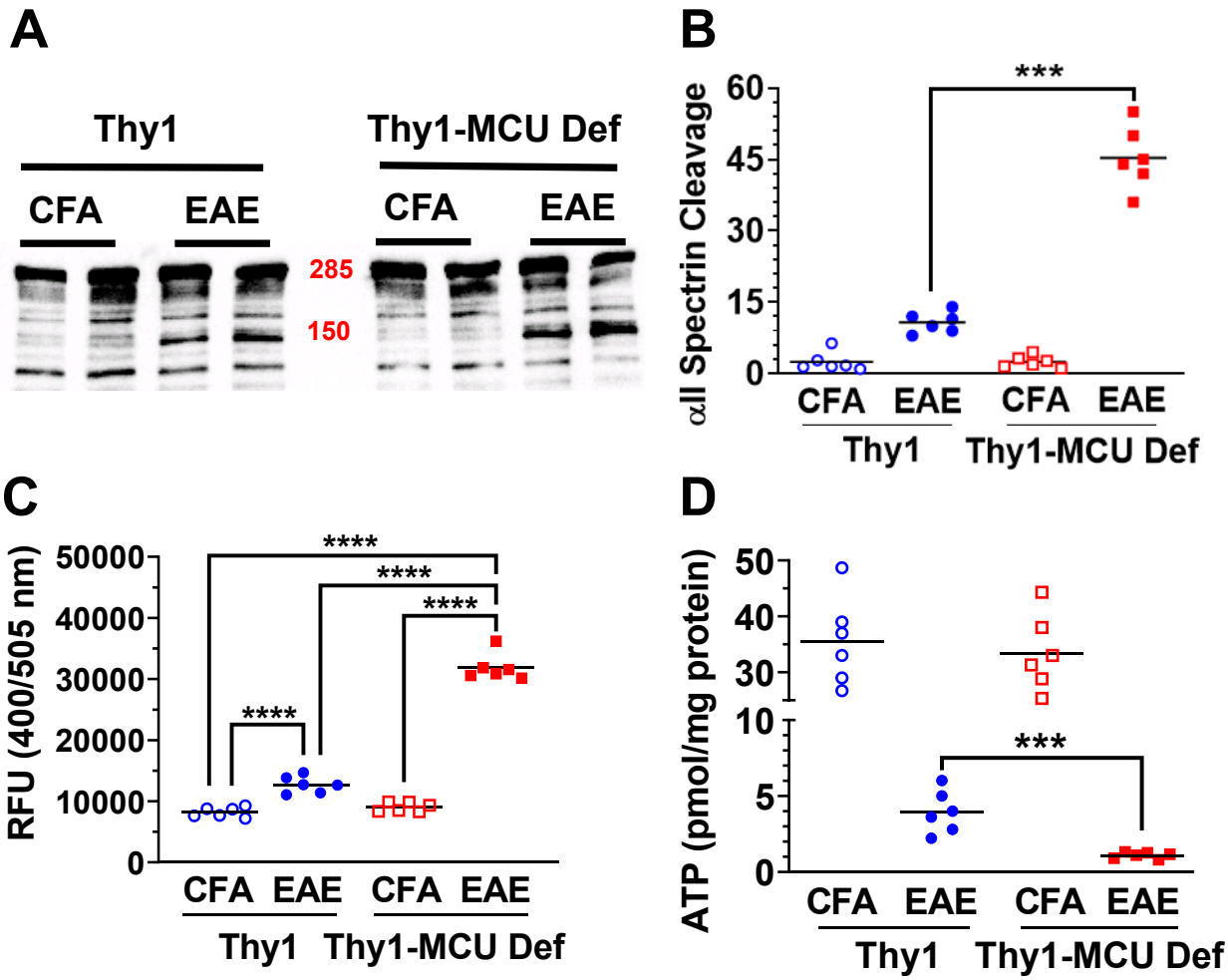

Figure 5. Calpain activation and ATP levels within the spinal cords of CFA/Thy1, EAE/Thy1, CFA/Thy1-MCU Def and EAE/Thy1-MCU Def mice at DPI 16. (A) Representative western blots probed for intact αII-spectrin (285 kDa) and cleaved αII-spectrin (150 kDa). (B) Calpain activation was quantified as a ratio of cleaved to intact αII-spectrin. αII-spectrin cleavage was significantly higher in EAE/Thy1-MCU Def relative to EAE/Thy1 mice (***p<0.001) while there were no differences in CFA/Thy1 or CFA/Thy1-MCU Def mice. (C) Calpain activation was also tested by fluorometric calpain activity assay. Relative florescent units (RFUs) were significantly increased in the spinal cords of EAE/Thy1-MCU Def mice when compared to EAE/Thy1 controls indicating a higher activity of calpain (****p<0.0001). (D) ATP concentrations were significantly lower in the spinal cords of EAE/Thy1 and EAE/Thy1-MCU Def mice when compared to CFA/Thy1 and CFA/Thy1-MCU Def mice (****p<0.0001). ATP levels in EAE/Thy1-MCU Def mice were at 15% of those detected in EAE/Thy1 controls (***p<0.001). Bars represent the mean. Data were analyzed by Kruskal-Wallis ANOVA followed by Dunn's tests. Adapted from (Holman et al., 2020).

3.2 Assessment of Mitochondrial and Autophagic Changes in EAE/Thy1-MCU Def Mice

After having established a higher disease severity, suppression of remyelination, axonal damage, calpain activation, and failure of ATP production in EAE/Thy1-MCU Def mice than EAE/Thy1 controls, EM imaging was performed to better understand the pathological differences within axons of these mice. The L5 portion of corticospinal tracts in mice humanely euthanized at DPI 16 at equivalent CS were imaged to understand the effects of Thy1-MCU Def on mitochondrial morphology, autophagy, cytoskeletal density and myelination within healthy and damaged axons. Based on the morphological observations made from EM imaging, spinal cord samples at DPI 16 were then also probed for autophagosome marker LC3b to understand how autophagy is localized in the spinal cords of these mice. Finally, qRT-PCR was performed to detect expression of autophagy-related (atg) genes as a measure of autophagic flux as well as mitochondrial complex genes as a measure of mitochondrial dysfunction.

3.2.1 EAE/Thy1-MCU Def Mice Show Morphological Features of Mitochondrial Dysfunction and Excessive Autophagy in Myelinated L5 Spinal Cord Axons

To examine the effects of Thy1-MCU Def on mitochondrial function in EAE, EM was used to visualize these organelles in myelinated L5 spinal cord axons of EAE/Thy1 and EAE/Thy1-MCU Def mice at the onset of peak disease (DPI 16). Images were compared from both groups in mice at equivalent CS to assess for pathological differences. Representative images are arranged to show images of

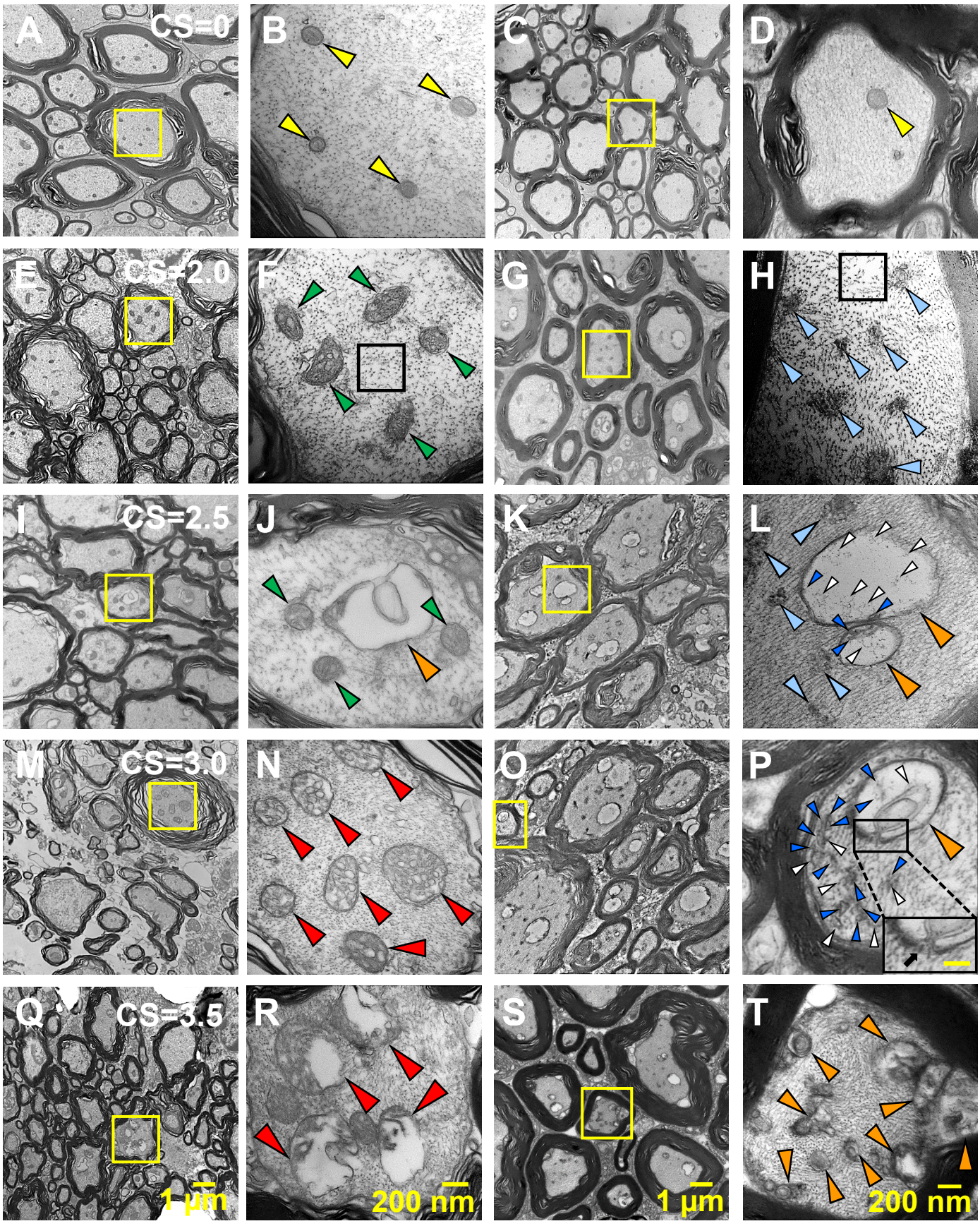
EAE/Thy1
EAE/Thy1-MCU Def
A
CS=0
B
C
D
E
CS=2.0
F
G
H
I
CS=2.5
J
K
L
M
CS=3.0
N
O
P
Q
CS=3.5
R
S
T
1 µm
200 nm
1 µm
200 nm

Figure 6. Representative spinal cord (L5) EM images of EAE/Thy1 and EAE/Thy1-MCU Def mice with increasing CS (CS=0, A-D; CS=2.0, E-H; CS=2.5, I-L; CS=3.0, M-P; CS=3.5, Q-T) at DPI 16. Boxes: yellow (A, C, E, G, I, K, M, O, Q and S) indicate regions shown in the adjacent images (B, D, F, H, J, L, N, P, R and T) and black (panels F and H) show areas quantified for cytoskeletal optical density. Arrowheads: yellow (B and D), green (F and J), light blue (H and L) and large red (N and R) - normal, activated, fragmented and swollen mitochondria, respectively; large orange (J, L and P) - autophagosome; small blue (L and P) - mitochondrial fragments; small white (L and P) -cytoskeletal fragments; small orange (T) - condensed (late) autophagosomes. Small black rectangle (P) shows an active autophagosome. Black rectangle (P) show an enlarged view of an autophagosome (yellow bar = 350 nm). The black arrow indicates cytoskeletal fragments entering the mouth of an autophagosome. Adapted from (Holman et al., 2020).

myelinated axons (A, C, E, G, I, K, M, O, Q and S) containing yellow boxes to indicate magnified regions shown in the adjacent images (B, D, F, H, J, L, N, P, R and T). In Thy1 and Thy1-MCU Def mice immunized with CFA (CS= 0), axons contained small mitochondria (yellow arrowheads; diameter ~150 nm; Fig. 6A-D) that were not activated and were evenly distributed. Distinct differences in mitochondrial morphologies and cytoskeletal integrity were first seen in the myelinated axons of Thy1 and Thy1-MCU Def mice with moderate EAE (walking deficits; CS=2.0; Fig. 6E-H). In EAE/Thy1 controls, the axonal cytoskeleton appeared normal while mitochondria were larger, elongated and displayed dense cristae (green arrowheads; Fig. 6E and F). These changes were very rarely observed in EAE/Thy1-MCU Def mice whose axons contained far fewer activated mitochondria (Fig. 7A). Instead, EAE/Thy1-MCU Def axons contained numerous condensed and fragmented mitochondria (light blue arrowheads) associated with disorganized and damaged microtubules (Fig. 6G and H; Fig. 7B). Optical density measurements taken from areas indicated by the black boxes in Fig. 6F and H confirmed cytoskeletal loss in EAE/Thy1-MCU relative to EAE/Thy1 mice at CS=2.0 (Fig. 7C). At CS=2.5, while EAE/Thy1 mice continued to exhibit elongated and activated mitochondria (Fig. 6I and J), further mitochondrial fragmentation was apparent in EAE/Thy1-MCU Def axons and was accompanied by the presence of large autophagosomes (large orange arrowheads) containing mitochondrial (small blue arrowheads) and cytoskeletal debris (small white arrowheads; Fig. 6K and L). By comparison, mitochondria were still activated and autophagosomes were far less common and did not appear to contain

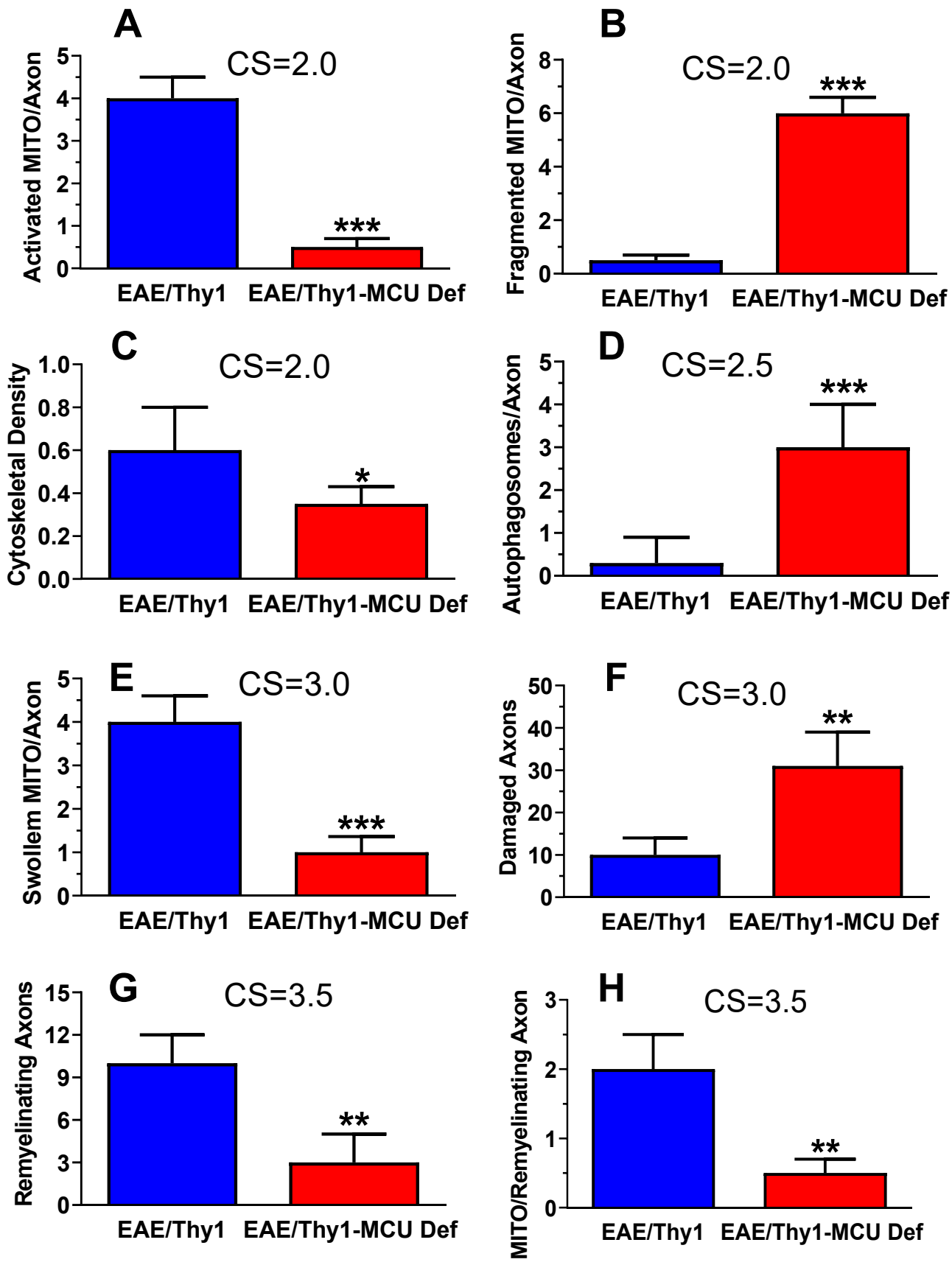
A
CS=2.0
Activated MITO/Axon
0
1
2
3
4
5
***
EAE/Thy1
EAE/Thy1-MCU Def
B
CS=2.0
Fragmented MITO/Axon
0
2
4
6
8
***
EAE/Thy1
EAE/Thy1-MCU Def
C
CS=2.0
Cytoskeletal Density
0.0
0.2
0.4
0.6
0.8
1.0
*
EAE/Thy1
EAE/Thy1-MCU Def
D
CS=2.5
Autophagosomes/Axon
0
1
2
3
4
5
***
EAE/Thy1
EAE/Thy1-MCU Def
E
CS=3.0
Swollem MITO/Axon
0
1
2
3
4
5
***
EAE/Thy1
EAE/Thy1-MCU Def
F
CS=3.0
Damaged Axons
0
10
20
30
40
50
**
EAE/Thy1
EAE/Thy1-MCU Def
G
CS=3.5
Remyelinating Axons
0
3
6
9
12
15
**
EAE/Thy1
EAE/Thy1-MCU Def
H
CS=3.5
MITO/Remyelinating Axon
0
1
2
3
**
EAE/Thy1
EAE/Thy1-MCU Def

Figure 7. Quantification of EAE/Thy1 and EAE/Thy1-MCU Def mice EM spinal cord images at each level of CS. At a CS=2.0 EAE/Thy1-MCU Def mice showed (A) fewer activated mitochondria/axon (MITO; ***p<0.001), (B) significantly higher numbers of condensed and fragmented MITO/axon (***p<0.001) and (C) decreased cytoskeletal density (*p<0.05) compared to EAE/Thy1 mice. (D) At a CS=2.5 numbers of autophagosomes/axon were significantly higher in EAE/Thy1-MCU Def mice (***p<0.001). At a CS=3.0 (E) numbers of swollen MITO/axon were lowered and (F) number of damaged axons within a given area were elevated in EAE/Thy1-MCU Def mice (***p<0.001, **p<0.01). Finally, at a CS=3.5 (G) number of remyelinating axons in an area and (H) number of MITO/remyelinating axon were significantly higher in EAE/Thy1 when compared to EAE/Thy1-MCU Def mice (**p<0.01, **p<0.01). Bars represent the mean ± SEM (n=4/group). Data were analyzed by Mann-Whitney U Tests. Adapted from (Holman et al., 2020).

cytoskeletal debris in EAE/Thy1 axons (Fig. 6I and J; Fig 7D). With EAE progression to CS=3.0, numerous swollen mitochondria with damaged cristae were detected in EAE/Thy1 but not EAE/Thy1-MCU Def axons (red arrowheads; Fig. 6M and N; Fig. 7E). At this clinical stage, autophagosomes were frequently seen digesting mitochondria and cytoskeletal debris in EAE/Thy1-MCU Def but not EAE/Thy1 axons (black arrow in black box; Fig. 6O and P). This stage of disease was also accompanied by enhanced axonal damage in EAE/Thy1-MCU Def mice (Fig. 7F). At CS=3.5, massively swollen mitochondria with disintegrating cristae were observed in EAE/Thy1 axons (Fig. 6Q and R). EAE/Thy1-MCU Def axons had an overwhelming presence of numerous late (condensed) autophagosomes (small orange arrowheads; Fig. 6S and T).

3.2.2 Differences in Mitochondrial Content and Morphologies in the Demyelinated and Remyelinating Axons of EAE/Thy1 and EAE/Thy1-MCU Def Mice

In addition to the analysis of myelinated L5 spinal cord axons (Fig. 6) of EAE/Thy1 and EAE/Thy1-MCU Def mice, EM was also employed to study demyelinated and remyelinating axons within mice with severe EAE (CS=3.5) at DPI 16. Images were compared from both groups of mice to assess for pathological differences. Representative images are arranged to show images of remyelinating or demyelinated axons (A, C, E, G, I, K, M and O) containing yellow boxes to indicate magnified regions shown in the adjacent images (B, D, F, H, J, L, N and P). In addition to causing metabolic collapse in myelinated axons, analysis also suggested that mitochondrial dysfunction and excessive autophagy impaired the remyelination of EAE/Thy1-MCU Def axons. At CS=3.5,

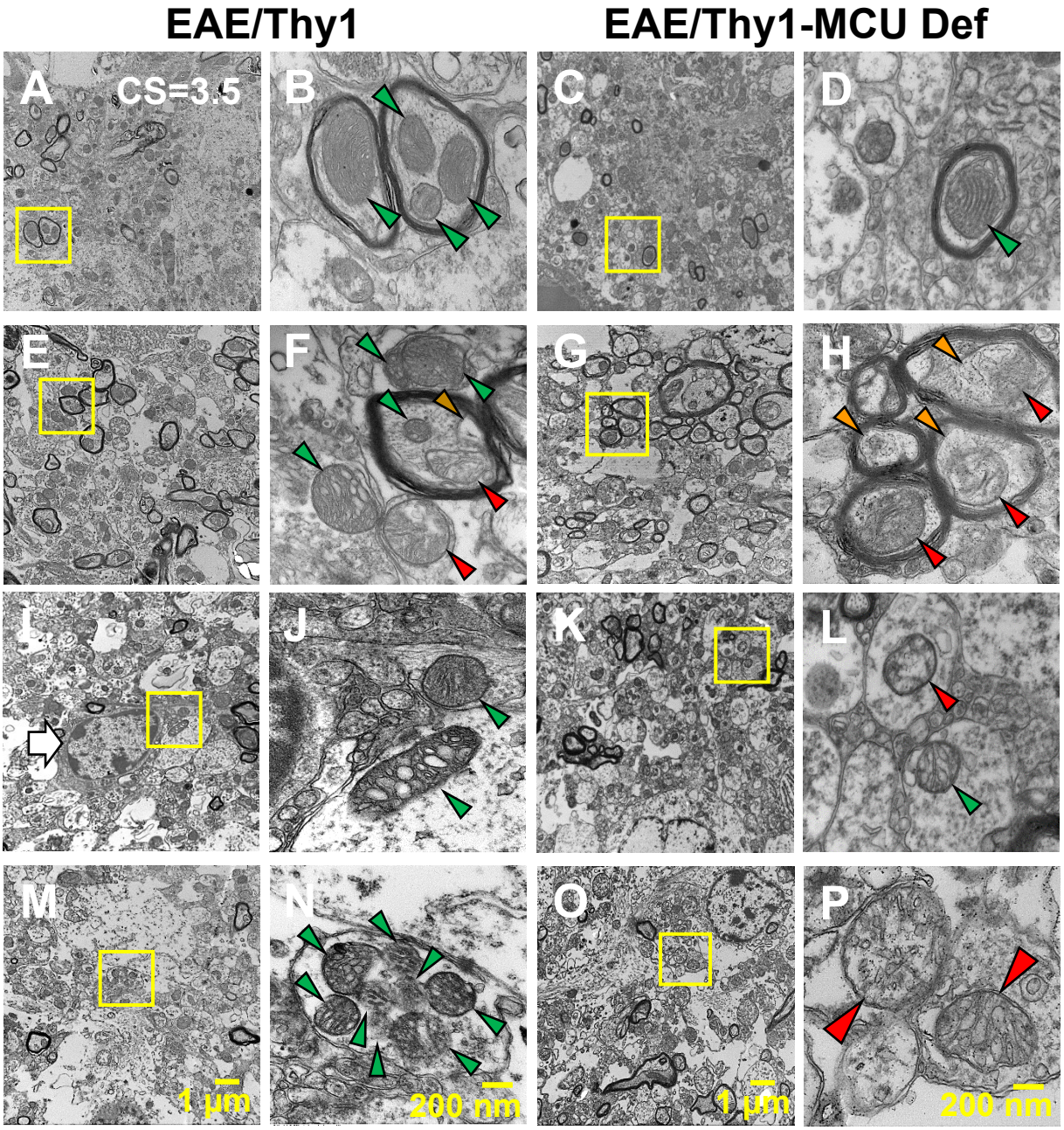

Figure 8. Representative spinal cord (L5) EM images of EAE/Thy1 and EAE/Thy1-MCU Def mice showing remyelinating (A-H) or demyelinated (I-P) axons at comparable CS (CS=3.5). Boxes: yellow (A, C, E, G, I, K, M, and O) indicate regions shown in the adjacent images (B, D, F, H, J, L, N and P). Arrowheads: green (B, D, F, J, L and N) and red (F, H, L and P) - activated and damaged mitochondria, respectively; brown (F) - mitophagosome; large red (P) - massively swollen but intact mitochondria; orange (H) - autophagosome. Adapted from (Holman et al., 2020).

the number of remyelinating axons was 75% lower in EAE/Thy1-MCU Def mice than EAE/Thy1 controls (Fig. 7G; Fig. 8A-D). Furthermore, the number of intact mitochondria was reduced in the remyelinating axons of EAE/Thy1-MCU Def relative to EAE/Thy1 mice (Fig. 7H; green arrows; Fig. 8A-D). Damaged mitochondria were also observed more frequently in the remyelinating axons of EAE/Thy1 and EAE/Thy1-MCU Def mice (red arrowheads; Fig. 8E-H). Unlike remyelinating EAE/Thy1 axons, remyelinating EAE/Thy1-MCU Def axons typically showed signs of autophagic damage (orange arrowheads; Fig. 8E-H). In demyelinated EAE/Thy1 axons, two or more activated mitochondria were usually present (Fig. 8I, J, M and N). By contrast, demyelinated EAE/Thy1-MCU Def axons either lacked mitochondria or contained a single activated or damaged mitochondrion (Fig. 8K and L). In some damaged EAE/Thy1-MCU Def axons, a single massively swollen mitochondrion with intact outer and inner mitochondrial membranes could be seen (Fig. 8O and P).

3.2.3 Mitochondrial Gene Expression is Suppressed in EAE/Thy1-MCU Def Mice

To further examine the effects of Thy1-MCU Def on mitochondrial function in the EAE model, we examined mRNA levels for succinate dehydrogenase subunit A (SDHA), cytochrome oxidase subunit 4 (mt-CO4) and peroxisome proliferator-activated receptor gamma coactivator 1 alpha (PGC-1α) in the spinal cords of CFA/Thy1, EAE/Thy1, CFA/Thy1-MCU Def and EAE/Thy1-MCU Def mice at DPI 16. SDHA, mt-CO4 and PGC-1α mRNA levels were reduced in EAE/Thy1-MCU Def relative to CFA/Thy1, EAE/Thy1 and CFA/Thy1-MCU Def mice (Fig. 9A-C).

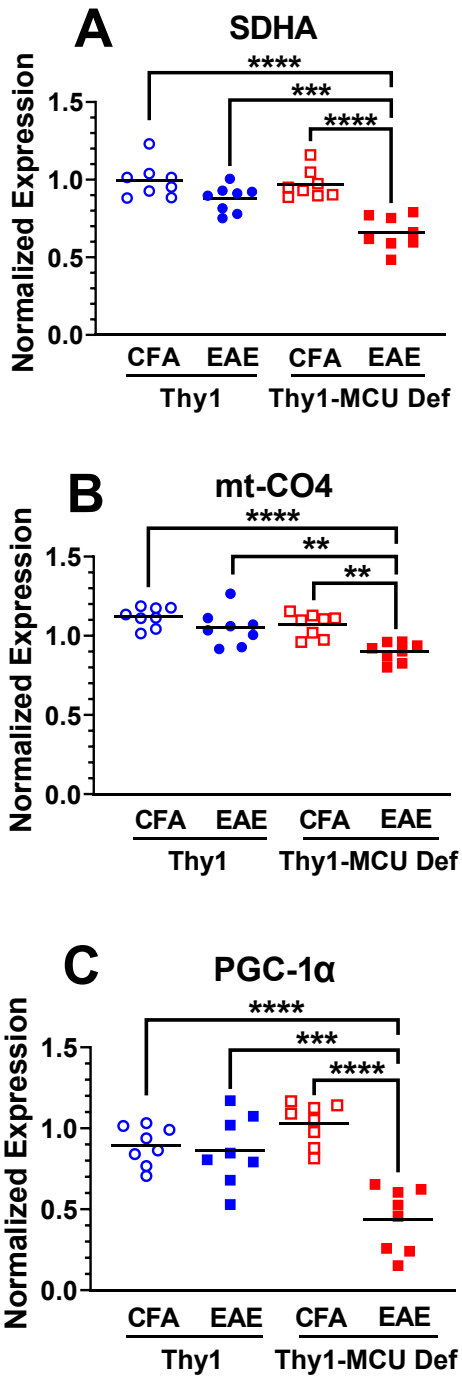

Figure 9. Normalized relative mRNA levels for mitochondrial complex genes in the spinal cords of CFA/Thy1, EAE/Thy1, CFA/Thy1-MCU Def and EAE/Thy1-MCU Def mice at DPI 16. No differences were seen between CFA/Thy1, EAE/Thy1 and CFA/ compared to all other groups (**p<0.01, ***p<0.001 and ****p<0.0001). Bars represent the mean. Data were analyzed using a Kruskal-Wallis ANOVA followed by Dunn's multiple comparisons tests. Adapted from (Holman et al., 2020).

3.2.4 Atg Gene mRNAs are Elevated in EAE/Thy1-MCU Def Mice Relative to EAE/Thy1 Mice

In view of the morphological evidence observed in EM of excessive autophagy in the axons of EAE/Thy1-MCU Def mice, autophagy related gene 5 and 7 (atg5 and atg7) mRNA levels were then compared in the spinal cords of CFA/Thy1, EAE/Thy1, CFA/Thy1-MCU Def and EAE/Thy1-MCU Def mice at DPI 16. While no differences were observed between CFA/Thy1, EAE/Thy1 and CFA/Thy1-MCU Def mice, EAE/Thy1-MCU Def mice showed elevated levels of both atg5 and atg7 mRNA levels when compared to all other groups (Fig. 10A and B).

3.2.5 Spinal Cords of EAE/Thy1-MCU Def Mice Exhibit More LC3 Positive Neurons and a Higher Correspondence of eYFP and LC3 Expression Than EAE/Thy1 Counterparts

Immunolabelling for the autophagosomal marker LC3 was performed in order to see how autophagy is localized within neurons of the spinal cords of EAE/Thy1 and EAE/Thy1-MCU Def mice at DPI 16. Labelling of eYFP positive Thy1 neurons was present and equally expressed in the spinal cords of both groups (Fig. 11A, B and G). Within those same areas, there was a significantly higher number of LC3 positive neurons in EAE/Thy1-MCU Def when compared to EAE/Thy1 mice (Fig. 11C, D and G). Lastly, there was a significantly higher correspondence of LC3 to eYFP positive neurons within EAE/Thy1-MCU Def mice (Fig. 11E, F and G).

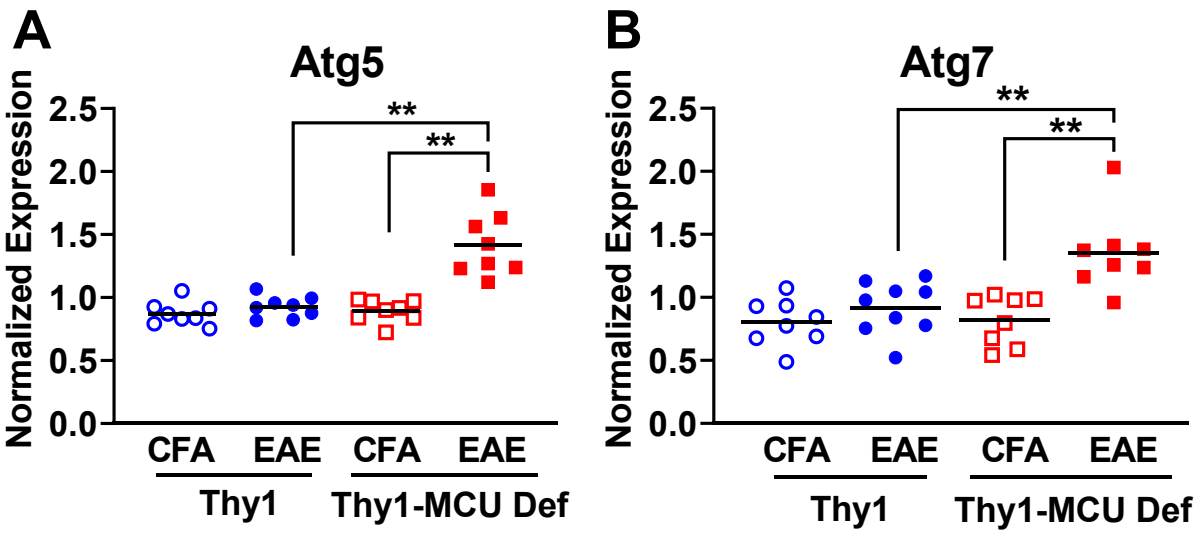

Figure 10. Atg5 and atg7 mRNA levels in total RNA extracts from the spinal cords of CFA/Thy1, EAE/Thy1, CFA/Thy1-MCU Def and EAE/Thy1-MCU Def mice at DPI 16 (A and B). Levels of atg5 and atg7 mRNAs were not significantly different between CFA/Thy1, EAE/Thy1 and CFA/Thy1-MCU Def mice but were upregulated in the spinal cords of EAE/Thy1-MCU Def mice compared to all other groups (**p<0.01). Bars represent the mean. Data were analyzed using a Kruskal-Wallis ANOVA followed by Dunn's tests. Adapted from (Holman et al., 2020).

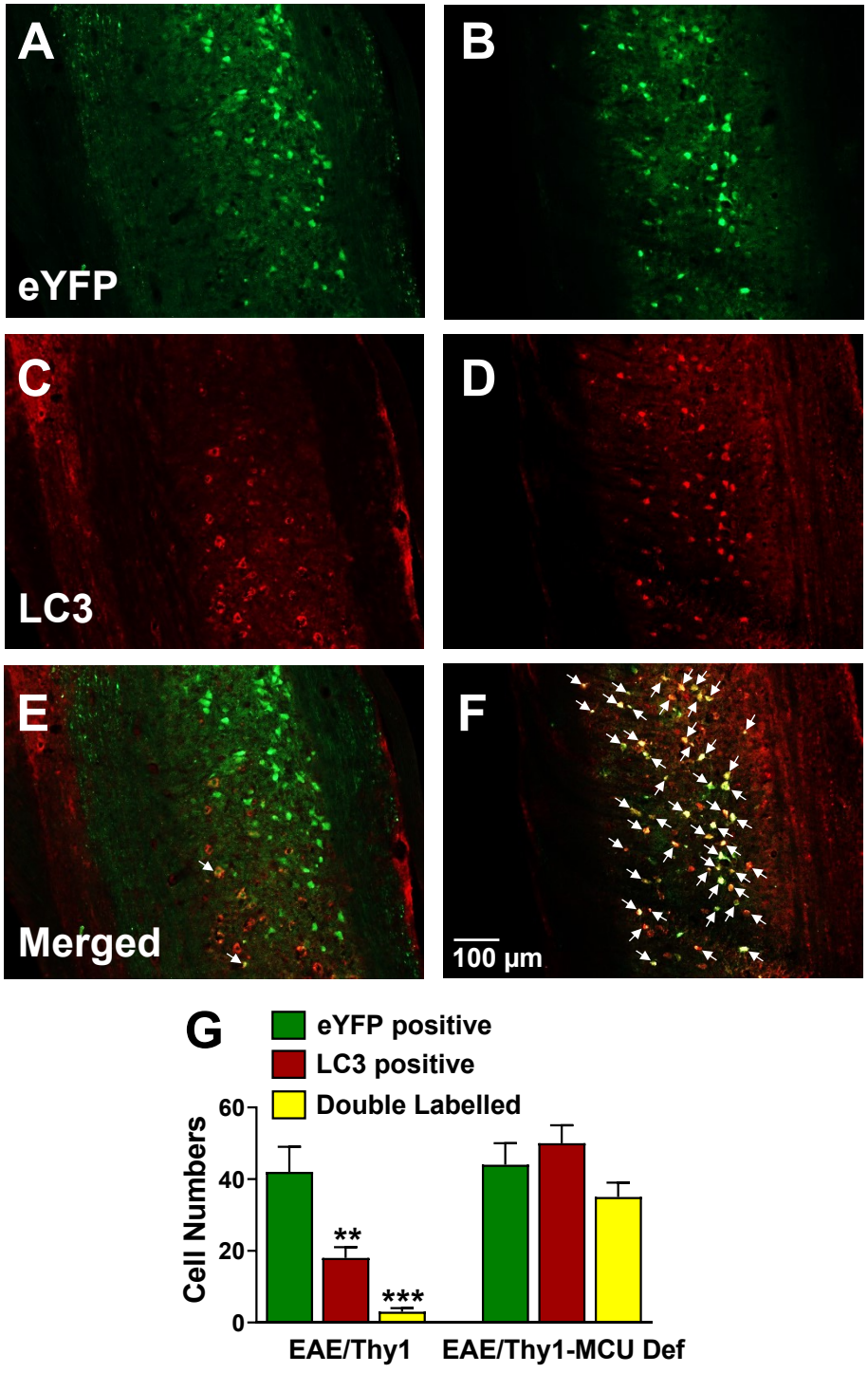

Figure 11. Representative images of eYFP (green; A and B), LC3 (red; C and D) and eYFP/LC3 (arrows; E and F) positive neurons in the spinal cords of EAE/Thy1 (A, C and E) and EAE/Thy1-MCU Def (B, D and F) mice. (G) In areas with equivalent numbers of eYFP positive neurons, EAE/Thy1-MCU Def mice exhibit higher numbers of LC3 positive neurons (**$p<0.01$) and a greater degree of neuron double labelling for LC3 and eYFP (***$p<0.001$) than EAE/Thy1 mice. Bars represent the mean ± SEM (n=5/group). Data were analyzed by Kruskal-Wallis ANOVA followed by Dunn's tests. Adapted from (Holman et al., 2020).

3.3 Differential Immune Cell Activation in EAE/Thy1-MCU Def Mice

With a better understanding of how Thy1-MCU Def lead to exacerbation of EAE, increase in mitochondrial dysfunction and upregulation of autophagic damage, we decided to look at immune cell activation and CNS infiltration in order to establish whether Thy1-MCU Def causes any changes in immune response within the EAE model. Given that Thy1-MCU Def is exclusively neuronal, alteration to immune response would help shed some light onto how mitochondrial dysfunction is capable of affecting autoimmunity in EAE. CFA/Thy1, EAE/Thy1, CFA/Thy1-MCU Def and EAE/Thy1-MCU Def mice were humanely euthanized at DPI 16 and their splenocytes and CNS tissues harvested for determination of T cell and myeloid cell concentrations by FACS analysis. Additionally, qRT-PCR was performed on spinal cord homogenates for probing of inflammatory gene expression to better understand whether Thy1-MCU Def promotes a pro-inflammatory or pro-repair environment within EAE.

3.3.1 Immune Cell Activation and Infiltration is Elevated in EAE/Thy1-MCU Def Mice

Flow cytometry was employed to compare peripheral (by measurement of splenocytes) and CNS (brain and spinal cord) T lymphocyte and myeloid cell populations of CFA/Thy1, EAE/Thy1, CFA/Thy1-MCU Def and EAE/Thy1-MCU Def mice at DPI 16. $CD4^+$ and $CD8^+$ T cell populations were significantly increased in the spleen of EAE/Thy1-MCU Def compared to CFA/Thy1, EAE/Thy1 and CFA/Thy1-MCU Def mice (Fig. 12A). However, peripheral $CD4^+$ and $CD8^+$ T cell populations were not significantly elevated in EAE/Thy1 mice

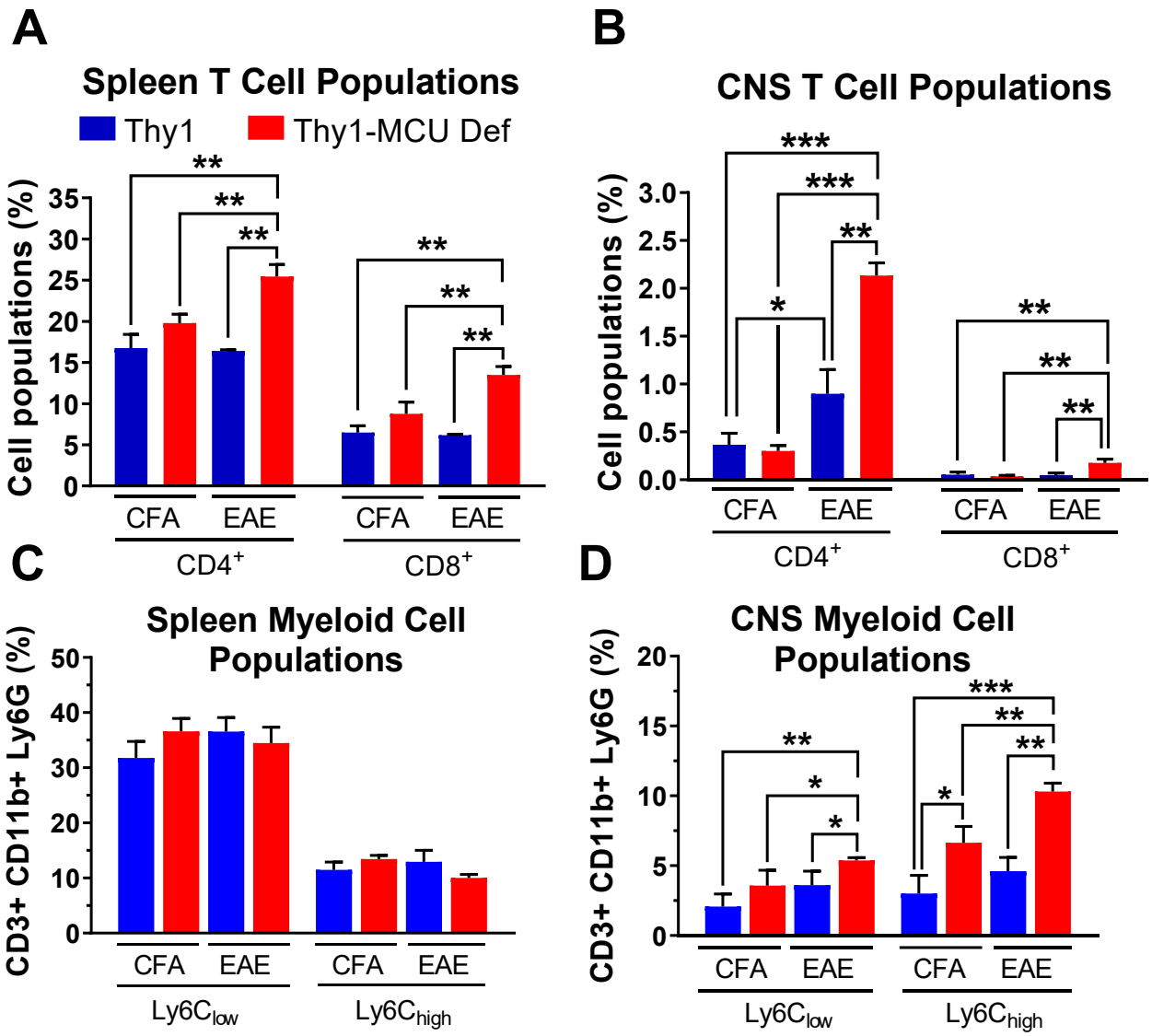

Figure 12. FACS analysis of immune cell populations in the spleens (A and C) and CNS (B and D) of adult female CFA/Thy1, EAE/Thy1, CFA/Thy1-MCU Def and EAE/Thy1-MCU Def mice at DPI 16. (A) Peripheral $CD4^+$ and $CD8^+$ T lymphocyte population concentrations did not show significant difference between CFA/Thy1, EAE/Thy1 and CFA/Thy1-MCU Def mice but EAE/Thy1-MCU Def mice showed a significant increase compared to all other groups (**p<0.01). (B) $CD4^+$ T cell populations were upregulated in the CNS of both EAE/Thy1 (*p<0.05) and EAE/Thy1-MCU Def (***p<0.001) mice when compared to their CFA controls although this increase was higher in EAE/Thy1-MCU Def mice (**p<0.01). $CD8^+$ T cell populations were upregulated in the CNS of EAE/Thy1-MCU Def mice only (**p<0.01). (C) $Ly6C_{low}$ and $Ly6C_{high}$ myeloid cell populations were unaltered in the periphery of all mice. (D) $Ly6C_{low}$ and $Ly6C_{high}$ populations were upregulated in the CNS of EAE/Thy1-MCU Def mice (*p<0.05, **p<0.01) and there was an increased infiltration of $Ly6C_{high}$ cells in the CNS of non-diseased CFA/Thy1-MCU Def mice. Bars show mean ± SEM (n=5/group). Data were analyzed by Kruskal-Wallis ANOVA followed by Dunn's tests. Adapted from (Holman et al., 2020).

when compared to CFA controls (Fig. 12A). $CD4^+$ T cell infiltration in the CNS was elevated in both EAE/Thy1 and EAE/Thy1-MCU Def mice relative to their CFA controls while $CD8^+$ populations were only elevated in the CNS of EAE/Thy1-MCU Def mice (Fig. 12B). By comparison, $CD4^+$ and $CD8^+$ T cells were more prevalent in the CNS of EAE/Thy1-MCU Def compared to EAE/Thy1 mice (Fig. 12B). The percentages of $Ly6C_{low}$ and $Ly6C_{high}$ myeloid cells in the spleen were similar for all four groups (Fig. 12C). Increased CNS immune cell infiltration in EAE/Thy1-MCU Def mice was also characterized by higher $Ly6C_{low}$ and $Ly6C_{high}$ myeloid CNS cell percentages than CFA/Thy1, EAE/Thy1 and CFA/Thy1-MCU Def mice (Fig. 12D). The only other difference observed was an elevated concentration of $Ly6C_{high}$ cells, known to become pro-inflammatory macrophages and dendritic cells, in the CNS of CFA/Thy1-MCU Def relative to CFA/Thy1 mice (Fig. 12D).

3.3.2 Cytokine mRNA Levels Reflect Increased Pro-Inflammatory and Blunted Pro-Repair Responses in the Spinal Cords of EAE/Thy1-MCU Def Mice

Lastly, mRNA levels for pro-inflammatory [interferon-γ (IFN-γ), tumour necrosis factor-α (TNF-α), interleukin-1 (IL-1β), IL-6, IL-12 (p35) and chemokine (C-C motif) ligand 5 (CCL-5)] and pro-repair [transforming growth factor-β (TGF-β) and IL-10] cytokines were compared in the spinal cords of CFA/Thy1, EAE/Thy1, CFA/Thy1-MCU Def and EAE/Thy1-MCU Def mice at DPI 16. Relative to the non-diseased CFA/Thy1 and CFA/Thy1-MCU Def controls, pro-inflammatory (IFN-γ, IL-1β, TNF-α, IL-6, IL-12 (p35) and CCL-5) mRNA levels were elevated in both EAE/Thy1 and EAE/Thy1-MCU Def mice (Fig. 13A-F).

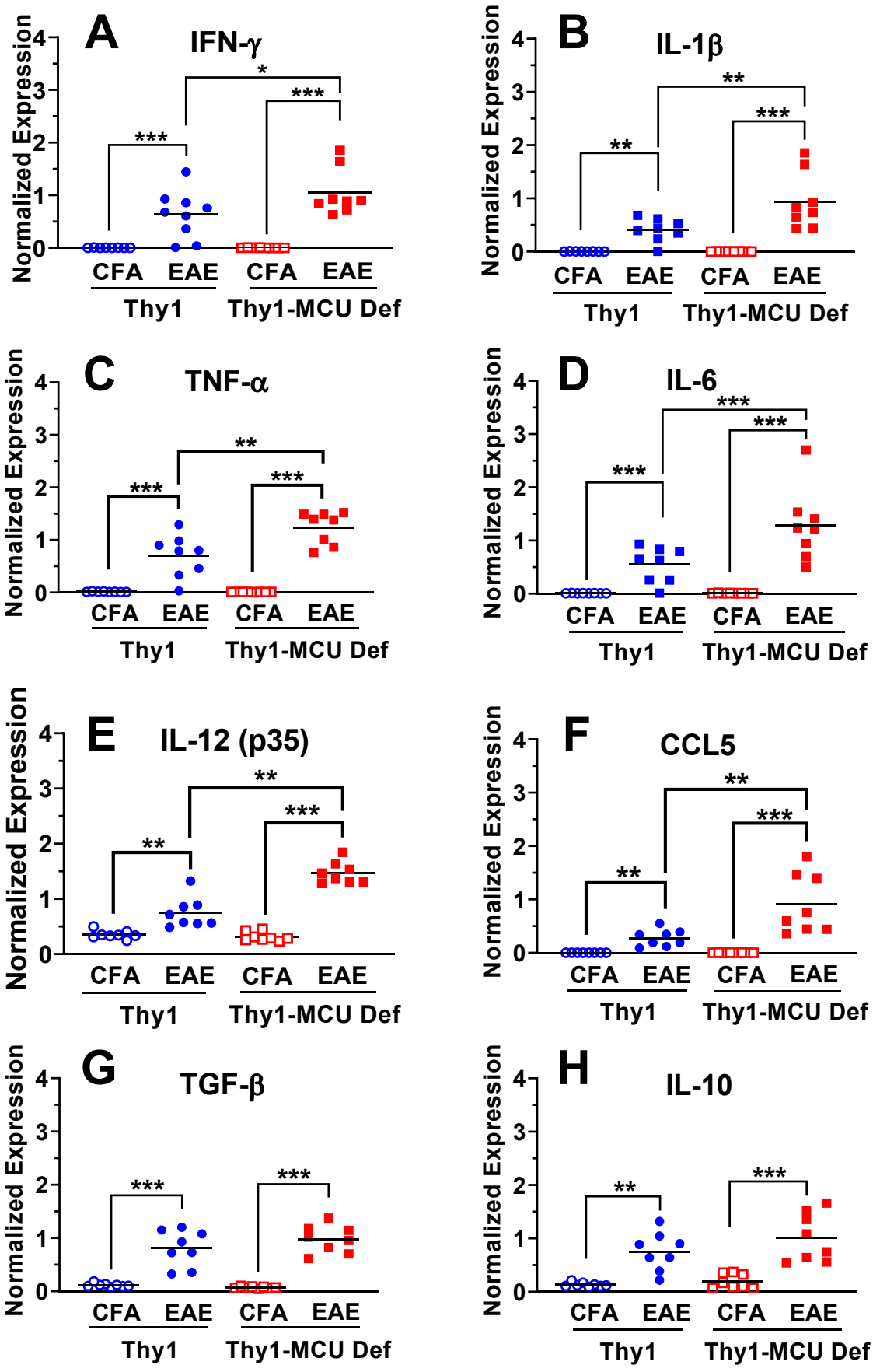
A
IFN-γ
B
IL-1β
C
TNF-α
D
IL-6
E
IL-12 (p35)
F
CCL5
G
TGF-β
H
IL-10
Normalized Expression
CFA
EAE
Thy1
Thy1-MCU Def

Figure 13. qRT-PCR was used to measure cytokine (IFNγ, IL-1β, TNFα, IL-6, IL-12 (p35), TGF-β and IL-10; A-E, G and H) and chemokine (CCL-5; F) mRNA levels in total RNA extracts from the spinal cords of adult female CFA/Thy1, EAE/Thy1, CFA/Thy1-MCU Def and EAE/Thy1-MCU Def mice at DPI 16. (A-F) Pro-inflammatory cytokine (IFN-γ, IL-1β, TNF-α, IL-6, IL-12 (p35) and CCL-5) levels were elevated in both EAE/Thy1 and EAE/Thy1-MCU Def mice when compared to CFA/Thy1 and CFA/Thy1-MCU Def controls. However, EAE/Thy1-MCU Def mice had consistently higher levels of these cytokines compared to the EAE/Thy1 mice. (G and H) Pro-repair cytokine levels were higher in the spinal cords of both EAE/Thy1 and EAE/Thy1-MCU Def mice when compared to their non-diseased CFA/Thy1 and CFA/Thy1-MCU Def counterparts. There was no significant difference in pro-repair cytokine levels between EAE/Thy1 and EAE/Thy1-MCU Def mice (*$p<0.05$, **$p<0.01$ and ***$p<0.001$). Bars represent the mean. Data were analyzed by Kruskal-Wallis ANOVA followed by Dunn's multiple comparisons tests. Adapted from (Holman et al., 2020).

By comparison to EAE/Thy1 mice, mRNA levels for these pro-inflammatory cytokines were all higher in EAE/Thy1-MCU Def mice (Fig. 13A-F). Pro-repair cytokine (TGF-β and IL-10) mRNA levels were increased in EAE/Thy1 and EAE/Thy1-MCU Def relative to their CFA/Thy1 and CFA/Thy1-MCU Def controls at the onset of remyelination (Fig. 13G and H). However, TGF-β and IL-10 mRNA levels were not significantly different in EAE/Thy1 and EAE/Thy1-MCU Def mice. This therefore indicates that despite an increase in pro-inflammatory cytokine mRNA levels, there was not a corresponding increase of pro-repair cytokines in EAE/Thy1-MCU Def mice.

Chapter 4 – Discussion

4.1 Oral Administration of TMX Leads to MCU Deletion in the Spinal Cords but not Immune Cells of Thy1-MCU Def Mice

Western blots showed that MCU protein levels were decreased by 30% in the spinal cord tissues of Thy1-MCU Def mice relative to Thy1 controls 2 weeks after the oral administration of TMX. These results are consistent with previous findings in which Thy1-MCU deletion using the SLICK-H/Cre-LoxP system led to a 50% reduction of MCU levels relative to the forebrain of Thy1 mice (Nichols et al., 2018). Less than 100% reduction in MCU levels is to be expected given that the Thy1 promoter regions used for expression contain the sequences required for neuronal expression but lack the sequences for expression in non-neuronal CNS cell types (https://www.jax.org/strain/012708). Testing for eYFP expression in oligodendrocytes and other glial cells of the SLICK-H breed has shown that CreER^{T2} activity is exclusive to Thy1-expressing neurons (Heimer-McGinn and Young, 2011). Consistency of both cortical and motor neuron expression of Thy1 (Young et al., 2008b) as well as high recombination efficiencies of the Cre-LoxP system within those neuronal populations (Heimer-McGinn and Young, 2011) have been shown previously in the SLICK-H strain.

MCU levels were not altered within the splenocytes of TMX treated Thy1-MCU Def mice. Thy1 is weakly expressed by T cells and other immune cell subtypes (Haeryfar and Hoskin, 2004) but clear evidence confirming the absence of CreER^{T2} activity in immune cell populations of SLICK-H mice is lacking. Given that EAE is a T cell mediated model of autoimmunity (Fletcher et al., 2010;

Kurschus, 2015; Okuda et al., 2002) any alteration of mitochondrial function by MCU deletion could lead to a differential immune response. Therefore, the present results indicate that immune cells are unaffected by neuronal Thy1-MCU deletion.

4.2 Characterization of Increased Disease Severity in EAE/Thy1-MCU Def Mice

EAE/Thy1-MCU Def mice experienced marked elevation of motor deficit when compared to EAE/Thy1 controls as revealed by significantly higher CS beginning a day after disease onset. Disease onset and peak disease occurred earlier in EAE/Thy1-MCU Def mice and the number of days spent at a CS≥1.5 was significantly higher. To help characterize spinal cord pathology in the two groups, we proceeded to analyze axonal damage and demyelination at DPI 16 and DPI 30.

4.2.1 Axonal Damage is Higher in EAE/Thy1-MCU Def Mice Than EAE/Thy1 Controls and Increases from DPI 16 to 30 in EAE/Thy1-MCU Def Mice

Axonal damage in EAE has previously been assessed using various approaches. Trapp et al. 1998 showed that bulbous ends of transected axons could be identified under confocal microscopy with SMI32 labelling. Libbey et al. 2014 then showed that SMI32 punctate labelling could be combined with YFP labelling to identify damaged axons and neurons. We extended this technique by showing that Thy1-eYFP aggregates at the ends of transected axons and thereby serve as an additional technique for the measurement of axonal damage. This novel method was used in the current study to show that axonal damage is significantly

higher at both DPI 16 and 30 in EAE/Thy1-MCU Def compared to EAE/Thy1 mice. This was also reflected by EM imaging at DPI 16 which indicated that there were a higher number of damaged axons in EAE/Thy1-MCU Def than EAE/Thy1 mice. This amount was expected because clinical scores have been shown to be highly correlated with axonal damage (Budde et al., 2008; Wujek et al., 2002). Additionally, increased axonal damage over time, even after remission from peak disease, is a common feature of EAE (Jones et al., 2013; Prinz et al., 2015; Recks et al., 2013). This process is similar in MS lesions where axon loss is highest in actively demyelinating lesions but continues at lower levels in chronic demyelinated plaques (Haines et al., 2011; Kornek et al., 2000). Prinz et al. 2015 did not see significant changes in axonal pathology from peak disease until 6 months DPI. This is corroborated by the lack of increased axonal damage in EAE/Thy1 mice from DPI 16 to 30. Overall, eYFP labelling was effective at discerning the degree of axonal damage in EAE mice and it showed a higher degree of injury in EAE/Thy1-MCU Def relative to EAE/Thy1 mice followed by an increase of axonal damage in EAE/Thy1-MCU Def mice from DPI 16 to DPI 30. This increase in damage likely contributed to the severe motor deficits seen in EAE/Thy1-MCU Def.

4.2.2 Demyelination at Peak Disease is not Significantly Different Between EAE/Thy1 and EAE/Thy1-MCU Def Mice

Demyelination was found to be equivalent between EAE/Thy1 and EAE/Thy1-MCU Def mice at peak disease (DPI 16) despite the stark differences in motor deficits observed by the measurement of CS. As previously mentioned, axonal transection may be a contributor but it is also known that demyelination impairs

action potential propagation resulting in a transition from saltatory to continuous conduction (Hamada et al., 2017; Quandt and Davis, 1992; Smith, 1994). Ion gradients that mediate neurotransmission are largely maintained by the Na^+/K^+ ATPase and thus depend on mitochondrial fidelity and ATP production (Alizadeh et al., 2015; Trapp and Stys, 2009). Given the suppression of ATP production observed in EAE/Thy1-MCU Def mice at DPI 16, failed Na^+/K^+ exchange may have lead to high intracellular Na^+ levels which would have further impaired action potential propagation (Coggan et al., 2015). Metabolic collapse may therefore have contributed to the increase of motor deficits in EAE/Thy1-MCU Def mice in the absence of greater demyelination at DPI 16 compared to EAE/Thy1 controls.

4.2.3 Remyelination is Suppressed in the Spinal Cords of EAE/Thy1-MCU Def Mice

The EAE model of MS has been shown to induce demyelination followed by a moderate degree of remyelination after the onset of peak disease (Jones et al., 2008; Kornek et al., 2000; Mei et al., 2016). However, remyelination in EAE often occurs on a longer time scale than was observed in the current study and is contradicted by studies that show increases in demyelination over time (Prinz et al., 2015; Recks et al., 2013). The present study shows a reduction in WML from DPI 16 to 30 in EAE/Thy1 mice. By contrast, remyelination was completely absent in EAE/Thy1-MCU Def mice which had similar WML between DPI 16 and 30 and significantly higher WML than EAE/Thy1 mice at DPI 30. This finding was supported by the reduced number of remyelinating axons observed in EM images of EAE/Thy1-MCU Def mice when compared to EAE/Thy1 controls.

Remyelination in EAE and MS is dependent upon the recruitment of oligodendrocyte precursor cells (OPCs) to active lesions and their differentiation into myelin-producing oligodendrocytes (Hashemian et al., 2019; Mei et al., 2016). This has been shown through pharmacological activation of OPC proliferation and differentiation with the FDA approved drugs fingolimod (Brinkmann et al., 2002; Hashemian et al., 2019) and pioglitazone (Chedrawe et al., 2018; Peymani et al., 2018). Concurrently, non-remyelinating MS lesions show either failed OPC recruitment or differentiation (Franklin, 2002). The activation of OPC differentiation is dependent upon ATP release from neighbouring neurons for signalling at purinergic receptors (Kashfi et al., 2017; Welsh and Kucenas, 2018). Purinergic receptors on oligodendrocytes have also been implicated in the initiation of myelination (Welsh and Kucenas, 2018). Therefore, decreased ATP levels within the spinal cords of EAE/Thy1-MCU Def mice may have contributed to failed remyelination at DPI 30 by reducing the recruitment and activation of OPCs and oligodendrocytes. This is also a prominent feature of non-remyelinating lesions of progressive MS patients (Magalon et al*.,* 2012).

4.3 Suppressed ATP Synthesis, Mitochondrial Gene Expression and Calpain Activation in EAE/Thy1-MCU Def Mice Recapitulate Key Features of Progressive MS

In keeping with a massive depolarization of the Ψ_m in the spinal cord axons of EAE mice at peak disease (Sadeghian et al., 2016) we observed a 90% reduction of ATP concentrations in spinal cord extracts from EAE/Thy1 mice at DPI 16. EAE/Thy1-MCU Def mice showed a further 85% reduction in ATP

concentrations. Reduction of high capacity Ca^{2+} uptake into mitochondria prevents allosteric activation of Ca^{2+}-dependent dehydrogenases to produce reducing equivalents that drive oxidative phosphorylation (Giorgi et al., 2012; Trapp and Stys, 2009). This leads to a dissipation of the Ψ_m in patients with mitochondrial diseases which appears to be recapitulated in EAE/Thy1-MCU Def mice.

4.3.1 Impaired Mitochondrial Function in EAE/Thy1-MCU Def Mice

Impaired ATP production was accompanied by reduced mRNA levels for SDHA, mt-CO4 and PGC-1α in EAE/Thy1-MCU Def relative to EAE/Thy1 mice. SDHA activity has previously been shown to be upregulated in both EAE (Ng et al., 2019; Packialakshmi and Zhou, 2018) and MS lesions (Mahad et al., 2009). Additionally, SDHA expression in SPMS lesions was found to be unaltered meaning that the reduction of mRNA expression in EAE/Thy1-MCU Def mice is not present in MS patients (Dutta et al., 2006). However, activity of mt-CO4 has been shown to be unaltered in wild-type EAE mice (Ng et al., 2019) while downregulation of mt-CO4 expression in EAE/Thy1-MCU Def mice is consistent with findings in active MS lesions (Mahad et al., 2008). This subunit is essential in cytochrome c function and its absence reduces ATP production, compromises Ψ_m and induces apoptosis that may have suppressed ATP levels in EAE/Thy-MCU Def mice (Li et al., 2006). Finally, PGC-1α is moderately downregulated in wild-type EAE mice at DPI 16 (Dang et al., 2019) but is markedly lowered in MS lesions and found to increase ROS formation and enhance ROS-induced cell death (Witte et al., 2013). These findings in EAE/Thy1-MCU Def mice are

consistent with impaired CNS mitochondrial function and biogenesis in MS including downregulation of mt-CO4 and PGC-1α in active lesions (Campbell and Mahad, 2012; Dutta et al., 2006; Mahad et al., 2008; Witte et al., 2013; Witte et al., 2014).

4.3.2 Failed Ca^{2+} Buffering and Calpain Activation in EAE/Thy1-MCU Def Mice

As previously mentioned, high amounts of energy are required to fuel Na^+/K^+ ATPase that maintains ion gradients crucial for the propagation of action potentials along the axon (Trapp and Stys, 2009). With a reduction of ATP production in EAE/Thy1-MCU Def mice, expulsion of Na^+ is impaired leading to high Na^+ concentrations in the axoplasm of denuded axons (Waxman et al., 2004). This elevation of axoplasmic Na^+ may then lead to a reversal of the Na^+/Ca^{2+} exchanger (NCX) which depends on the electrochemical gradient to expel Ca^{2+} from the inside of axons (Alizadeh et al., 2015; Stys et al., 1992; Trapp and Stys, 2009). The Ψ_m drives MCU activity responsible for Ca^{2+} buffering in the axoplasm (Giorgi et al., 2012) . Failed mitochondrial Ca^{2+} buffering paired with increased Ca^{2+} influx via the NCX may lead to axonal Ca^{2+} overloading in MS resulting in the overactivation of Ca^{2+}-dependent proteases such as calpain (Alizadeh et al., 2015; Stys et al., 1992). This overactivation of calpain activity in the EAE model was evident in both western blotting for αII Spectrin cleavage and the fluorometric measurements of calpain activity. Moreover, spinal cord calpain activity is elevated by Thy1-MCU Def in EAE mice. Mitochondrial dysfunction also appeared to have catastrophic metabolic consequences for EAE/Thy1-MCU Def axons under immune-mediated attack as suggested by mitochondrial

fragmentation, cytoskeletal integrity loss and increased autophagosome formation. EAE/Thy1-MCU Def mice therefore appear to recapitulate key features of metabolic dysfunction in progressive MS that are not seen to the same degree, if at all in EAE/Thy1 mice.

4.4 Distinct Axon Injury Mechanisms in EAE/Thy1 and EAE/Thy1-MCU Def Mice

4.4.1 Mitochondrial Morphology in EAE/Thy1 and EAE/Thy1-MCU Def Mice

To better understand how Thy1-MCU Def promoted axonal loss in the EAE model, the morphological features of L5 spinal cord axons in EAE/Thy1 and EAE/Thy1-MCU Def mice at equivalent clinical severities were examined with the use of EM. Our studies revealed that mitochondrial morphology and positioning during autoimmune-mediated demyelination were dependent on MCU function. At the onset of walking deficits in EAE/Thy1 mice (CS=2.0), axonal mitochondria appeared larger, elongated in shape, and displayed dense cristae indicative of an activated state commonly observed within the lesions of MS patients and EAE mice (Gomes and Scorrano, 2011; Kiryu-Seo et al., 2010; Recks et al., 2013). By stark contrast, mitochondria in EAE/Thy1-MCU Def mice were condensed, similar to mitochondria exposed to hypertonic environments (Hackenbrock, 1966; Mannella, 2008). Mitochondrial condensation may become pathological leading to severe fragmentation as has been observed during excitotoxicity mediated by glutamate-induced mitochondrial Ca^{2+} overloading in a mouse model of glaucoma (Coughlin et al., 2015; Ju et al., 2009). As in MS spinal cord pathology, microtubules also appear disorganized (Mao and Reddy, 2010). Densitometric

measurements also verified cytoskeletal loss in EAE/Thy1-MCU Def axons typical of chronic MS plaques (Dutta et al., 2006).

At CS=3.0, EAE/Thy1 mice began to exhibit swollen mitochondria with disorganized cristae which are reminiscent of mitochondria undergoing hypoxic damage and producing excessive amounts of reactive oxygen species (ROS) (Nichols et al., 2017; Recks et al., 2013). Swollen mitochondria were positioned at denuded sites in remyelinating and demyelinated EAE/Thy1 axons, presumably to provide additional Ca^{2+} buffering and ATP production. By contrast, EAE/Thy1-MCU Def axons had very few functional mitochondria and showed only single, massively swollen mitochondria at denuded sites. The undocking of mitochondria from cytoskeletal motors at energetically favourable sites (nodes of Ranvier in non-pathological axons) (Kang et al., 2008; Pivovarova and Andrews, 2010) is a process controlled mainly by the KIF5-Milton-MIRO complex which allows mobile mitochondria to disengage from the cytoskeleton in the presence of high Ca^{2+} concentrations (Cai and Sheng, 2009; Sheng and Cai, 2012). With the complete failure of Ca^{2+} buffering in EAE/Thy1-MCU Def mitochondria, it is possible that axons became oversaturated with Ca^{2+} to the point that MIRO complexes were constitutively disengaging mitochondria from the cytoskeleton thereby preventing the strategic recruitment of mitochondria to denuded sites. Ca^{2+}-dependent release of mitochondria from kinesin heavy chain KIF5 allows for competitive binding of syntaphilin (SNPH) which anchors mitochondria to the cytoskeleton and inhibits ATPase activity of KIF5 (Chen and Sheng, 2013; Short, 2020). With axonal Ca^{2+} overloading in EAE/Thy1-MCU Def mice, it is possible

that fragmented mitochondria were constitutively bound in place to the cytoskeleton by SNPH. As these mitochondria were targeted for autophagic digestion, the attached cytoskeleton may have been shredded and dragged into autophagosomes which would explain the large amounts of internalized cytoskeletal debris and reduction in cytoskeletal density.

At CS=3.5, swelling of EAE/Thy1 mitochondria reached critical mass leading to a dissolution of cristae that has been described before in severe EAE and instances of intense mitochondrial stress (Hackenbrock, 1966; Qi et al., 2006; Recks et al., 2013). EM studies have previously shown that mitochondria in demyelinated MS lesions appear to be small and irregular in size with extremely disorganized and damaged cristae (Mahad et al., 2009). The mitochondria in MS brain tissues have similar features of swollen and damaged mitochondria observed in both EAE/Thy1 and EAE/Thy1-MCU Def mice. However, axonal mitochondria appeared fragmented and condensed in EAE/Thy1-MCU Def mice. However, there is a scarcity of studies showing EM images of mitochondrial morphology in MS thereby preventing any direct comparisons with EAE/Th1-MCU Def mice. Mitochondrial morphology has, however, been shown to be a natural mechanism used for energetic adaptation in stressful environments (Gomes et al., 2011; Gomes and Scorrano, 2011; Mannella, 2008). Given the dramatic changes in mitochondrial morphology seen in EAE/Thy1-MCU Def mice, future EM studies of mitochondria are important for progressive MS research.

4.4.2 EAE/Thy1-MCU Def Mice Model Excessive Autophagy Induction in MS

Autophagy acts primarily as a cell survival mechanism during nutrient starvation. However, in certain pathological states it also induces cell death by excessively degrading cellular contents (Fuchs and Steller, 2011; Marino et al., 2014). We have previously shown that the expression of atg5 in the CNS is strongly correlated with MS disease severity (Alirezaei et al., 2009). The ability of autophagy inhibitors to reduce paralysis and spinal cord damage in EAE mice further suggests a pathological role for autophagy in MS (Bhattacharya et al., 2014; Li et al., 2019).

At a CS=2.5, large autophagosomes were more common in the axons of EAE/Thy1-MCU Def than EAE/Thy1 mice. Furthermore, these autophagosomes became more numerous with EAE progression. The higher levels of atg5 and atg7 mRNAs and greater co-localization of LC3 in Thy1-expressing spinal neurons of EAE/Thy1-MCU Def than EAE/Thy1 mice are also indicative of autophagy induction. Ca^{2+} regulation plays a significant role in autophagy (Sun et al., 2016). Adenosine monophosphate kinase (AMPK) is activated by AMP in conditions of energy depletion (i.e. high AMP to ATP ratio) (Ding and Yin, 2012; Jeon, 2016; Sun et al., 2016). This leads to the inhibition of mTOR which is also suppressed by ROS production during cellular stress (Ding and Yin, 2012). Inhibition of mTOR activates autophagosome formation (Ding and Yin, 2012; Kapuy et al., 2014; Kosztelnik et al., 2019). For this reason, mitochondrial dysfunction and suppressed production of ATP could be very strong contributors

to the upregulation of autophagy in EAE/Thy1-MCU Def mice. This non-selective autophagic induction leads to indiscriminate degradation of axoplasmic contents such as mitochondria and microtubules (Ding and Yin, 2012). These findings are consistent with *in vitro* evidence of autophagy induction by suppressed MCU activity (Cardenas et al., 2010; Kondratskyi et al., 2018; Mallilankaraman et al., 2012). However, autophagy upregulation by rapamycin has also been shown to be protective in EAE (Feng et al., 2017) indicating that an optimal level of autophagy is required for recovery from autoimmune-mediated demyelination.

As disease severity increased to CS=3.0, clear signs of mitophagy were apparent in the axonal mitochondria of EAE/Thy1 mice. These mitochondria were characterized by mitochondrial swelling and loss of cristae integrity which became more pronounced at CS=3.5. These findings indicate that mitochondria in EAE/Thy1 axons undergo a healthy degree of mitophagy whereas mitochondrial collapse in EAE/Thy1-MCU Def axons triggers excessive autophagy. The injurious effects of excessive autophagy are suggested by increased damaged axons, reduced remyelinating axons and decreased numbers of intact mitochondria within the remyelinating axons of EAE/Thy1-MCU Def compared to EAE/Thy1 mice. EAE/Thy1-MCU Def mice therefore recapitulate the upregulation of autophagy characteristic of MS lesions (Alirezaei et al., 2009; Patergnani et al., 2018).

4.5 Patterns of Immune Cell Infiltration and Cytokine Expression in EAE/Thy1-MCU Def Mice Reflect a Pro-Inflammatory Bias That Promotes Axonal Damage

Flow cytometric measurements indicated that infiltration of T lymphocytes ($CD4^+$ and $CD8^+$) and myeloid cells ($Ly6C_{low}$ and $Ly6C_{high}$) was elevated in the CNS of EAE/Thy1-MCU Def relative to EAE/Thy1 mice. These infiltrates were composed primarily of $CD4^+$ T cells and $Ly6C_{high}$ myeloid cells. These findings indicate that increased EAE disease severity in Thy1-MCU Def mice was associated with a pro-inflammatory bias.

4.5.1 $CD4^+$ and $CD8^+$ Immune Cell Populations are Upregulated in the Periphery and CNS of EAE/Thy1-MCU Def Mice

EAE induction uses myelin antigen (such as MOG_{35-55}) emulsified with an immune adjuvant to induce autoreactivity towards myelin of the CNS in CD4+ T helper cells (Chitnis, 2007; Constantinescu et al., 2011). This replicates the predominance of $CD4^+$ T cells in acute lesions of MS while $CD8^+$ cells tend to be dominant in chronic lesions (Chitnis, 2007; Raine, 1994). Accordingly, EAE/Thy1-MCU Def mice showed a substantially larger infiltration of $CD4^+$ T cells in the CNS than EAE/Thy1 controls. Upon entry to the CNS, $CD4^+$ T cells are re-activated by antigen presenting cells (APCs) and then produce pro-inflammatory cytokines IFN-γ and TNF-α which mobilize the innate immune system resulting in inflammatory spinal cord damage (Corsini et al., 1996; Dendrou et al., 2015; Olsson et al., 1990; Olsson, 1995). This promotes the recruitment and infiltration of monocytes to the CNS (Dendrou et al., 2015; Monaghan et al., 2019). Cross-presentation by dendritic cells then induces the activation and infiltration of $CD8^+$ cytotoxic T cells which are correlated with higher rates of axonal damage in MS

(Bitsch et al., 2000; Dendrou et al., 2015). EAE/Thy1-MCU Def mice were the only group that showed elevated levels of $CD8^+$ T cells thereby replicating T cell mechanisms in chronic MS lesion pathology. These actions are supported by higher mRNA expression of pro-inflammatory cytokines (IFN-γ, IL-1β, IL-6, IL-12 (p35) and CCL5) produced by encephalitogenic T lymphocytes, dendritic cells, neutrophils and M1 macrophages in the spinal cords of EAE/Thy1-MCU Def than EAE/Thy1 mice (Arango and Descoteaux, 2014; Domingues et al., 2010; Maimone et al., 1993).

4.5.2 Monocyte Populations are Upregulated in the CNS but not Periphery of EAE/Thy1-MCU Def Mice

The two monocyte lineages in mice are the classical $Ly6C^{high}$ with high expression of C-C chemokine receptor 2 ($CCR2^{hi}$) and low levels of CX3C chemokine receptor 1 ($CX3CR1^{low}$) and the non-classical $Ly6C^{low}$ which are $CCR2^{low}CX3CR1^{hi}$. These lineages are comparable to classical and non-classical human monocytes, respectively (Kratofil et al., 2017; Monaghan et al., 2019). $Ly6C^{high}$ monocytes up-regulate pro-inflammatory molecules and are one of the main TNF producers early in inflammation. These monocytes also differentiate into dendritic cells and M1 macrophages known to promote CNS damage in the EAE model (Benakis et al., 2014; Katsumoto et al., 2014; King et al., 2009; Shechter et al., 2013). $Ly6C^{high}$ monocytes deficient of CCR2 are incapable of developing EAE which indicates how central they are to CNS inflammation in this MS model (Fife et al., 2000). This may be because $Ly6C^{high}$ monocytes differentiate into antigen presenting cells that are responsible for the re-activation of infiltrating $CD4^+$ T cells (Monaghan et al., 2019). Overall, the upregulation of

Ly6C^{high} monocytes in EAE/Thy1-MCU Def mice is indicative of a pro-inflammatory environment similar to that seen in MS. Ly6C^{low} monocytes are derived from Ly6C^{high} populations, patrol the vasculature and may play a minor role in EAE (Benakis et al., 2014; Kratofil et al., 2017). However, Ly6C^{low} monocytes do become more prevalent during the resolution of inflammation and seem to contribute to the development of a pro-repair environment (Benakis et al., 2014). This mechanism did not appear to operate in EAE/Thy1-MCU Def mice because pro-repair cytokines failed to be elevated and the overall elevation of Ly6C^{low} monocyte levels was minimal compared to EAE/Thy1 controls. Ly6C$_{high}$ and Ly6C$_{low}$ cell populations in the spleen were unchanged between EAE/Thy1 and EAE/Thy1-MCU Def mice. This indicates that monocyte levels were not elevated globally in EAE/Thy1-MCU Def mice but, were instead increased secondary to enhanced CNS damage. This aligns with the inside-out theory that early mitochondrial and axonal damage in the CNS contributes to the priming of autoreactive immune cells in MS (Faissner et al., 2019; Geurts et al., 2010; Mao and Reddy, 2010).

4.6 EAE/Thy1-MCU Deficiency as a New Preclinical Model of MS

Progressive MS is in need of accurate preclinical models for the testing of potential therapeutics (Faissner et al., 2019). Based on the results presented in the present study, I propose that unlike wild-type mice, EAE/Thy-MCU Def mice effectively model many of the pathological features consistent with “inside-out” disease mechanisms implicated in MS disease progression (Chrzanowski et al., 2019; Milo et al., 2019; Scheld et al., 2016). EAE/Thy1-MCU Def mice model key

features of MS such as mitochondrial dysfunction, upregulation of injurious autophagy, downregulation of mitochondrial respiratory complex genes, suppression of ATP production, Ca^{2+} overloading and calpain overactivation, all of which contribute to severe motor deficits, suppression of remyelination, increased axonal damage and a higher recruitment of immune infiltrates. Drug screening efforts based on the reversal of these MCU-dependent metabolic deficits may therefore rapidly identify novel neuroprotective and remyelinating agents for progressive MS. Testing of these therapeutic candidates in EAE/Thy1-MCU mice may thus offer a novel approach to prioritize them for clinical development.

4.7 Limitations

4.7.1 Conclusions Based on Correlative Data Require Further Experimentation

The current findings suggest that mitochondrial dysfunction suppressed Ca^{2+} buffering, ATP synthesis and mitochondrial gene expression resulting in the metabolic collapse of EAE/Thy1-MCU Def axons at DPI 16 which was characterized by excessive autophagy and increased inflammation relative to EAE/Thy1 controls. However, we acknowledge that causality is not proven by these correlations. In the same way, MS etiopathogenesis has been debated for decades, making any concrete conclusions difficult (Compston and Coles, 2002; Faissner et al., 2019; Mao and Reddy, 2010). EAE is also mechanistically complex and not fully understood. My findings suggest that mechanisms at work in EAE/Thy1-MCU Def mice may also be relevant for MS disease progression.

However, this conclusion could obviously be strengthened by further experimentation and validation to move from correlation to causality. Some of these experiments are outlined in the “Future Directions” portion of the discussion.

4.7.2 The Exclusive Use of Female Mice for Experimentation

The present study was performed exclusively with the use of female mice thereby excluding any of the male sex from experimentation. It has been shown that there are sex differences in EAE, but female mice are superior to males for testing of neuropathic pain (Papenfuss et al., 2004; Rahn et al., 2014). Additionally, female humans are more susceptible to MS than males as shown by an approximate 3:1 incidence which is steadily increasing (Harbo et al., 2013; Stys et al., 2012). For these reasons, female mice were chosen, and male mice were excluded to reduce variability while staying within time and resource constraints. The present investigation would therefore have benefited from studies in male animals.

4.7.3 Relative Unreliability of Clinical Scoring

The clinical scoring system used is semi-quantitative in nature and employs an ordinal scale for assessment of motor disability and behavioural deficits in the EAE model. Variations of this scoring system are used diffusely but have been shown to be inconsistent and suboptimal for quantitating disease severity due to their ordinality (Fiander et al., 2017b; Fleming et al., 2005). Kinematic gait analyses in the sagittal plain have been shown by our lab to be a highly reliable and sensitive quantitative measure of motor deficit in EAE mice (Chedrawe et al.,

2018; Fiander et al., 2017a; Fiander et al., 2017b). Unfortunately, when EAE/Thy1-MCU Def mice were subjected to treadmill recording, 70% were too fatigued or disabled to produce any measurable gait outcomes (data not shown). Fatigue is a common symptom of MS and is thought to originate from the increased energy requirements of denuded axons paired with mitochondrial dysfunction (Mao and Reddy, 2010). Further behavioural analyses would therefore lend to a better functional characterization of EAE/Thy1-MCU Def mice and provide a potentially more accurate representation of the pathological differences between them and EAE/Thy1 mice.

4.8 Future Directions

4.8.1 Testing of Drug Candidates for MS Using the EAE/Thy-MCU Def Model

The EAE/Thy1-MCU Def mouse model shares several mechanisms of spinal cord damage with progressive MS (Faissner et al., 2019). The following drugs, if effective at reversing the exacerbation of EAE observed in Thy1-MCU Def mice, may therefore be effective drug therapies for progressive MS.

Mitochondrial respiration - Drugs targeting mitochondrial morphology (Gomes et al., 2011) and oxidative phosphorylation efficiency may promote the reversal of suppressed ATP production in EAE/Thy1-MCU Def mice. Vitamin B_1 (thiamine) is responsible for activation of the thiamine- and Ca^{2+}-dependent enzymes pyruvate dehydrogenase and alpha-ketoglutarate dehydrogenase of the citric acid cycle (Parker, Jr. et al., 1984; Traaseth et al., 2004). Thiamine administration has been shown to reduce fatigue in MS (Costantini et al., 2013) by activation of oxidative

phosphorylation and suppression of the pro-inflammatory cytokine CCL2 in the spinal cord (Khosravi-Largani et al., 2018). Administration of thiamine could therefore suppress inflammation and promote the activation of Ca^{2+}-dependent dehydrogenases in EAE/Thy1-MCU Def mice. Mitochonic acid 5 (MA-5) promotes cell survival in mitochondrial diseases by activating oligomerization of ATP synthase (Khosravi-Largani et al., 2018). Furthermore, this compound is orally bioavailable (Matsuhashi et al., 2017). Ginkgo biloba extract has been shown to improve respiration of mitochondria and reduce fatigue in MS (Suzuki et al., 2016). Reversal of mitochondrial deficits by any of these drugs in EAE/Thy1-MCU Def mice would encourage testing in progressive MS.

Autophagy - Rapamycin is an inhibitor of mTOR which is implicated in the AMPK energy sensitive pathway of autophagy in the cell (Eckert, 2012; Johnson et al., 2006). Preliminary results have shown some beneficial effects in RRMS (Bagherpour et al., 2018; Vergo et al., 2011). Testing in the EAE/Thy1-MCU Def model may reveal applications for PPMS or SPMS.

Calpain activation - SNJ1945 is an orally bioavailable calpain inhibitor that has been shown to reduce CS in mice subjected to EAE by preventing inflammation and reducing neurodegeneration (Liang and Le, 2015).

Remyelination - Retinoic acid receptors (RXR) have been implicated in remyelination by promoting the differentiation of OPCs into mature oligodendrocytes (Trager et al., 2014). Administration of the RXR agonist IRX4204 ameliorates EAE by attenuation of Th17 development and promoting

differentiation of T regulatory cells (Kremer et al., 2015). IRX4204 may therefore be an extremely useful drug for immune suppression in the short term (RRMS) and the prevention of neurodegeneration in the long term (progressive MS). Olesoxime is a compound that promotes the elongation of mitochondria in OPCs (Chandraratna et al., 2016) which then produce more ATP and less ROS (Magalon et al., 2016). This favours OPC differentiation and subsequent remyelination in lysolecithin and cuprizone models of MS (Gomes et al., 2011). Non-remyelinating MS lesions show either fewer numbers of OPCs or failure of OPCs to differentiate (Magalon et al., 2012) indicating that the testing of these drugs in the EAE/Thy1-MCU Def model would present a clearer image of their therapeutic potential in MS.

Ion transport - As previously mentioned, Na^+ and Ca^{2+} overloading lead to reduced action potential propagation and many damaging effects in MS which are potentially shared by EAE/Thy1-MCU Def mice. Amiloride is an inhibitor of acid-sensing ion channel 1 (ASIC1) which is permeable to both ions. Amiloride has been shown to be neuroprotective in EAE (Franklin, 2002) and is currently in Phase II clinical trials for SPMS (Connick et al., 2018).

4.8.2 Future Experimentation to Elucidate the Complexities of the EAE/Thy1 MCU Def Model

There are several future experiments that would help in understanding the intricacies of the EAE/Thy1-MCU Def model but more importantly, may also offer more insights into MS disease processes.

Testing of Adoptive Transfer From EAE/Thy1-MCU Def Mice - Adoptive transfer is a passive method for the induction of EAE in which the lymph nodes of primed donor mice are harvested and processed for the retrieval of T cells for culturing in MOG_{35-55} containing media. These activated T cells are then injected into naïve mice to induce EAE (Connick et al., 2018). Equivalent concentrations of primed EAE/Thy1 and EAE/Thy1-MCU Def mouse T cells could be transferred into naïve wild-type mice followed by measurements of CS, axonal damage and WML. Given the upregulation of immune cell infiltration in EAE/Thy1-MCU Def mice, adoptive transfer would distinguish whether exacerbation in these mice originated from mitochondrial dysfunction and metabolic collapse or increased encephalogenic T cell activity. If there is no difference in disease severity between Thy1 and Thy1-MCU Def mice exposed to adoptively transferred EAE, this outcome would further implicate neuronal mitochondrial dysfunction in the more severe disease course for EAE/Thy1-MCU Def mice.

Further Confirmation of Non-Selective Autophagy in EAE/Thy1-MCU Def Mice - LC3 is implicated in the docking of autophagosomes to lysosomes for degradation of internalized contents and was used in this study to examine general autophagy in the spinal cord. When a starvation-like state is induced in cells, LC3-I is conjugated to phosphatidylethanolamine to produce LC3-II which is integrated into autophagosomes (McCarthy et al., 2012). Upon lysosomal fusion, LC3-II is converted back to LC3-I. Autophagy induction during cellular starvation increases the ratio of LC3-II:LC3-I (Tanida et al., 2008). Western blotting for LC3-I and LC3-II in EAE/Thy1 and EAE/Thy1-MCU Def mice would

therefore further address whether autophagy is overactivated in EAE/Thy1-MCU Def mice.

Further Investigation of OPC Activation/Differentiation for Remyelination - As discussed previously, there is a diversity of commentary surrounding degree of remyelination in the EAE model. Some studies show very little remyelination while others report similar findings as the present study (Constantinescu et al., 2011; Hampton et al., 2008; Jones et al., 2008; Kornek et al., 2000; Mei et al., 2016; Prinz et al., 2015; Recks et al., 2013). For this reason, a direct quantification of the recruitment and differentiation of OPCs in spinal cord lesions would directly show whether remyelination is promoted in EAE/Thy1 mice and whether it is suppressed in EAE/Thy1-MCU Def mice. IHC staining for neuron-glia antigen 2 (NG2), a marker for OPCs and oligodendrocyte specific protein (OSP) for oligodendrocytes, would be useful to compare OPC recruitment and differentiation numbers in the spinal cord lesions of EAE/Thy1 and EAE/Thy1-MCU Def mice (Michalski et al., 2018; Suzuki et al., 2017).

4.9 Conclusions

Based on evidence that enhanced MCU-mediated Ca^{2+} uptake increases Ca^{2+} buffering, stimulates ATP synthesis and triggers mitochondrial undocking (Baughman et al., 2011; Chang et al., 2011; De et al., 2011; Glancy and Balaban, 2012; Hansford and Zorov, 1998; Okuda et al., 2002; Pan et al., 2013; Schwarz, 2013), I have proposed that the MCU plays a pivotal role in the survival of axons exposed to autoimmune-mediated demyelination. The first series of

experiments support this hypothesis by showing that disease severity, spinal cord demyelination and corticospinal axon injury were markedly elevated in EAE/Thy1-MCU Def relative to EAE/Thy1 mice at DPI 16 and 30. Furthermore, EAE/Thy1-MCU Def mice suffered more days at CS ≥ 1.5 and increased axonal injury from DPI 16 to DPI 30. These findings suggest that MCU dysfunction contributes to common features of progressive MS such as motor deficits, axonal injury and failed remyelination (Compston and Coles, 2008; Diaz-Sanchez et al., 2006; Faissner et al., 2019; Guyton et al., 2005; Kalyvas et al., 2009; Kornek et al., 2000; Mei et al., 2016; Shields et al., 1999).

Suppressed mitochondrial-mediated Ca^{2+} buffering contributed to increased axonal damage in these mice via overactivation of injurious Ca^{2+}-dependent proteases. Calpain activity was elevated by 3-fold in the spinal cords of EAE/Thy1-MCU Def compared to EAE/Thy1 mice at DPI 16. This suggests that reduced Ca^{2+} buffering in EAE/Thy1-MCU Def axons promoted injury by excessively activating this Ca^{2+}-dependent protease. Biochemical and histochemical studies have shown that CNS axon damage in EAE and MS are associated with injurious Ca^{2+}-dependent phospholipase and calpain inductions (Diaz-Sanchez et al., 2006; Guyton et al., 2005; Kalyvas et al., 2009; Shields et al., 1999). Furthermore, failure of Ca^{2+} entry into mitochondria led to reduced ATP production in EAE/Thy1-MCU Def mice which is thought to contribute to several pathological events observed in MS. ATP production is responsible for powering Na^{+}/K^{+} ATPase in denuded axons, preventing excessive autophagic induction and inducing the differentiation of OPCs (Sun et al., 2016; Trapp and

Stys, 2009). Therefore, suppression of ATP production in EAE/Thy1-MCU Def axons replicates Na^+ and Ca^{2+} imbalances, autophagy induction and failed OPC differentiation observed in progressive MS (Alizadeh et al., 2015; Ding and Yin, 2012; Dutta et al., 2006; Jeon, 2016; Stys et al., 1992; Welsh and Kucenas, 2018). Finally, Ca^{2+} overloading prevents proper mobilization and positioning of mitochondria by SNPH and the KIF5-Milton-MIRO complex at energetically favourable sites in EAE/Thy1-MCU Def mice as reflected by the lack of functional mitochondria at the denuded sites of these animals (Cai and Sheng, 2009; Chen and Sheng, 2013; Sheng and Cai, 2012; Short, 2020).

I therefore propose that EAE/Thy1-MCU Def mice model inside-out mechanisms implicated in MS disease progression. In addition to having provided an in-depth view into how mitochondrial dysfunction induces demyelination and suppresses myelin repair, this model will also be useful in identifying drug candidates that may mitigate metabolic collapse in progressive MS.

References

1998. Placebo-controlled multicentre randomised trial of interferon beta-1b in treatment of secondary progressive multiple sclerosis. European Study Group on interferon beta-1b in secondary progressive MS. *Lancet* 352 (9139): 1491-1497.

1999. TNF neutralization in MS: results of a randomized, placebo-controlled multicenter study. The Lenercept Multiple Sclerosis Study Group and The University of British Columbia MS/MRI Analysis Group. *Neurology* 53 (3): 457-465.

Ahmed SI, Aziz K, Gul A, Samar SS, and Bareeqa SB. 2019. Risk of Multiple Sclerosis in Epstein-Barr Virus Infection. *Cureus.* 11 (9): e5699.

Alirezaei M, Fox HS, Flynn CT, Moore CS, Hebb AL, Frausto RF, Bhan V, Kiosses WB, Whitton JL, Robertson GS, and Crocker SJ. 2009. Elevated ATG5 expression in autoimmune demyelination and multiple sclerosis. *Autophagy.* 5 (2): 152-158.

Alizadeh A, Dyck SM, and Karimi-Abdolrezaee S. 2015. Myelin damage and repair in pathologic CNS: challenges and prospects. *Front Mol. Neurosci.* 8: 35.

Alonso A, and Hernan MA. 2008. Temporal trends in the incidence of multiple sclerosis: a systematic review. *Neurology* 71 (2): 129-135.

Amor S, Smith PA, Hart B', and Baker D. 2005. Biozzi mice: of mice and human neurological diseases. *Journal of Neuroimmunology* 165 (1-2): 1-10.

Arango DG, and Descoteaux A. 2014. Macrophage cytokines: involvement in immunity and infectious diseases. *Front Immunol.* 5: 491.

Ascherio A, and Munger KL. 2007a. Environmental risk factors for multiple sclerosis. Part I: the role of infection. *Annals of Neurology* 61 (4): 288-299.

Ascherio A, and Munger KL. 2007b. Environmental risk factors for multiple sclerosis. Part II: Noninfectious factors. *Annals of Neurology* 61 (6): 504-513.

Baecher-Allan C, Kaskow BJ, and Weiner HL. 2018. Multiple Sclerosis: Mechanisms and Immunotherapy. *Neuron* 97 (4): 742-768.

Bagherpour B, Salehi M, Jafari R, Bagheri A, Kiani-Esfahani A, Edalati M, Kardi MT, and Shaygannejad V. 2018. Promising effect of rapamycin on multiple sclerosis. *Mult. Scler. Relat Disord.* 26: 40-45.

Barnett MH, and Prineas JW. 2004. Relapsing and remitting multiple sclerosis: pathology of the newly forming lesion. *Annals of Neurology* 55 (4): 458-468.

Baughman JM, Perocchi F, Girgis HS, Plovanich M, Belcher-Timme CA, Sancak Y, Bao XR, Strittmatter L, Goldberger O, Bogorad RL, Koteliansky V, and Mootha VK. 2011. Integrative genomics identifies MCU as an essential component of the mitochondrial calcium uniporter. *Nature* 476 (7360): 341-345.

Benakis C, Garcia-Bonilla L, Iadecola C, and Anrather J. 2014. The role of microglia and myeloid immune cells in acute cerebral ischemia. *Front Cell Neurosci.* 8: 461.

Bhattacharya A, Parillon X, Zeng S, Han S, and Eissa NT. 2014. Deficiency of autophagy in dendritic cells protects against experimental autoimmune encephalomyelitis. *Journal of Biological Chemistry* 289 (38): 26525-26532.

Bitsch A, Schuchardt J, Bunkowski S, Kuhlmann T, and Bruck W. 2000. Acute axonal injury in multiple sclerosis. Correlation with demyelination and inflammation. *Brain* 123 (Pt 6): 1174-1183.

Brinkmann V, Davis MD, Heise CE, Albert R, Cottens S, Hof R, Bruns C, Prieschl E, Baumruker T, Hiestand P, Foster CA, Zollinger M, and Lynch KR. 2002. The immune modulator FTY720 targets sphingosine 1-phosphate receptors. *Journal of Biological Chemistry* 277 (24): 21453-21457.

Brown JWL, Coles A, Horakova D, Havrdova E, Izquierdo G, Prat A, Girard M, Duquette P, Trojano M, Lugaresi A, Bergamaschi R, Grammond P, Alroughani R, Hupperts R, McCombe P, Van P, V, Sola P, Ferraro D, Grand'Maison F, Terzi M, Lechner-Scott J, Flechter S, Slee M, Shaygannejad V, Pucci E, Granella F, Jokubaitis V, Willis M, Rice C, Scolding N, Wilkins A, Pearson OR, Ziemssen T, Hutchinson M, Harding K, Jones J, McGuigan C, Butzkueven H, Kalincik T, and Robertson N. 2019. Association of Initial Disease-Modifying Therapy With Later Conversion to Secondary Progressive Multiple Sclerosis. *JAMA* 321 (2): 175-187.

Budde MD, Kim JH, Liang HF, Russell JH, Cross AH, and Song SK. 2008. Axonal injury detected by in vivo diffusion tensor imaging correlates with neurological disability in a mouse model of multiple sclerosis. *NMR in Biomedicine* 21 (6): 589-597.

Bustin SA, Benes V, Garson JA, Hellemans J, Huggett J, Kubista M, Mueller R, Nolan T, Pfaffl MW, Shipley GL, Vandesompele J, and Wittwer CT. 2009. The MIQE guidelines: minimum information for publication of quantitative real-time PCR experiments. *Clin. Chem* 55 (4): 611-622.

Cadavid D, Mellion M, Hupperts R, Edwards KR, Calabresi PA, DruloviÄ‡ J, Giovannoni G, Hartung HP, Arnold DL, Fisher E, Rudick R, Mi S, Chai Y, Li J, Zhang Y, Cheng W, Xu L, Zhu B, Green SM, Chang I, Deykin A, and Sheikh SI. 2019. Safety and efficacy of opicinumab in patients with relapsing multiple sclerosis (SYNERGY): a randomised, placebo-controlled, phase 2 trial. *Lancet Neurol.* 18 (9): 845-856.

Cai Q, and Sheng ZH. 2009. Mitochondrial transport and docking in axons. *Experimental Neurology* 218 (2): 257-267.

Calabrese M, Magliozzi R, Ciccarelli O, Geurts JJ, Reynolds R, and Martin R. 2015. Exploring the origins of grey matter damage in multiple sclerosis. *Nature Reviews: Neuroscience* 16 (3): 147-158.

Campbell G, and Mahad D. 2018. Neurodegeneration in Progressive Multiple Sclerosis. *Cold Spring Harb. Perspect. Med.* 8 (10).

Campbell GR, and Mahad DJ. 2012. Mitochondrial changes associated with demyelination: consequences for axonal integrity. *Mitochondrion.* 12 (2): 173-179.

Cardenas C, Miller RA, Smith I, Bui T, Molgo J, Muller M, Vais H, Cheung KH, Yang J, Parker I, Thompson CB, Birnbaum MJ, Hallows KR, and Foskett JK. 2010. Essential regulation of cell bioenergetics by constitutive InsP3 receptor Ca2+ transfer to mitochondria. *Cell* 142 (2): 270-283.

Chandraratna RA, Noelle RJ, and Nowak EC. 2016. Treatment with retinoid X receptor agonist IRX4204 ameliorates experimental autoimmune encephalomyelitis. *Am. J. Transl. Res.* 8 (2): 1016-1026.

Chang KT, Niescier RF, and Min KT. 2011. Mitochondrial matrix Ca2+ as an intrinsic signal regulating mitochondrial motility in axons. *Proc. Natl. Acad. Sci. U. S. A* 108 (37): 15456-15461.

Chedrawe MAJ, Holman SP, Lamport AC, Akay T, and Robertson GS. 2018. Pioglitazone is superior to quetiapine, clozapine and tamoxifen at alleviating experimental autoimmune encephalomyelitis in mice. *Journal of Neuroimmunology* 321: 72-82.

Chen Y, and Sheng ZH. 2013. Kinesin-1-syntaphilin coupling mediates activity-dependent regulation of axonal mitochondrial transport. *Journal of Cell Biology* 202 (2): 351-364.

Chitnis T. 2007. The role of CD4 T cells in the pathogenesis of multiple sclerosis. *International Review of Neurobiology* 79: 43-72.

Chrzanowski U, Bhattarai S, Scheld M, Clarner T, Fallier-Becker P, Beyer C, Rohr SO, Schmitz C, Hochstrasser T, Schweiger F, Amor S, Horn-Bochtler A, Denecke B, Nyamoya S, and Kipp M. 2019. Oligodendrocyte degeneration and concomitant microglia activation directs peripheral immune cells into the forebrain. *Neurochemistry International* 126: 139-153.

Chun J, and Hartung HP. 2010. Mechanism of action of oral fingolimod (FTY720) in multiple sclerosis. *Clin. Neuropharmacol.* 33 (2): 91-101.

Coggan JS, Bittner S, Stiefel KM, Meuth SG, and Prescott SA. 2015. Physiological Dynamics in Demyelinating Diseases: Unraveling Complex Relationships through Computer Modeling. *Int. J. Mol. Sci.* 16 (9): 21215-21236.

Compston A, and Coles A. 2002. Multiple sclerosis. *Lancet* 359 (9313): 1221-1231.

Compston A, and Coles A. 2008. Multiple sclerosis. *Lancet* 372 (9648): 1502-1517.

Connick P, De AF, Parker RA, Plantone D, Doshi A, John N, Stutters J, MacManus D, Prados CF, Barkhof F, Ourselin S, Braisher M, Ross M, Cranswick G, Pavitt SH, Giovannoni G, Gandini Wheeler-Kingshott CA, Hawkins C, Sharrack B, Bastow R, Weir CJ, Stallard N, Chandran S, and Chataway J. 2018. Multiple Sclerosis-Secondary Progressive Multi-Arm Randomisation Trial (MS-SMART): a multiarm phase IIb randomised, double-blind, placebo-controlled clinical trial comparing the efficacy of three neuroprotective drugs in secondary progressive multiple sclerosis. *BMJ Open.* 8 (8): e021944.

Constantinescu CS, Farooqi N, O'Brien K, and Gran B. 2011. Experimental autoimmune encephalomyelitis (EAE) as a model for multiple sclerosis (MS). *British Journal of Pharmacology* 164 (4): 1079-1106.

Corsini E, Dufour A, Ciusani E, Gelati M, Frigerio S, Gritti A, Cajola L, Mancardi GL, Massa G, and Salmaggi A. 1996. Human brain endothelial cells and astrocytes produce IL-1 beta but not IL-10. *Scandinavian Journal of Immunology* 44 (5): 506-511.

Costantini A, Nappo A, Pala MI, and Zappone A. 2013. High dose thiamine improves fatigue in multiple sclerosis. *BMJ Case. Rep.* 2013.

Coughlin L, Morrison RS, Horner PJ, and Inman DM. 2015. Mitochondrial morphology differences and mitophagy deficit in murine glaucomatous optic nerve. *Invest Ophthalmol. Vis. Sci.* 56 (3): 1437-1446.

Dang C, Han B, Li Q, Han R, and Hao J. 2019. Up-regulation of PGC-1a in neurons protects against experimental autoimmune encephalomyelitis. *FASEB Journal* 33 (12): 14811-14824.

De SD, Raffaello A, Teardo E, Szabo I, and Rizzuto R. 2011. A forty-kilodalton protein of the inner membrane is the mitochondrial calcium uniporter. *Nature* 476 (7360): 336-340.

Deluca HF, and Engstrom GW. 1961. Calcium uptake by rat kidney mitochondria. *Proc. Natl. Acad. Sci. U. S. A* 47: 1744-1750.

Dendrou CA, Fugger L, and Friese MA. 2015. Immunopathology of multiple sclerosis. *Nature Reviews: Immunology* 15 (9): 545-558.

Denic A, Johnson AJ, Bieber AJ, Warrington AE, Rodriguez M, and Pirko I. 2011. The relevance of animal models in multiple sclerosis research. *Pathophysiology.* 18 (1): 21-29.

Denton RM. 2009. Regulation of mitochondrial dehydrogenases by calcium ions. *Biochimica et Biophysica Acta: Protein Structure and Molecular Enzymology* 1787 (11): 1309-1316.

Denton RM, Randle PJ, and Martin BR. 1972. Stimulation by calcium ions of pyruvate dehydrogenase phosphate phosphatase. *Biochemical Journal* 128 (1): 161-163.

Diaz-Sanchez M, Williams K, DeLuca GC, and Esiri MM. 2006. Protein co-expression with axonal injury in multiple sclerosis plaques. *Acta Neuropathol.* 111 (4): 289-299.

Ding WX, and Yin XM. 2012. Mitophagy: mechanisms, pathophysiological roles, and analysis. *Biological Chemistry* 393 (7): 547-564.

Domingues HS, Mues M, Lassmann H, Wekerle H, and Krishnamoorthy G. 2010. Functional and pathogenic differences of Th1 and Th17 cells in experimental autoimmune encephalomyelitis. *PLoS. One.* 5 (11): e15531.

Dutta R, McDonough J, Yin X, Peterson J, Chang A, Torres T, Gudz T, Macklin WB, Lewis DA, Fox RJ, Rudick R, Mirnics K, and Trapp BD. 2006. Mitochondrial dysfunction as a cause of axonal degeneration in multiple sclerosis patients. *Annals of Neurology* 59 (3): 478-489.

Dutta R, and Trapp BD. 2012. Gene expression profiling in multiple sclerosis brain. *Neurobiol. Dis.* 45 (1): 108-114.

Eckert A. 2012. Mitochondrial effects of Ginkgo biloba extract. *Int. Psychogeriatr.* 24 Suppl 1: S18-S20.

Faissner S, Plemel JR, Gold R, and Yong VW. 2019. Progressive multiple sclerosis: from pathophysiology to therapeutic strategies. *Nature Reviews: Drug Discovery* 18 (12): 905-922.

Feng X, Hou H, Zou Y, and Guo L. 2017. Defective autophagy is associated with neuronal injury in a mouse model of multiple sclerosis. *Bosn. J. Basic Med. Sci.* 17 (2): 95-103.

Fiander MD, Chedrawe MA, Lamport AC, Akay T, and Robertson GS. 2017a. Sagittal Plane Kinematic Gait Analysis in C57BL/6 Mice Subjected to MOG35-55 Induced Experimental Autoimmune Encephalomyelitis. *J. Vis. Exp.* (129).

Fiander MD, Stifani N, Nichols M, Akay T, and Robertson GS. 2017b. Kinematic gait parameters are highly sensitive measures of motor deficits and spinal cord injury in mice subjected to experimental autoimmune encephalomyelitis. *Behavioural Brain Research* 317: 95-108.

Fife BT, Huffnagle GB, Kuziel WA, and Karpus WJ. 2000. CC chemokine receptor 2 is critical for induction of experimental autoimmune encephalomyelitis. *Journal of Experimental Medicine* 192 (6): 899-905.

Fischer MT, Sharma R, Lim JL, Haider L, Frischer JM, Drexhage J, Mahad D, Bradl M, van HJ, and Lassmann H. 2012. NADPH oxidase expression in active multiple sclerosis lesions in relation to oxidative tissue damage and mitochondrial injury. *Brain* 135 (Pt 3): 886-899.

Fleming KK, Bovaird JA, Mosier MC, Emerson MR, LeVine SM, and Marquis JG. 2005. Statistical analysis of data from studies on experimental autoimmune encephalomyelitis. *Journal of Neuroimmunology* 170 (1-2): 71-84.

Fletcher JM, Lalor SJ, Sweeney CM, Tubridy N, and Mills KHG. 2010. T cells in multiple sclerosis and experimental autoimmune encephalomyelitis. *Clinical and Experimental Immunology* 162 (1): 1-11.

Franklin RJ. 2002. Why does remyelination fail in multiple sclerosis? *Nature Reviews: Neuroscience* 3 (9): 705-714.

Franklin RJ, Ffrench-Constant C, Edgar JM, and Smith KJ. 2012. Neuroprotection and repair in multiple sclerosis. *Nat. Rev. Neurol.* 8 (11): 624-634.

Friese MA, Montalban X, Willcox N, Bell JI, Martin R, and Fugger L. 2006. The value of animal models for drug development in multiple sclerosis. *Brain* 129 (Pt 8): 1940-1952.

Frischer JM, Bramow S, Dal-Bianco A, Lucchinetti CF, Rauschka H, Schmidbauer M, Laursen H, Sorensen PS, and Lassmann H. 2009. The relation between inflammation and neurodegeneration in multiple sclerosis brains. *Brain* 132 (Pt 5): 1175-1189.

Fuchs Y, and Steller H. 2011. Programmed cell death in animal development and disease. *Cell* 147 (4): 742-758.

Gay FW, Drye TJ, Dick GW, and Esiri MM. 1997. The application of multifactorial cluster analysis in the staging of plaques in early multiple sclerosis. Identification and characterization of the primary demyelinating lesion. *Brain* 120 (Pt 8): 1461-1483.

GBD 2MSC. 2019. Global, regional, and national burden of neurological disorders, 1990-2016: a systematic analysis for the Global Burden of Disease Study 2016. *Lancet Neurol.* 18 (5): 459-480.

Geurts JJ, and Barkhof F. 2008. Grey matter pathology in multiple sclerosis. *Lancet Neurol.* 7 (9): 841-851.

Geurts JJ, Kooi EJ, Witte ME, and van d, V. 2010. Multiple sclerosis as an "inside-out" disease. *Annals of Neurology* 68 (5): 767-768.

Gilmour H, Ramage-Morin PL, and Wong SL. 2018. Multiple sclerosis: Prevalence and impact. *Health Rep.* 29 (1): 3-8.

Giorgi C, Agnoletto C, Bononi A, Bonora M, De ME, Marchi S, Missiroli S, Patergnani S, Poletti F, Rimessi A, Suski JM, Wieckowski MR, and Pinton P. 2012. Mitochondrial calcium homeostasis as potential target for mitochondrial medicine. *Mitochondrion.* 12 (1): 77-85.

Glancy B, and Balaban RS. 2012. Role of mitochondrial Ca2+ in the regulation of cellular energetics. *Biochemistry* 51 (14): 2959-2973.

Gomes LC, Di BG, and Scorrano L. 2011. During autophagy mitochondria elongate, are spared from degradation and sustain cell viability. *Nature Cell Biology* 13 (5): 589-598.

Gomes LC, and Scorrano L. 2011. Mitochondrial elongation during autophagy: a stereotypical response to survive in difficult times. *Autophagy.* 7 (10): 1251-1253.

Grzegorski T, and Losy J. 2017. Cognitive impairment in multiple sclerosis - a review of current knowledge and recent research. *Rev. Neurosci.* 28 (8): 845-860.

Guyton MK, Wingrave JM, Yallapragada AV, Wilford GG, Sribnick EA, Matzelle DD, Tyor WR, Ray SK, and Banik NL. 2005. Upregulation of calpain correlates with increased neurodegeneration in acute experimental autoimmune encephalomyelitis. *Journal of Neuroscience Research* 81 (1): 53-61.

Hackenbrock CR. 1966. Ultrastructural bases for metabolically linked mechanical activity in mitochondria. I. Reversible ultrastructural changes with change in metabolic steady state in isolated liver mitochondria. *Journal of Cell Biology* 30 (2): 269-297.

Haeryfar SM, and Hoskin DW. 2004. Thy-1: more than a mouse pan-T cell marker. *Journal of Immunology* 173 (6): 3581-3588.

Hafler DA, Compston A, Sawcer S, Lander ES, Daly MJ, De Jager PL, de Bakker PI, Gabriel SB, Mirel DB, Ivinson AJ, Pericak-Vance MA, Gregory SG, Rioux JD, McCauley JL, Haines JL, Barcellos LF, Cree B, Oksenberg JR, and Hauser SL. 2007. Risk alleles for multiple sclerosis identified by a genomewide study. *N. Engl. J. Med.* 357 (9): 851-862.

Hahn A, Vonck J, Mills DJ, Meier T, and Kuhlbrandt W. 2018. Structure, mechanism, and regulation of the chloroplast ATP synthase. *Science* 360 (6389).

Haines JD, Inglese M, and Casaccia P. 2011. Axonal damage in multiple sclerosis. *Mt. Sinai J. Med.* 78 (2): 231-243.

Hamada MS, and Kole MH. 2015. Myelin loss and axonal ion channel adaptations associated with gray matter neuronal hyperexcitability. *Journal of Neuroscience* 35 (18): 7272-7286.

Hamada MS, Popovic MA, and Kole MH. 2017. Loss of Saltation and Presynaptic Action Potential Failure in Demyelinated Axons. *Front Cell Neurosci.* 11: 45.

Hampton DW, Anderson J, Pryce G, Irvine KA, Giovannoni G, Fawcett JW, Compston A, Franklin RJ, Baker D, and Chandran S. 2008. An experimental model of secondary progressive multiple sclerosis that shows regional variation in gliosis, remyelination, axonal and neuronal loss. *Journal of Neuroimmunology* 201-202: 200-211.

Handel AE, Lincoln MR, and Ramagopalan SV. 2011. Of mice and men: experimental autoimmune encephalitis and multiple sclerosis. *Eur. J. Clin. Invest* 41 (11): 1254-1258.

Hansford RG, and Zorov D. 1998. Role of mitochondrial calcium transport in the control of substrate oxidation. *Mol. Cell Biochem.* 184 (1-2): 359-369.

Harbo HF, Gold R, and TintorÃ© M. 2013. Sex and gender issues in multiple sclerosis. *Ther. Adv. Neurol. Disord.* 6 (4): 237-248.

Hashemian M, Ghasemi-Kasman M, Parsian H, and Sadeghi F. 2019. Fingolimod (FTY720) improves the functional recovery and myelin preservation of the optic pathway in focal demyelination model of rat optic chiasm. *Brain Research Bulletin* 153: 109-121.

Hawkes CH, and Macgregor AJ. 2009. Twin studies and the heritability of MS: a conclusion. *Mult. Scler.* 15 (6): 661-667.

Heimer-McGinn V, and Young P. 2011. Efficient inducible Pan-neuronal cre-mediated recombination in SLICK-H transgenic mice. *Genesis.* 49 (12): 942-949.

Holick MF. 2004. Sunlight and vitamin D for bone health and prevention of autoimmune diseases, cancers, and cardiovascular disease. *American Journal of Clinical Nutrition* 80 (6 Suppl): 1678S-1688S.

Holman SP, Lobo AS, Novorolsky RJ, Nichols M, Fiander MD, Konda P, Kennedy BE, Gujar S, and Robertson GS. 2020. Neuronal mitochondrial calcium uniporter deficiency exacerbates axonal injury and suppresses remyelination in mice subjected to experimental autoimmune encephalomyelitis. *Experimental Neurology* 333: 113430.

Ignatius Arokia Doss PM, Roy AP, Wang A, Anderson AC, and Rangachari M. 2015. The Non-Obese Diabetic Mouse Strain as a Model to Study CD8(+) T Cell Function in Relapsing and Progressive Multiple Sclerosis. *Front Immunol.* 6: 541.

Jeon SM. 2016. Regulation and function of AMPK in physiology and diseases. *Exp. Mol. Med.* 48 (7): e245.

Johnson SK, Diamond BJ, Rausch S, Kaufman M, Shiflett SC, and Graves L. 2006. The effect of Ginkgo biloba on functional measures in multiple sclerosis: a pilot randomized controlled trial. *Explore. (NY)* 2 (1): 19-24.

Jones MV, Nguyen TT, Deboy CA, Griffin JW, Whartenby KA, Kerr DA, and Calabresi PA. 2008. Behavioral and pathological outcomes in MOG 35-55 experimental autoimmune encephalomyelitis. *Journal of Neuroimmunology* 199 (1-2): 83-93.

Jones MV, Nguyen TT, Ewaleifoh O, Lebson L, Whartenby KA, Griffin JW, and Calabresi PA. 2013. Accelerated axon loss in MOG35-55 experimental autoimmune encephalomyelitis (EAE) in myelin-associated glycoprotein-deficient (MAGKO) mice. *Journal of Neuroimmunology* 262 (1-2): 53-61.

Ju WK, Kim KY, Angert M, Duong-Polk KX, Lindsey JD, Ellisman MH, and Weinreb RN. 2009. Memantine blocks mitochondrial OPA1 and cytochrome c release and subsequent apoptotic cell death in glaucomatous retina. *Invest Ophthalmol. Vis. Sci.* 50 (2): 707-716.

Kalyvas A, Baskakis C, Magrioti V, Constantinou-Kokotou V, Stephens D, Lopez-Vales R, Lu JQ, Yong VW, Dennis EA, Kokotos G, and David S. 2009. Differing roles for members of the phospholipase A2 superfamily in experimental autoimmune encephalomyelitis. *Brain* 132 (Pt 5): 1221-1235.

Kang JS, Tian JH, Pan PY, Zald P, Li C, Deng C, and Sheng ZH. 2008. Docking of axonal mitochondria by syntaphilin controls their mobility and affects short-term facilitation. *Cell* 132 (1): 137-148.

Kapoor R, Ho PR, Campbell N, Chang I, Deykin A, Forrestal F, Lucas N, Yu B, Arnold DL, Freedman MS, Goldman MD, Hartung HP, Havrdova EK, Jeffery D, Miller A, Sellebjerg F, Cadavid D, Mikol D, and Steiner D. 2018. Effect of natalizumab on disease progression in secondary progressive multiple sclerosis (ASCEND): a phase 3, randomised, double-blind, placebo-controlled trial with an open-label extension. *Lancet Neurol.* 17 (5): 405-415.

Kappos L, Bar-Or A, Cree BAC, Fox RJ, Giovannoni G, Gold R, Vermersch P, Arnold DL, Arnould S, Scherz T, Wolf C, WallstrÃ¶m E, and Dahlke F. 2018. Siponimod versus placebo in secondary progressive multiple sclerosis (EXPAND): a double-blind, randomised, phase 3 study. *Lancet* 391 (10127): 1263-1273.

Kapuy O, Vinod PK, and BÃ¡nhegyi G. 2014. mTOR inhibition increases cell viability via autophagy induction during endoplasmic reticulum stress - An experimental and modeling study. *FEBS Open. Bio* 4: 704-713.

Kashfi S, Peymani M, Ghaedi K, Baharvand H, Nasr-Esfahani MH, and Javan M. 2017. Purinergic Receptor Expression and Potential Association with Human Embryonic Stem Cell-Derived Oligodendrocyte Progenitor Cell Development. *Cell J.* 19 (3): 386-402.

Katsumoto A, Lu H, Miranda AS, and Ransohoff RM. 2014. Ontogeny and functions of central nervous system macrophages. *Journal of Immunology* 193 (6): 2615-2621.

Khosravi-Largani M, Pourvali-Talatappeh P, Rousta AM, Karimi-Kivi M, Noroozi E, Mahjoob A, Asaadi Y, Shahmohammadi A, Sadeghi S, Shakeri S, Ghiyasvand K, and Tavakoli-Yaraki M. 2018. A review on potential roles of vitamins in incidence, progression, and improvement of multiple sclerosis. *eNeurologicalSci.* 10: 37-44.

King IL, Dickendesher TL, and Segal BM. 2009. Circulating Ly-6C+ myeloid precursors migrate to the CNS and play a pathogenic role during autoimmune demyelinating disease. *Blood* 113 (14): 3190-3197.

Kiryu-Seo S, Ohno N, Kidd GJ, Komuro H, and Trapp BD. 2010. Demyelination increases axonal stationary mitochondrial size and the speed of axonal mitochondrial transport. *Journal of Neuroscience* 30 (19): 6658-6666.

Koch-Henriksen N, and Sorensen PS. 2010. The changing demographic pattern of multiple sclerosis epidemiology. *Lancet Neurol.* 9 (5): 520-532.

Kondratskyi A, Kondratska K, Skryma R, Klionsky DJ, and Prevarskaya N. 2018. Ion channels in the regulation of autophagy. *Autophagy.* 14 (1): 3-21.

Kornek B, Storch MK, Weissert R, Wallstroem E, Stefferl A, Olsson T, Linington C, Schmidbauer M, and Lassmann H. 2000. Multiple Sclerosis and Chronic Autoimmune Encephalomyelitis : A Comparative Quantitative Study of Axonal Injury in Active, Inactive, and Remyelinated Lesions. *Am. J. Pathol.* 157 (1): 267-276.

Kosztelnik M, Kurucz A, Papp D, Jones E, Sigmond T, Barna J, Traka MH, Lorincz T, Szarka A, Banhegyi G, Vellai T, Korcsmaros T, and Kapuy O. 2019. Suppression of AMPK/aak-2 by NRF2/SKN-1 down-regulates autophagy during prolonged oxidative stress. *FASEB Journal* 33 (2): 2372-2387.

Kratofil RM, Kubes P, and Deniset JF. 2017. Monocyte Conversion During Inflammation and Injury. *Arterioscler. Thromb. Vasc. Biol.* 37 (1): 35-42.

Kremer D, KÃ¼ry P, and Dutta R. 2015. Promoting remyelination in multiple sclerosis: current drugs and future prospects. *Mult. Scler.* 21 (5): 541-549.

Kurnellas MP, Nicot A, Shull GE, and Elkabes S. 2005. Plasma membrane calcium ATPase deficiency causes neuronal pathology in the spinal cord: a potential mechanism for neurodegeneration in multiple sclerosis and spinal cord injury. *FASEB Journal* 19 (2): 298-300.

Kurschus FC. 2015. T cell mediated pathogenesis in EAE: Molecular mechanisms. *Biomed. J.* 38 (3): 183-193.

Kurtzke JF, Beebe GW, and Norman JE, Jr. 1985. Epidemiology of multiple sclerosis in US veterans: III. Migration and the risk of MS. *Neurology* 35 (5): 672-678.

Kwong JQ, Lu X, Correll RN, Schwanekamp JA, Vagnozzi RJ, Sargent MA, York AJ, Zhang J, Bers DM, and Molkentin JD. 2015. The Mitochondrial Calcium Uniporter Selectively Matches Metabolic Output to Acute Contractile Stress in the Heart. *Cell Rep.* 12 (1): 15-22.

Lehninger AL. 1979. Some aspects of energy coupling by mitochondria. *Advances in Experimental Medicine and Biology* 111: 1-16.

Li W, Feng J, Gao C, Wu M, Du Q, Tsoi B, Wang Q, Yang D, and Shen J. 2019. Nitration of Drp1 provokes mitophagy activation mediating neuronal injury in experimental autoimmune encephalomyelitis. *Free Radic. Biol. Med.* 143: 70-83.

Li Y, Park JS, Deng JH, and Bai Y. 2006. Cytochrome c oxidase subunit IV is essential for assembly and respiratory function of the enzyme complex. *Journal of Bioenergetics and Biomembranes* 38 (5-6): 283-291.

Liang P, and Le W. 2015. Role of autophagy in the pathogenesis of multiple sclerosis. *Neurosci. Bull.* 31 (4): 435-444.

Lodygin D, Hermann M, Schweingruber N, FlÃ¼gel-Koch C, Watanabe T, Schlosser C, Merlini A, KÃ¶rner H, Chang HF, Fischer HJ, Reichardt HM, Zagrebelsky M, Mollenhauer B, KÃ¼gler S, Fitzner D, Frahm J, Stadelmann C, Haberl M, Odoardi F, and FlÃ¼gel A. 2019. Beta-Synuclein-reactive T cells induce autoimmune CNS grey matter degeneration. *Nature* 566 (7745): 503-508.

Loma I, and Heyman R. 2011. Multiple sclerosis: pathogenesis and treatment. *Curr. Neuropharmacol.* 9 (3): 409-416.

Lublin F, Miller DH, Freedman MS, Cree BAC, Wolinsky JS, Weiner H, Lubetzki C, Hartung HP, Montalban X, Uitdehaag BMJ, Merschhemke M, Li B, Putzki N, Liu FC, Haring DA, and Kappos L. 2016. Oral fingolimod in primary progressive multiple sclerosis (INFORMS): a phase 3, randomised, double-blind, placebo-controlled trial. *Lancet* 387 (10023): 1075-1084.

Lublin FD, Reingold SC, Cohen JA, Cutter GR, SÃ¸rensen PS, Thompson AJ, Wolinsky JS, Balcer LJ, Banwell B, Barkhof F, Bebo B, Jr., Calabresi PA, Clanet M, Comi G, Fox RJ, Freedman MS, Goodman AD, Inglese M, Kappos L, Kieseier BC, Lincoln JA, Lubetzki C, Miller AE, Montalban X, O'Connor PW, Petkau J, Pozzilli C, Rudick RA, Sormani MP, StÃ¼ve O, Waubant E, and Polman CH. 2014. Defining the clinical course of multiple sclerosis: the 2013 revisions. *Neurology* 83 (3): 278-286.

Luongo TS, Lambert JP, Yuan A, Zhang X, Gross P, Song J, Shanmughapriya S, Gao E, Jain M, Houser SR, Koch WJ, Cheung JY, Madesh M, and Elrod JW. 2015. The Mitochondrial Calcium Uniporter Matches Energetic Supply with Cardiac Workload during Stress and Modulates Permeability Transition. *Cell Rep.* 12 (1): 23-34.

Magalon K, Le GM, El WB, Moulis M, Pruss R, Bordet T, Cayre M, Belenguer P, Carre M, and Durbec P. 2016. Olesoxime favors oligodendrocyte differentiation through a functional interplay between mitochondria and microtubules. *Neuropharmacology* 111: 293-303.

Magalon K, Zimmer C, Cayre M, Khaldi J, Bourbon C, Robles I, Tardif G, Viola A, Pruss RM, Bordet T, and Durbec P. 2012. Olesoxime accelerates myelination and promotes repair in models of demyelination. *Annals of Neurology* 71 (2): 213-226.

Mahad D, Ziabreva I, Lassmann H, and Turnbull D. 2008. Mitochondrial defects in acute multiple sclerosis lesions. *Brain* 131 (Pt 7): 1722-1735.

Mahad DJ, Ziabreva I, Campbell G, Lax N, White K, Hanson PS, Lassmann H, and Turnbull DM. 2009. Mitochondrial changes within axons in multiple sclerosis. *Brain* 132 (Pt 5): 1161-1174.

Maimone D, Reder AT, and Gregory S. 1993. T cell lymphokine-induced secretion of cytokines by monocytes from patients with multiple sclerosis. *Cell Immunol.* 146 (1): 96-106.

Mallilankaraman K, Cardenas C, Doonan PJ, Chandramoorthy HC, Irrinki KM, Golenar T, Csordas G, Madireddi P, Yang J, Muller M, Miller R, Kolesar JE, Molgo J, Kaufman B, Hajnoczky G, Foskett JK, and Madesh M. 2012. MCUR1 is an essential component of mitochondrial Ca2+ uptake that regulates cellular metabolism. *Nature Cell Biology* 14 (12): 1336-1343.

Mallucci G, Peruzzotti-Jametti L, Bernstock JD, and Pluchino S. 2015. The role of immune cells, glia and neurons in white and gray matter pathology in multiple sclerosis. *Progress in Neurobiology* 127-128: 1-22.

Mannella CA. 2008. Structural diversity of mitochondria: functional implications. *Annals of the New York Academy of Sciences* 1147: 171-179.

Mao P, and Reddy PH. 2010. Is multiple sclerosis a mitochondrial disease? *Biochimica et Biophysica Acta: Protein Structure and Molecular Enzymology* 1802 (1): 66-79.

Marino G, Niso-Santano M, Baehrecke EH, and Kroemer G. 2014. Self-consumption: the interplay of autophagy and apoptosis. *Nature Reviews: Molecular Cell Biology* 15 (2): 81-94.

Matsuhashi T, Sato T, Kanno SI, Suzuki T, Matsuo A, Oba Y, Kikusato M, Ogasawara E, Kudo T, Suzuki K, Ohara O, Shimbo H, Nanto F, Yamaguchi H, Saigusa D, Mukaiyama Y, Watabe A, Kikuchi K, Shima H, Mishima E, Akiyama Y, Oikawa Y, Hsin-Jung HO, Akiyama Y, Suzuki C, Uematsu M, Ogata M, Kumagai N, Toyomizu M, Hozawa A, Mano N, Owada Y, Aiba S, Yanagisawa T, Tomioka Y, Kure S, Ito S, Nakada K, Hayashi KI, Osaka H, and Abe T. 2017. Mitochonic Acid 5 (MA-5) Facilitates ATP Synthase Oligomerization and Cell Survival in Various Mitochondrial Diseases. *EBioMedicine.* 20: 27-38.

McCarthy DP, Richards MH, and Miller SD. 2012. Mouse models of multiple sclerosis: experimental autoimmune encephalomyelitis and Theiler's virus-induced demyelinating disease. *Methods Mol. Biol.* 900: 381-401.

McRae BL, Vanderlugt CL, Dal Canto MC, and Miller SD. 1995. Functional evidence for epitope spreading in the relapsing pathology of experimental autoimmune encephalomyelitis. *Journal of Experimental Medicine* 182 (1): 75-85.

Mei F, Lehmann-Horn K, Shen YA, Rankin KA, Stebbins KJ, Lorrain DS, Pekarek K, Sagan A, Xiao L, Teuscher C, von BÃ¼dingen HC, Wess J, Lawrence JJ, Green AJ, Fancy SP, Zamvil SS, and Chan JR. 2016. Accelerated remyelination during inflammatory demyelination prevents axonal loss and improves functional recovery. *Elife.* 5.

Michalski D, Keck AL, Grosche J, Martens H, and HÃ¤rtig W. 2018. Immunosignals of Oligodendrocyte Markers and Myelin-Associated Proteins Are Critically Affected after Experimental Stroke in Wild-Type and Alzheimer Modeling Mice of Different Ages. *Front Cell Neurosci.* 12: 23.

Milo R, and Kahana E. 2010. Multiple sclerosis: geoepidemiology, genetics and the environment. *Autoimmunity Reviews* 9 (5): A387-A394.

Milo R, Korczyn AD, Manouchehri N, and Stuve O. 2019. The temporal and causal relationship between inflammation and neurodegeneration in multiple sclerosis. *Mult. Scler.*: 1352458519886943.

Mokhtarian F, Huan CM, Roman C, and Raine CS. 2003. Semliki Forest virus-induced demyelination and remyelination--involvement of B cells and anti-myelin antibodies. *Journal of Neuroimmunology* 137 (1-2): 19-31.

Monaghan KL, Zheng W, Hu G, and Wan ECK. 2019. Monocytes and Monocyte-Derived Antigen-Presenting Cells Have Distinct Gene Signatures in Experimental Model of Multiple Sclerosis. *Front Immunol.* 10: 2779.

Montalban X, Hauser SL, Kappos L, Arnold DL, Bar-Or A, Comi G, De SJ, Giovannoni G, Hartung HP, Hemmer B, Lublin F, Rammohan KW, Selmaj K, Traboulsee A, Sauter A, Masterman D, Fontoura P, Belachew S, Garren H, Mairon N, Chin P, and Wolinsky JS. 2017. Ocrelizumab versus Placebo in Primary Progressive Multiple Sclerosis. *N. Engl. J. Med.* 376 (3): 209-220.

Ng X, Sadeghian M, Heales S, and Hargreaves IP. 2019. Assessment of Mitochondrial Dysfunction in Experimental Autoimmune Encephalomyelitis (EAE) Models of Multiple Sclerosis. *Int. J. Mol. Sci.* 20 (20).

Nichols M, Elustondo PA, Warford J, Thirumaran A, Pavlov EV, and Robertson GS. 2017. Global ablation of the mitochondrial calcium uniporter increases glycolysis in cortical neurons subjected to energetic stressors. *J. Cereb. Blood Flow Metab* 37 (8): 3027-3041.

Nichols M, Pavlov EV, and Robertson GS. 2018. Tamoxifen-induced knockdown of the mitochondrial calcium uniporter in Thy1-expressing neurons protects mice from hypoxic/ischemic brain injury. *Cell Death. Dis.* 9 (6): 606.

Niescier RF, Chang KT, and Min KT. 2013. Miro, MCU, and calcium: bridging our understanding of mitochondrial movement in axons. *Front Cell Neurosci.* 7: 148.

Niescier RF, Hong K, Park D, and Min KT. 2018. MCU Interacts with Miro1 to Modulate Mitochondrial Functions in Neurons. *Journal of Neuroscience* 38 (20): 4666-4677.

Okuda Y, Okuda M, and Bernard CC. 2002. The suppression of T cell apoptosis influences the severity of disease during the chronic phase but not the recovery from the acute phase of experimental autoimmune encephalomyelitis in mice. *Journal of Neuroimmunology* 131 (1-2): 115-125.

Olsson T. 1995. Cytokine-producing cells in experimental autoimmune encephalomyelitis and multiple sclerosis. *Neurology* 45 (6 Suppl 6): S11-S15.

Olsson T, Zhi WW, Hojeberg B, Kostulas V, Jiang YP, Anderson G, Ekre HP, and Link H. 1990. Autoreactive T lymphocytes in multiple sclerosis determined by antigen-induced secretion of interferon-gamma. *J. Clin. Invest* 86 (3): 981-985.

Packialakshmi B, and Zhou X. 2018. Experimental autoimmune encephalomyelitis (EAE) up-regulates the mitochondrial activity and manganese superoxide dismutase (MnSOD) in the mouse renal cortex. *PLoS. One.* 13 (4): e0196277.

Page WF, Kurtzke JF, Murphy FM, and Norman JE, Jr. 1993. Epidemiology of multiple sclerosis in U.S. veterans: V. Ancestry and the risk of multiple sclerosis. *Annals of Neurology* 33 (6): 632-639.

Pan X, Liu J, Nguyen T, Liu C, Sun J, Teng Y, Fergusson MM, Rovira II, Allen M, Springer DA, Aponte AM, Gucek M, Balaban RS, Murphy E, and Finkel T. 2013. The physiological role of mitochondrial calcium revealed by mice lacking the mitochondrial calcium uniporter. *Nature Cell Biology* 15 (12): 1464-1472.

Papenfuss TL, Rogers CJ, Gienapp I, Yurrita M, McClain M, Damico N, Valo J, Song F, and Whitacre CC. 2004. Sex differences in experimental autoimmune encephalomyelitis in multiple murine strains. *J Neuroimmunol.* 150 (1-2): 59-69.

Parker WD, Jr., Haas R, Stumpf DA, Parks J, Eguren LA, and Jackson C. 1984. Brain mitochondrial metabolism in experimental thiamine deficiency. *Neurology* 34 (11): 1477-1481.

Patergnani S, Castellazzi M, Bonora M, Marchi S, Casetta I, Pugliatti M, Giorgi C, Granieri E, and Pinton P. 2018. Autophagy and mitophagy elements are increased in body fluids of multiple sclerosis-affected individuals. *"Journal of Neurology, Neurosurgery and Psychiatry"* 89 (4): 439-441.

Peruzzotti-Jametti L, and Pluchino S. 2018. Targeting Mitochondrial Metabolism in Neuroinflammation: Towards a Therapy for Progressive Multiple Sclerosis. *Trends in Molecular Medicine* 24 (10): 838-855.

Peymani M, Ghaedi K, Hashemi MS, Ghoochani A, Kiani-Esfahani A, Nasr-Esfahani MH, and Baharvand H. 2018. Ameliorating the Effect of Pioglitazone on LPS-Induced Inflammation of Human Oligodendrocyte Progenitor Cells. *Cell Mol. Neurobiol.* 38 (2): 517-527.

Pivovarova NB, and Andrews SB. 2010. Calcium-dependent mitochondrial function and dysfunction in neurons. *FEBS Journal* 277 (18): 3622-3636.

Prinz J, Karacivi A, Stormanns ER, Recks MS, and Kuerten S. 2015. Time-Dependent Progression of Demyelination and Axonal Pathology in MP4-Induced Experimental Autoimmune Encephalomyelitis. *PLoS. One.* 10 (12): e0144847.

Purves D, Augustine GJ, and Fitzpatrick D. 2001. Neuroscience. 2nd edition: Functional Properties of the Na+/K+ Pump.

Qi X, Lewin AS, Sun L, Hauswirth WW, and Guy J. 2006. Mitochondrial protein nitration primes neurodegeneration in experimental autoimmune encephalomyelitis. *Journal of Biological Chemistry* 281 (42): 31950-31962.

Quandt FN, and Davis FA. 1992. Action potential refractory period in axonal demyelination: a computer simulation. *Biological Cybernetics* 67 (6): 545-552.

Rahn EJ, Iannitti T, Donahue RR, and Taylor BK. 2014. Sex differences in a mouse model of multiple sclerosis: neuropathic pain behavior in females but not males and protection from neurological deficits during proestrus. *Biol. Sex Differ.* 5 (1): 4.

Raine CS. 1994. The Dale E. McFarlin Memorial Lecture: the immunology of the multiple sclerosis lesion. *Annals of Neurology* 36 Suppl: S61-S72.

Recks MS, Stormanns ER, Bader J, Arnhold S, Addicks K, and Kuerten S. 2013. Early axonal damage and progressive myelin pathology define the kinetics of CNS histopathology in a mouse model of multiple sclerosis. *Clinical Immunology* 149 (1): 32-45.

Riise T, Nortvedt MW, and Ascherio A. 2003. Smoking is a risk factor for multiple sclerosis. *Neurology* 61 (8): 1122-1124.

Rivers TM, Sprunt DH, and Berry GP. 1933. OBSERVATIONS ON ATTEMPTS TO PRODUCE ACUTE DISSEMINATED ENCEPHALOMYELITIS IN MONKEYS. *Journal of Experimental Medicine* 58 (1): 39-53.

Rizzuto R, De SD, Raffaello A, and Mammucari C. 2012. Mitochondria as sensors and regulators of calcium signalling. *Nature Reviews: Molecular Cell Biology* 13 (9): 566-578.

Robinson AP, Harp CT, Noronha A, and Miller SD. 2014. The experimental autoimmune encephalomyelitis (EAE) model of MS: utility for understanding disease pathophysiology and treatment. *Handb. Clin. Neurol.* 122: 173-189.

Rottenberg H, and Scarpa A. 1974. Calcium uptake and membrane potential in mitochondria. *Biochemistry* 13 (23): 4811-4817.

Sadeghian M, Mastrolia V, Rezaei HA, Mosley A, Mullali G, Schiza D, Sajic M, Hargreaves I, Heales S, Duchen MR, and Smith KJ. 2016. Mitochondrial dysfunction is an important cause of neurological deficits in an inflammatory model of multiple sclerosis. *Sci. Rep.* 6: 33249.

Saxton WM, and Hollenbeck PJ. 2012. The axonal transport of mitochondria. *Journal of Cell Science* 125 (Pt 9): 2095-2104.

Scheld M, Ruther BJ, Grosse-Veldmann R, Ohl K, Tenbrock K, Dreymuller D, Fallier-Becker P, Zendedel A, Beyer C, Clarner T, and Kipp M. 2016. Neurodegeneration Triggers Peripheral Immune Cell Recruitment into the Forebrain. *Journal of Neuroscience* 36 (4): 1410-1415.

Schwarz TL. 2013. Mitochondrial trafficking in neurons. *Cold Spring Harb. Perspect. Biol.* 5 (6).

Seok J, Warren HS, Cuenca AG, Mindrinos MN, Baker HV, Xu W, Richards DR, McDonald-Smith GP, Gao H, Hennessy L, Finnerty CC, LÃ³pez CM, Honari S, Moore EE, Minei JP, Cuschieri J, Bankey PE, Johnson JL, Sperry J, Nathens AB, Billiar TR, West MA, Jeschke MG, Klein MB, Gamelli RL, Gibran NS, Brownstein BH, Miller-Graziano C, Calvano SE, Mason PH, Cobb JP, Rahme LG, Lowry SF, Maier RV, Moldawer LL, Herndon DN, Davis RW, Xiao W, and Tompkins RG. 2013. Genomic responses in mouse models poorly mimic human inflammatory diseases. *Proc. Natl. Acad. Sci. U. S. A* 110 (9): 3507-3512.

Shechter R, Miller O, Yovel G, Rosenzweig N, London A, Ruckh J, Kim KW, Klein E, Kalchenko V, Bendel P, Lira SA, Jung S, and Schwartz M. 2013. Recruitment of beneficial M2 macrophages to injured spinal cord is orchestrated by remote brain choroid plexus. *Immunity.* 38 (3): 555-569.

Sheng ZH, and Cai Q. 2012. Mitochondrial transport in neurons: impact on synaptic homeostasis and neurodegeneration. *Nature Reviews: Neuroscience* 13 (2): 77-93.

Shields DC, Schaecher KE, Saido TC, and Banik NL. 1999. A putative mechanism of demyelination in multiple sclerosis by a proteolytic enzyme, calpain. *Proc. Natl. Acad. Sci. U. S. A* 96 (20): 11486-11491.

Short B. 2020. Syntaphilin puts the brakes on axonal mitochondria.

Sintzel MB, Rametta M, and Reder AT. 2018. Vitamin D and Multiple Sclerosis: A Comprehensive Review. *Neurol. Ther.* 7 (1): 59-85.

Skripuletz T, Bussmann JH, Gudi V, Koutsoudaki PN, Pul R, Moharregh-Khiabani D, Lindner M, and Stangel M. 2010. Cerebellar cortical demyelination in the murine cuprizone model. *Brain Pathol.* 20 (2): 301-312.

Smith KJ. 1994. Conduction properties of central demyelinated and remyelinated axons, and their relation to symptom production in demyelinating disorders. *Eye (Lond)* 8 (Pt 2): 224-237.

Smith ME. 1999. Phagocytosis of myelin in demyelinative disease: a review. *Neurochemical Research* 24 (2): 261-268.

Steinman L, and Zamvil SS. 2006. How to successfully apply animal studies in experimental allergic encephalomyelitis to research on multiple sclerosis. *Annals of Neurology* 60 (1): 12-21.

Stirling DP, and Stys PK. 2010. Mechanisms of axonal injury: internodal nanocomplexes and calcium deregulation. *Trends in Molecular Medicine* 16 (4): 160-170.

Stys PK, and Lopachin RM. 1998. Mechanisms of calcium and sodium fluxes in anoxic myelinated central nervous system axons. *Neuroscience* 82 (1): 21-32.

Stys PK, Waxman SG, and Ransom BR. 1992. Ionic mechanisms of anoxic injury in mammalian CNS white matter: role of Na+ channels and Na(+)-Ca2+ exchanger. *Journal of Neuroscience* 12 (2): 430-439.

Stys PK, Zamponi GW, van MJ, and Geurts JJ. 2012. Will the real multiple sclerosis please stand up? *Nature Reviews: Neuroscience* 13 (7): 507-514.

Sun F, Xu X, Wang X, and Zhang B. 2016. Regulation of autophagy by Ca(2). *Tumour. Biol.* 37 (12): 15467-15476.

Suzuki N, Sekimoto K, Hayashi C, Mabuchi Y, Nakamura T, and Akazawa C. 2017. Differentiation of Oligodendrocyte Precursor Cells from Sox10-Venus Mice to Oligodendrocytes and Astrocytes. *Sci. Rep.* 7.

Suzuki T, Yamaguchi H, Kikusato M, Hashizume O, Nagatoishi S, Matsuo A, Sato T, Kudo T, Matsuhashi T, Murayama K, Ohba Y, Watanabe S, Kanno S, Minaki D, Saigusa D, Shinbo H, Mori N, Yuri A, Yokoro M, Mishima E, Shima H, Akiyama Y, Takeuchi Y, Kikuchi K, Toyohara T, Suzuki C, Ichimura T, Anzai J, Kohzuki M, Mano N, Kure S, Yanagisawa T, Tomioka Y, Toyomizu M, Tsumoto K, Nakada K, Bonventre JV, Ito S, Osaka H, Hayashi K, and Abe T. 2016. Mitochonic Acid 5 Binds Mitochondria and Ameliorates Renal Tubular and Cardiac Myocyte Damage. *J. Am. Soc. Nephrol.* 27 (7): 1925-1932.

Tanida I, Ueno T, and Kominami E. 2008. LC3 and Autophagy. *Methods Mol. Biol.* 445: 77-88.

Thompson AJ, Toosy AT, and Ciccarelli O. 2010. Pharmacological management of symptoms in multiple sclerosis: current approaches and future directions. *Lancet Neurol.* 9 (12): 1182-1199.

Torkildsen A, Myhr KM, and BÃ¸ L. 2016. Disease-modifying treatments for multiple sclerosis - a review of approved medications. *Eur. J. Neurol.* 23 Suppl 1 (Suppl 1): 18-27.

Traaseth N, Elfering S, Solien J, Haynes V, and Giulivi C. 2004. Role of calcium signaling in the activation of mitochondrial nitric oxide synthase and citric acid cycle. *Biochimica et Biophysica Acta: Protein Structure and Molecular Enzymology* 1658 (1-2): 64-71.

Trager N, Smith A, Wallace IG, Azuma M, Inoue J, Beeson C, Haque A, and Banik NL. 2014. Effects of a novel orally administered calpain inhibitor SNJ-1945 on immunomodulation and neurodegeneration in a murine model of multiple sclerosis. *Journal of Neurochemistry* 130 (2): 268-279.

Trapp BD, Peterson J, Ransohoff RM, Rudick R, Mork S, and Bo L. 1998. Axonal transection in the lesions of multiple sclerosis. *N. Engl. J. Med.* 338 (5): 278-285.

Trapp BD, and Stys PK. 2009. Virtual hypoxia and chronic necrosis of demyelinated axons in multiple sclerosis. *Lancet Neurol.* 8 (3): 280-291.

Tsunoda I, and Fujinami RS. 2002. Inside-Out versus Outside-In models for virus induced demyelination: axonal damage triggering demyelination. *Springer Seminars in Immunopathology* 24 (2): 105-125.

Tsutsui S, and Stys PK. 2013. Metabolic injury to axons and myelin. *Experimental Neurology* 246: 26-34.

Vergo S, Craner MJ, Etzensperger R, Attfield K, Friese MA, Newcombe J, Esiri M, and Fugger L. 2011. Acid-sensing ion channel 1 is involved in both axonal injury and demyelination in multiple sclerosis and its animal model. *Brain* 134 (Pt 2): 571-584.

Vidal M, Morris R, Grosveld F, and Spanopoulou E. 1990. Tissue-specific control elements of the Thy-1 gene. *EMBO Journal* 9 (3): 833-840.

Virtanen JO, and Jacobson S. 2012. Viruses and multiple sclerosis. *CNS. Neurol. Disord. Drug Targets.* 11 (5): 528-544.

Waxman SG, Craner MJ, and Black JA. 2004. Na+ channel expression along axons in multiple sclerosis and its models. *Trends in Pharmacological Sciences* 25 (11): 584-591.

Weiner HL. 2008. A shift from adaptive to innate immunity: a potential mechanism of disease progression in multiple sclerosis. *J. Neurol.* 255 Suppl 1: 3-11.

Welsh TG, and Kucenas S. 2018. Purinergic signaling in oligodendrocyte development and function. *Journal of Neurochemistry* 145 (1): 6-18.

Wingerchuk DM. 2012. Smoking: effects on multiple sclerosis susceptibility and disease progression. *Ther. Adv. Neurol. Disord.* 5 (1): 13-22.

Witte ME, Mahad DJ, Lassmann H, and van HJ. 2014. Mitochondrial dysfunction contributes to neurodegeneration in multiple sclerosis. *Trends in Molecular Medicine* 20 (3): 179-187.

Witte ME, Nijland PG, Drexhage JA, Gerritsen W, Geerts D, van Het HB, Reijerkerk A, de Vries HE, van d, V, and van HJ. 2013. Reduced expression of PGC-1alpha partly underlies mitochondrial changes and correlates with neuronal loss in multiple sclerosis cortex. *Acta Neuropathol.* 125 (2): 231-243.

Wujek JR, Bjartmar C, Richer E, Ransohoff RM, Yu M, Tuohy VK, and Trapp BD. 2002. Axon loss in the spinal cord determines permanent neurological disability in an animal model of multiple sclerosis. *Journal of Neuropathology & Experimental Neurology* 61 (1): 23-32.

Young EA, Fowler CD, Kidd GJ, Chang A, Rudick R, Fisher E, and Trapp BD. 2008a. Imaging correlates of decreased axonal Na+/K+ ATPase in chronic multiple sclerosis lesions. *Annals of Neurology* 63 (4): 428-435.

Young P, Qiu L, Wang D, Zhao S, Gross J, and Feng G. 2008b. Single-neuron labeling with inducible Cre-mediated knockout in transgenic mice. *Nature Neuroscience* 11 (6): 721-728.

Appendix 1: Copyright Permission

Neuronal mitochondrial calcium uniporter deficiency exacerbates axonal injury and suppresses remyelination in mice subjected to experimental autoimmune encephalomyelitis

Author:
Scott P. Holman,Aurelio S. Lobo,Robyn J. Novorolsky,Matthew Nichols,Maximillian D.J. Fiander,Prathyusha Konda,Barry E. Kennedy,Shashi Gujar,George S. Robertson

Publication: Experimental Neurology

Publisher: Elsevier

Date: November 2020

Please note that, as the author of this Elsevier article, you retain the right to include it in a thesis or dissertation, provided it is not published commercially. Permission is not required, but please ensure that you reference the journal as the original source. For more information on this and on your other retained rights, please visit: https://www.elsevier.com/about/our-business/policies/copyright#Author-rights

BACK CLOSE WINDOW